MULTI-TEMPORAL WATER EXTENT ANALYSIS OF A HYPERSALINE PLAYA LAKE USING LANDSAT IMAGERY

A THESIS SUBMITTED TO
THE GRADUATE SCHOOL OF NATURAL AND APPLIED SCIENCES
OF
MIDDLE EAST TECHNICAL UNIVERSITY

BY

ECENUR CEYHAN

IN PARTIAL FULFILLMENT OF THE REQUIREMENTS
FOR
THE DEGREE OF MASTER OF SCIENCE
IN
GEOLOGICAL ENGINEERING

JUNE 2016

Approval of the thesis:

MULTI-TEMPORAL WATER EXTENT ANALYSIS OF A HYPERSALINE PLAYA LAKE USING LANDSAT IMAGERY

submitted by **ECENUR CEYHAN** in partial fulfillment of the requirements for the degree of **Master of Science in Geological Engineering Department, Middle East Technical University** by,

Prof. Dr. Gülbin Dural Ünver _____
Dean, Graduate School of **Natural and Applied Science**
Prof. Dr. Erdin Bozkurt _____
Head of Department, **Geological Engineering**
Assoc. Prof. Dr. Koray K. Yılmaz _____
Supervisor, **Geological Engineering Dept., METU**
Prof. Dr. M. Lütfi Süzen _____
Co-Supervisor, **Geological Engineering Dept., METU**

Examining Committee Members:
Prof. Dr. Nurkan Karahanoğlu _____
Geological Engineering Dept., METU
Assoc. Prof. Dr. Koray K. Yılmaz _____
Geological Engineering Dept., METU
Prof. Dr. M. Lütfi Süzen _____
Geological Engineering Dept., METU
Assoc. Prof. Dr. İsmail Yücel _____
Civil Engineering Dept., METU
Assoc. Prof. Dr. B. Taner San _____
Geological Engineering Dept., Akdeniz University

Date: 16/06/2016

I hereby declare that all information in this document has been obtained and presented in accordance with academic rules and ethical conduct. I also declare that, as required by these rules and conduct, I have fully cited and referenced all material and results that are not original to this work.

Name, Last name : Ecenur Ceyhan

Signature :

ABSTRACT

MULTI-TEMPORAL WATER EXTENT ANALYSIS OF A HYPERSALINE PLAYA LAKE USING LANDSAT IMAGERY

Ceyhan, Ecenur

M.S., Department of Geological Engineering

Supervisor: Assoc. Prof. Dr. Koray K. Yılmaz

Co-Supervisor: Prof. Dr. M. Lütfi Süzen

June 2016, 82 pages

Distinguishing inland water bodies from satellite imagery has always been one of the main practices of remote sensing. In some cases this differentiation can directly be obtained by visual interpretation. However, in case of hyper-saline playa lakes, presence of high albedo salt crust in the lake bed hampers visual interpretation and requires further attention. Lake Tuz is a hypersaline playa lake which is ranked as the second largest lake in Turkey. Spatio-temporal changes in lake water extent is an important issue both economically and hydrologically including salt production, lake water balance, drought and over-exploitation issues. This study investigates the spatio-temporal changes in Lake Tuz water extent using single-band thresholding and multi-band indices extracted from Landsat 5 TM and Landsat 7 ETM+ images. The applicability of different satellite-derived indices including Normalized Difference Water Index (NDWI), Modified NDWI (MNDWI), Automated Water Extraction Index (AWEI) and Tasseled Cap Wetness (TCW) were investigated for the extraction of lake water extent from Landsat imagery. Our analysis indicated

that, NDWI is superior to other tested indices in separating wet/dry pixels over the lake bottom covered with salt crust. Using a NDWI thresholding procedure, the annual and seasonal variation in the Lake Tuz water extent were determined and further linked to hydro-meteorological variables. The strongest link with lake extent was observed with annual precipitation. Moreover, time series investigation of the lake extent indicated that the lake dries consistently from North to South. The drying pattern can be related with the prevailing northerly winds.

Keywords: Lake Tuz, playa lake, water extent, Landsat TM/ETM+, NDWI

ÖZ

BİR HİPERSALİN PLAYA GÖLÜNÜN LANDSAT GÖRÜNTÜLERİ İLE ZAMANA BAĞLI SU SINIRI DEĞİŞİMİNİN ANALİZİ

Ceyhan, Ecenur

Yüksek Lisans, Jeoloji Mühendisliği Bölümü

Tez Yöneticisi: Doç. Dr. Koray K. Yılmaz

Yardımcı Tez Yöneticisi: Prof. Dr. M. Lütfi Süzen

Haziran 2016, 82 Sayfa

İç suların ayırt edilmesi uzaktan algılamanın temel uygulamalarından biri olmuştur. Bazı durumlarda bu ayırt etme direk görsel yorumlama ile elde edilebilir. Ancak hipersalin sığ göller söz konusu olduğunda, göl tabanında bulunan yüksek albedolu tuz katmanı görsel yorumlamayı olumsuz etkiler ve ileri çalışmalar gerektirir. Tuz Gölü, hipersalin sığ bir göldür ve Türkiye'nin en büyük ikinci gölüdür. Göl su sınırlarındaki zamansal ve mekansal değişimler; tuz üretimi, göl su bütçesi, kuraklık ve aşırı kullanım konuları da dahil olmak üzere hem ekonomik hem de hidrolojik olarak önemlidir. Bu çalışma, Landsat 5 TM ve Landsat 7 ETM+ görüntülerinden elde edilen tek bantlı eşik değerlerini ve çok bantlı indeksleri kullanarak Tuz Gölü su sınırının zamansal ve mekansal değişimini araştırmaktadır. Landsat görüntülerinden göl su sınırının elde edilebilmesi için Normalize Edilmiş Su Farklılık İndeksi (NDWI), Modifiye Normalize Edilmiş Su Farklılık İndeksi (MNDWI), Otomatikleştirilmiş Su Çıkarma İndeksi (AWEI) ve Tasseled Cap Nemlilik indeksi (TCW) dahil olmak üzere uydu kaynaklı farklı indekslerin

uygulanabilirliği araştırılmıştır. Yapılan analizler tabanı tuz katmanı ile kaplı olan bu gölde ıslak/kuru piksellerin ayırt edilmesinde NDWI'nın diğer test edilen indekslerden daha üstün olduğunu işaret etmiştir. NDWI eşik değerlerinin belirlenmesi ile Tuz Gölü'nün su sınırlarının yıllık ve mevsimlik değişimleri belirlenmiş ve sonrasında yağış ve rüzgar gibi hidro-meteorolojik değişkenlerle ilişkilendirilmiştir. En güçlü bağlantı göl su sınırı ile yıllık yağış arasında gözlemlenmiştir. Buna ek olarak, göl su sınırının zaman serisi olarak incelenmesi gölün tutarlı olarak Kuzey'den Güney'e doğru kuruduğunu göstermiştir. Kuruma şablonu bölgede yaygın olan Kuzey yönlü rüzgarlar ile ilişkili olabilir.

Anahtar Kelimeler: Tuz Gölü, playa gölü, su sınırı, Landsat TM/ETM+, NDWI

To my beloved family…

ACKNOWLEDGEMENT

I would like to express my deepest gratitude to my thesis supervisor Assoc. Prof. Dr. Koray K. Yılmaz for his theoretical guidance, support and patience throughout the study. I also would like to thank my co-supervisor Prof. Dr. M. Lütfi Süzen for his valuable contributions, guidance and criticism. It has been a great honor to work with them.

I am very thankful to my father for encouraging me to start my master's study and supporting me in this journey. I cannot thank enough to my mother for being exactly who she is and raising me as a strong woman just like herself. I also would like to thank my little sister Cansu Kılıç, her presence has always driven me to be a better person.

I wish to thank Dilge Varlı and Hatice Kılıç for their love, encouragement and support as valuable colleagues and friends.

I would like to thank to General Directorate of Meteorology and General Directorate of State Hydraulic Works for providing the meteorological and hydrological data, respectively. Their contributions are greatly appreciated.

I would like to thank TÜBİTAK for awarding me with Priority Areas Master's Scholarship for my study (Program no: 2210-C).

Last but certainly not least, I would like thank my spouse for his generous patience, encourage and love.

TABLE OF CONTENTS

LIST OF TABLES

TABLES:

LIST OF FIGURES

FIGURES:

LIST OF ABBREVIATIONS

AEZF	Altınekin Fault Zone
AWEI	Automated Water Extraction Index
CFZ	Cihanbeyli Fault Zone
DSI	Devlet Su İşleri
ETM+	Enhanced Thematic Mapper Plus
GDM	General Directorate of Meteorology
IQR	Interquartile Range
KCB	Konya Closed Basin
KMB	Kırşehir Massif Block
MGM	Meteoroloji Genel Müdürlüğü
MNDWI	Modified Normalized Difference Water Index
MTA	Maden Tetkik ve Arama Genel Müdürlüğü
NDVI	Normalized Difference Vegetation Index
NDWI	Normalized Difference Water Index
QPS	Quaternary Paleolake Sediments
SCL	Scan Line Corrector
SZB	Sakaray Zone Block
SZF	Sultanhanı Fault Zone
TAB	Tauride-Anatolide Block
TCW	Tasseled Cap Wetness
TFZ	Lake Tuz Fault Zone
TM	Thematic Mapper
USGS	United States Geological Survey
YZF	Yeniceoba Fault Zone

CHAPTER 1

INTRODUCTION

1.1. Purpose and Scope

Mapping water bodies has crucial importance on flood, coastal line change, wetland and lake monitoring and evaluation of water resources. Production of the water body maps by ground measurements has certain difficulties since the water body may be moving fast, not readily accessible or it may be time and money consuming. Using remotely sensed images provides significant conveniences for overcoming these problems.

Lake Tuz is the shallowest and second largest lake in Turkey. Apart from this, Lake Tuz has unique characteristics making it very important both ecologically and economically. The habitat of the lake includes endemic flora, fauna and suitable for hosting migratory bird species including flamingos (Çınar Mühendislik, 2010). With this great ecological significance Lake Tuz became a specially protected environment area in 2000. Moreover, the salty water of Lake Tuz is being used by the salinas which produce the majority of Turkey's salt demand making the lake economically very significant.

The lake bottom is covered with a salt crust which has high albedo. Because of this unique property Lake Tuz is being used for absolute radiometric calibration test site for accurate radiometric calibration of remote sensing sensors (Gürol et al. 2010). However, the salt crust creates problems for water body mapping by remotely sensed images. The high albedo crust covers the whole lake and the shallow water

cannot compensate its effect enough to differentiate wet and dry parts in remotely sensed images.

The purposes of this study are; (1) finding the most suitable method among single-band thresholding and some multi-band indices to differentiate wet and dry pixels (2) finding the threshold value separating the dry and wet pixels (3) extracting the changes in the extent of Lake Tuz seasonally and annually (4) investigating the relation between the lake extent and hydro-meteorological variables. The scope of the work includes comparison of Normalized Difference Water Index (NDWI), Modified Normalized Difference Water Index (MNDWI), Automated Water Extraction Index (AWEI) and Tasseled Cap Wetness (TCW), and each band of the selected images. Based on the degree of success in differentiating dry and wet pixels the best method was selected and a threshold values that best separates dry/wet pixels was determined. Using the selected threshold, annual and seasonal changes of the lake extent were determined. Finally, the relationship between water extent and hydro-meteorological variables such as precipitation, evaporation, temperature and wind were investigated.

This study differs from other works related to hypersaline lake studies. First of all, this study investigates both single bands and multi-band indices in selection of the best method. The moist class is also included in the study for determining a more precise threshold. The lake extents were investigated both annually and seasonally. Moreover, the relationship between the changes in the lake extent and hydro-meteorological variables were investigated.

Geology of the study area is provided in Section 2.2.3 as literature review. The relationship between the selected method and lake extent are out of the scope of this study.

1.2. Location of the Study Area

Lake Tuz is located in the Central Anatolia, between N 38° 15' - N 39° 15' latitudes and E 33° 00'- E 33° 00' longitudes. The lake and surrounding swamp areas cover an area of 1500 km^2. However, the maximum water extent reaches to 900 km^2

approximately. It is bordered by Ankara, Aksaray and Konya provinces. Ankara-Aksaray-Aydın Highway in the East, Ankara-Konya Highway in the West and Aksaray-Konya in the South are the major highways used in reaching the study area. Moreover, there are stabilized and asphalt roads connecting the settlements. These roads can be used to reach to the study area. The location of Lake Tuz is shown in Figure 1.

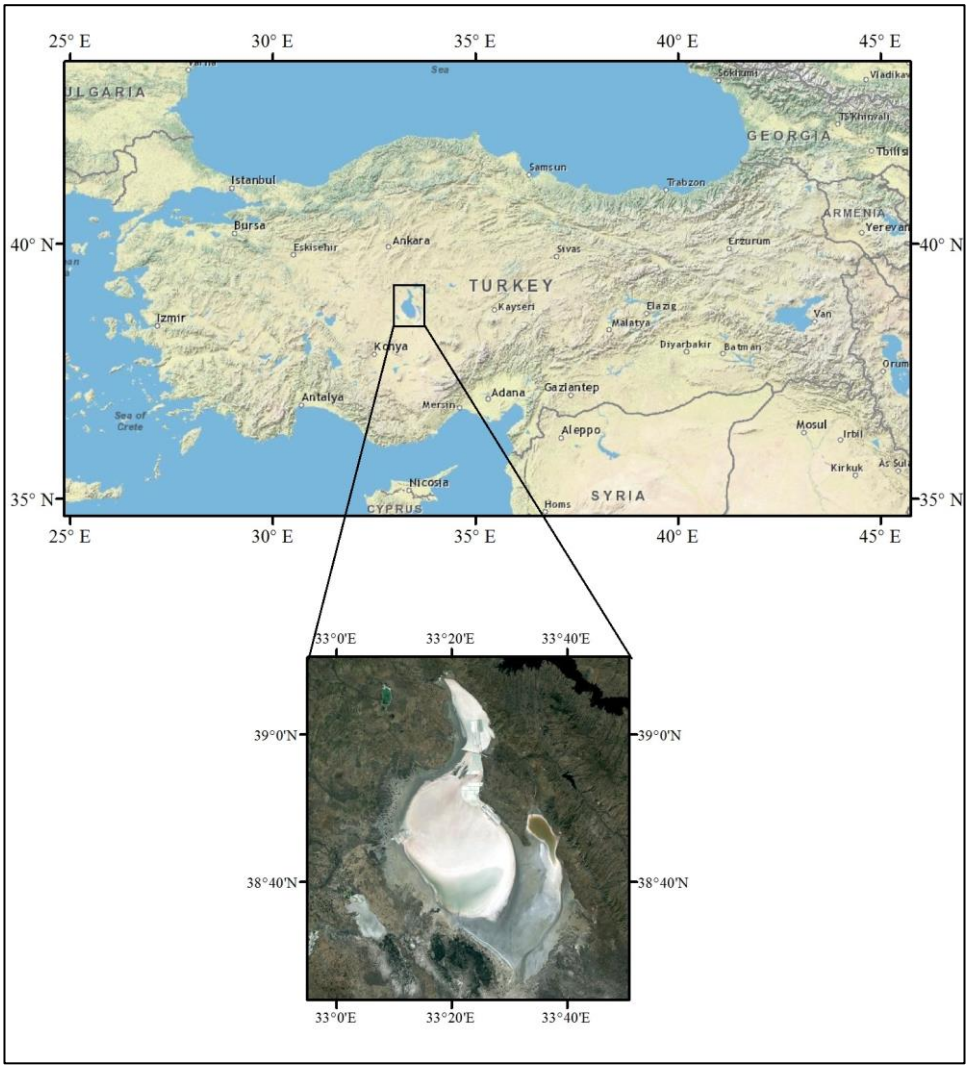

Figure 1: Location map of the study area

CHAPTER 2

LITERATURE REVIEW

2.1. Overview of Remote Sensing

2.1.1. Principles of Remote Sensing and Properties of Landsat TM and ETM+ Sensors

The most general definition of remote sensing is gathering information of a target without actually being in contact with it. In geological point of view, remote sensing refers to observing Earth's water or land surfaces by measuring reflected or emitted electromagnetic radiation. There are different mechanisms generating electromagnetic radiation such as decay of radioactive materials, acceleration of electrical charges, thermal movement of molecules or atoms. The sun is a major source and can produce full spectrum of electromagnetic radiation (Figure 2).

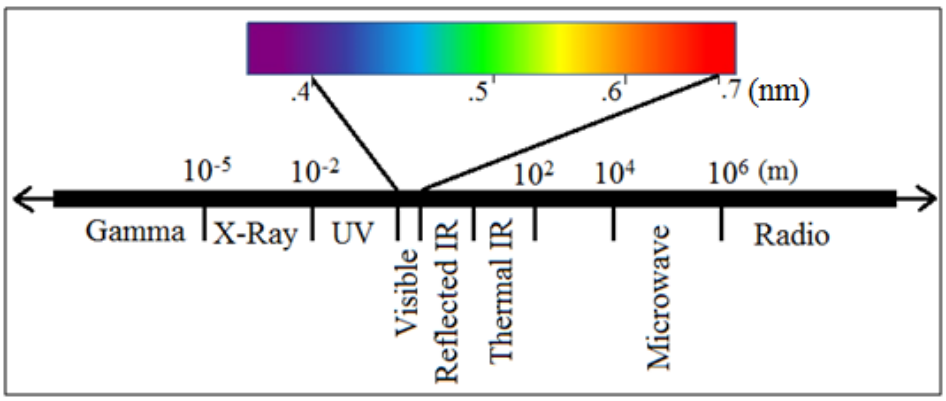

Figure 2: The electromagnetic spectrum and its segments with corresponding wavelengths (The Electromagnetic Spectrum, 2013)

Every material interacts with electromagnetic radiation in different amounts depending on chemical, physical properties of the material and the wavelength of the incident radiant energy. The unique response of different materials was named as *spectral signature* of materials (Parker and Wolff, 1965). Spectral signature curves of water, soil and vegetation is provided in Figure 3.

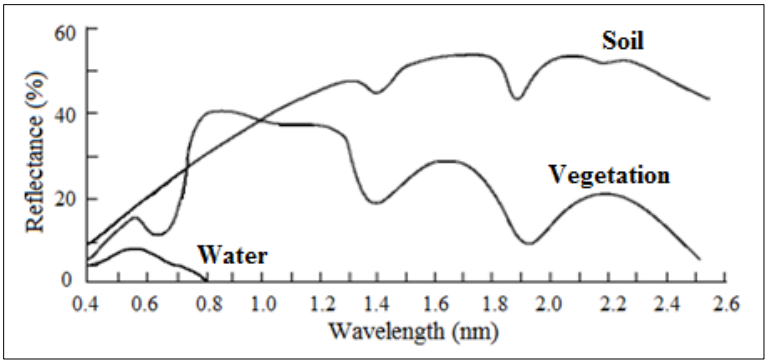

Figure 3: Electromagnetic spectral signature curves of major land cover types (adapted from Richards and Jia, 1999)

Remote sensing basically depends on the interaction of electromagnetic radiance and the material. The remote sensing process is summarized in Figure 4. The electromagnetic radiation is emitted from a source and interacts with ground surface features. After the interaction, energy is transmitted to a remote sensor. The data output can be obtained from the satellites.

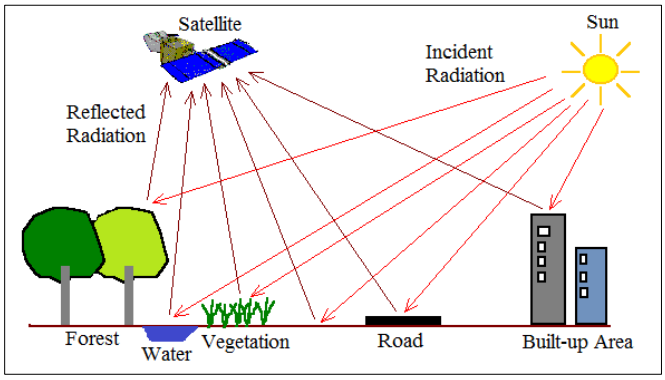

Figure 4: Generalized remote sensing process

If a sensor can provide its own energy it is said to be an active sensor and if it relies on another source such as Sun, the sensor is said to be a passive sensor (Campbell and Wynne, 2011). Landsat satellites are one of the most commonly used examples of passive sensors.

Thematic mapper sensor is a multispectral scanning, Earth resource sensor developed after MSS aimed to reach a higher resolution (Landsat Missions, 2016). Landsat 4 and 5 have thematic mapper (TM) sensor. The thematic mapper has a spatial resolution of 30m (120m for thermal band) and a temporal resolution of 16 days. Landsat 4 was operative between years 1982-2001. Landsat 5 was launched in 1984. Although it had some failures during its mission, Landsat 5 was technically operative until it was put into a disposal orbit in 2013. With a 29 year lifespan, Landsat 5 is still the longest operating Earth observation satellite. The Enhanced Thematic Mapper Plus (ETM+) has a high resolution panchromatic band in addition to bands TM sensors have. It is carried by Landsat 7 satellite. The spatial and spectral resolution properties of TM and ETM+ sensors are listed in Table 1.

Table 1: Spectral and spatial resolutions of TM and ETM+ sensors

Band	TM		ETM+	
	Spectral Resolution (nm)	Spatial Resolution (m)	Spectral Resolution (nm)	Spatial Resolution (m)
1	0.45-0.52	30	0.45-0.52	30
2	0.52-0.60	30	0.53-0.60	30
3	0.63-0.69	30	0.63-0.69	30
4	0.76-0.90	30	0.77-0.90	30
5	1.55-1.75	30	1.55-1.75	30
6	10.40-12.50	120	10.40-12.50	60
7	2.08-2.35	30	2.09-2.35	30
8			0.52-0.90	15

2.1.2. Indices Used in Water Body Mapping

Water body mapping is one of the major practices of remote sensing. Over time, differences on the target area required development of new methods to delineate water area.

Normalized Difference Vegetation Index (NDVI) is one of the most widely used indices in remote sensing applications (Equation 1). This index was proposed by Kriegler et al. (1969) to differentiate vegetation from the surroundings. The assumption behind development of this index is that water stress in healthy vegetation has a considerably higher reflectivity in the visible part of the spectrum when compared to near-infrared part.

$$NDVI = (NIR - Red) / (NIR + Red) \quad (1)$$

Although NDVI was developed to target vegetation, it also showed a success in delineating water bodies. Rokni et al. (2014) compared different indices including NDVI in mapping the extent of Lake Urmia. In the study, the overall accuracy of NDVI was calculated as 99.06 % and 98.91 % for years 2000 and 2010, respectively.

The Tasseled Cap was proposed by Kauth and Thomas (1976) as a graphical description to differentiate many agricultural crops captured by Landsat 4 MSS satellite. This graphical expression was developed by defining a new coordinate system including soil line and vegetation. After Landsat 4 satellite started to carry TM sensor, The Tasseled Cap was modified into the TM Tasseled Cap by Christ and Cicone (1984). In the study wetness axis was added to brightness, greenness, yellowness and non-such axes. Brightness axis shows the background reflectance variations of soil, greenness is the level of green vegetation variations, yellowness stands for the yellowing of vegetation by getting older, non-such axis is the perpendicular projection of an axis onto other axes and treated as a random noise resulted from atmospheric conditions. For Landsat TM the coefficients of Tasseled Cap Functions were calculated and Tasseled Cap Wetness (TCW) equation is given in Equation 2.

$$TCW = 0.1446\,TM1 + 0.1761\,TM2 + 0.3322\,TM3 + 0.3396\,TM4 - 0.6210\,TM5 - 0.4186\,TM7 \quad (2)$$

Normalized Difference Water Index (NDWI) was proposed by McFeeters (1996). The index was developed to detect water content changes and uses green and near infrared parts of the spectrum (Equation 3). McFeeters set the threshold to zero between water and non-water areas. In the study, positive NDWI values were interpreted as water while negative values were interpreted as non-water areas.

$$NDWI = (Green - NIR) / (Green + NIR) \quad (3)$$

Gao (1996) developed another Normalized Difference Water Index (NDWI) to detect liquid water in vegetation (Equation 4). This index was proposed as a complimentary index to NDVI rather than a substitute for it. Both channels used in this index are located in near infrared part of the spectrum where the reflectance of vegetation canopies is high.

$$NDWI = (NIR - SWIR) / (NIR + SWIR) \quad (4)$$

Xu (2006) found some drawbacks in the NDWI proposed by McFeeters. The positive values in NDWI were supposed to delineate water bodies but built-up features could be misinterpreted as water. Xu modified the NDWI by replacing the near infrared component with shortwave infrared and proposed Modified Normalized Difference Water Index (MNDWI). MNDWI is given by:

$$MNDWI = (Green - SWIR) / (Green + SWIR) \quad (5)$$

Rogers and Kearney (2004) used NDWI in another form:

$$NDWI = (TM3 - TM5) / (TM3 + TM5) \quad (6)$$

The aim of the study was to differentiate three main targets of remote sensing; vegetation, soil and water. The authors concluded that using red and shortwave infrared bands (3^{rd} and 5^{th} bands of Landsat 5 TM) instead of green-near infrared or

near infrared- shortwave infrared bands resulted in a maximum separation between soil, water and vegetation classes. Feyisa et al. (2014) called attention to accuracy problems in water extraction indices. In this study, Automated Water Extraction Index (AWEI) was proposed using Landsat 5 TM images. This index was devised so that it can improve accuracy in water extraction constantly when there exists noise resulted from the environment and it can offer a stable threshold between water and its surroundings. The accuracy of AWEI was compared with Modified Normalized Difference Water Index and Maximum Likelihood classifiers and it was concluded that the proposed method had a significantly higher accuracy in four out of five study sites. $AWEI_{nsh}$ (Equation 7) was developed so that it can also separate dark, built-up areas from water. Moreover, it was formulated so that the coefficients force non-water areas to negative values and water areas to positive values at the same time. $AWEI_{sh}$ (Eqution 8), on the other hand, was proposed as a further improvement of $AWEI_{nsh}$ in a case that shadow is effective in the target area.

$$AWEI_{nsh} = 4 \times (TM2 - TM5) - (0.25 \times TM4 + 2.75 \times TM7) \quad (7)$$

$$AWEI_{sh} = TM1 + 2.5 \times TM2 - 1.5 \times (TM4 + TM5) - 0.25 \times TM7 \quad (8)$$

2.2. Characterization of the Study Area

2.2.1. Description of the Study Area

Lake Tuz is located in Konya Closed Basin in Central Anatolia. In terms of surface area, Lake Tuz is the second largest lake of Turkey but it is the shallowest one. It is located approximately 905m above the sea level. Its maximum dimensions are 80km in N-S direction and 60km in E-W direction. The physiography of the study area is shown in Figure 5.

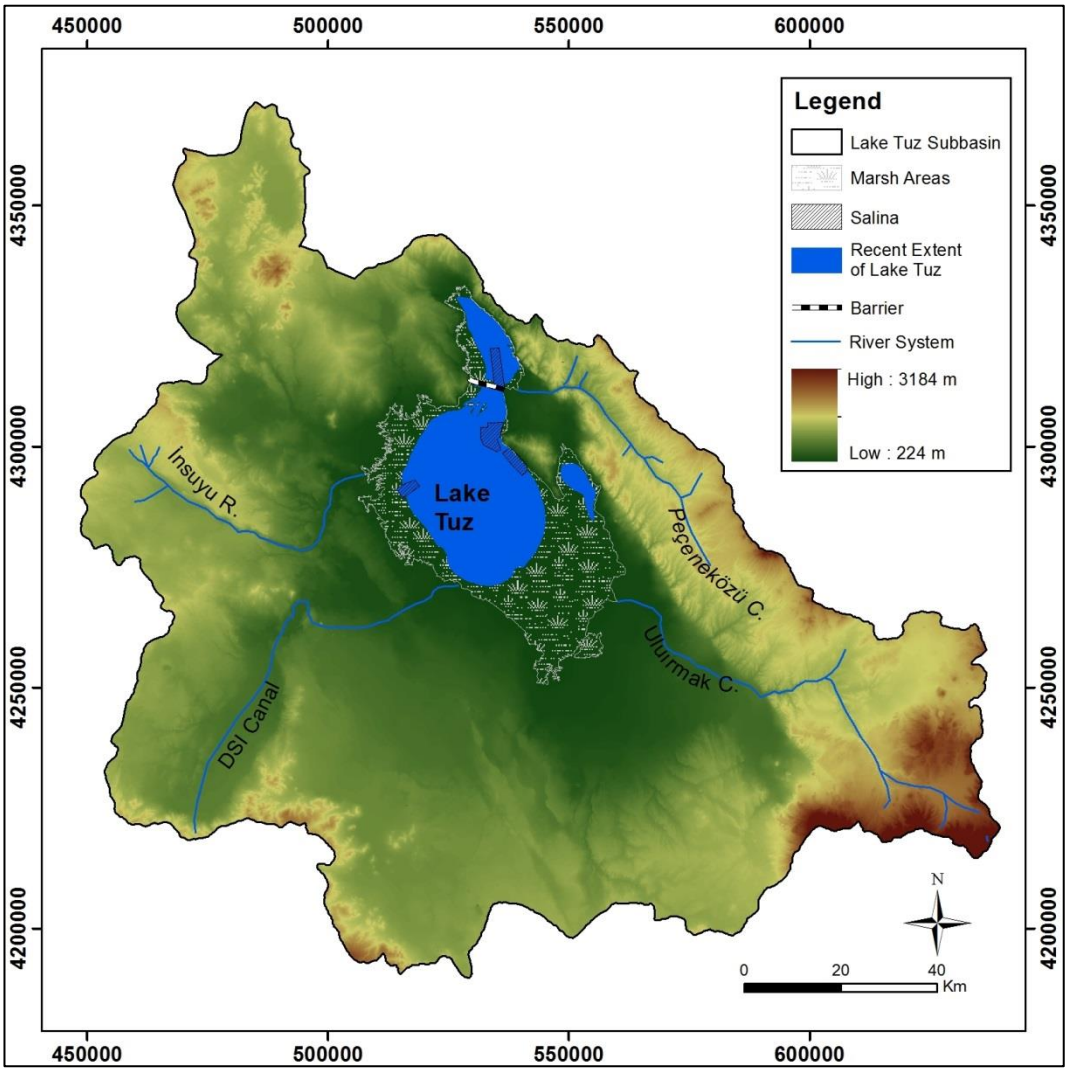

Figure 5: Physiography of the study area

Because of the high salinity vegetation is not present in Lake Tuz. But it forms a perfect wintering ground for a lot of aquatic bird species. Flamingos, avocets, ruddy shelducks can live in groups around Lake Tuz because they can find food and swim in Lake Tuz even in winter because the lake never freezes. The islands and swamps that form in the lake in spring are very suitable places for incubation of collared pratincoles, ruddy sheldrake and some seagull species (Ministry of Environment and Urbanization, 2014).

There is not any stream discharging out from the lake. Only a few streams discharge into Lake Tuz. Around Şereflikoçhisar Peçeneközü Creek, around Aksaray

Uluırmak Creek, and from the west Insuyu River discharges into Lake Tuz. Moreover, DSI constructed a 150km long canal discharging to the southern part of the lake in 1974 to dewater Çumra Plain for agricultural purposes. The canal also discharges overflow and waste water of Konya. Construction of ponds and reshaping of the river channels increased the aridity around the lake and reduced the area of marshes (Çınar Mühendislik, 2010). DSI constructed Şereflikoçhisar (Peçenek) Dam on Peçenek Creek in 2011 to supply potable water. The volume of the dam is 2840 dam^3. Mamasın Dam is located on Uluırmak Creek in Aksaray. The dam was constructed in 1962 for irrigation and supplying potable water and has volume of 400 dam^3. In the western part of the lake, Cihanbeyli Dam is located on İnsuyu River. It is constructed in 1989 for irrigation purpose and has volume of 619 dam^3 (Baraj Arama, 2014).

Çamur and Mutlu (1995) noted that ion concentrations change from high to low as; Cl, Na, SO_4, Mg, K, Ca and HCO_3. These ion concentrations make Lake Tuz NaCl type brine. The concentration of the main ions, Na and Cl, are almost constant throughout a year. The salinity of the lake is approximately 30% and the salt demand of Turkey is mainly supplied by Kayacık, Yavşan and Kaldırım Salinas. Every year, approximately 10cm of salt crust forms due to evaporation of the lake water.

With decreasing salt production DSI constructed a soil barrier on the lake in early 1990s. This barrier is located in E-W direction in the northern part of the lake. The main role of the barrier is to block water migration resulted from elevation differences and meteorological effects. The barrier also serves as a wall of a salina. Moreover, the barrier provides an easy transportation across the lake, to the inner parts of the lake and pools of the salina.

With its unique properties, Lake Tuz became a specially protected environment area in 2000. Also, Lake Tuz is being used for absolute radiometric calibration test site for accurate radiometric calibration coefficients for remote sensing sensors (Gürol et al. 2010).

2.2.2. Climate

The climate of Lake Tuz Subbasin is continental. Basically, the winters are cold and wet, summers are hot and dry. Four meteorological stations operated by General Directorate of Meteorology in Lake Tuz Subbasin have been included in this study. The locations of these stations are provided in Figure 6. The meteorological stations are located in Kulu, Cihanbeyli, Şereflikoçhisar and Aksaray. All of these stations are currently active. General information about the stations is summarized in Table 2.

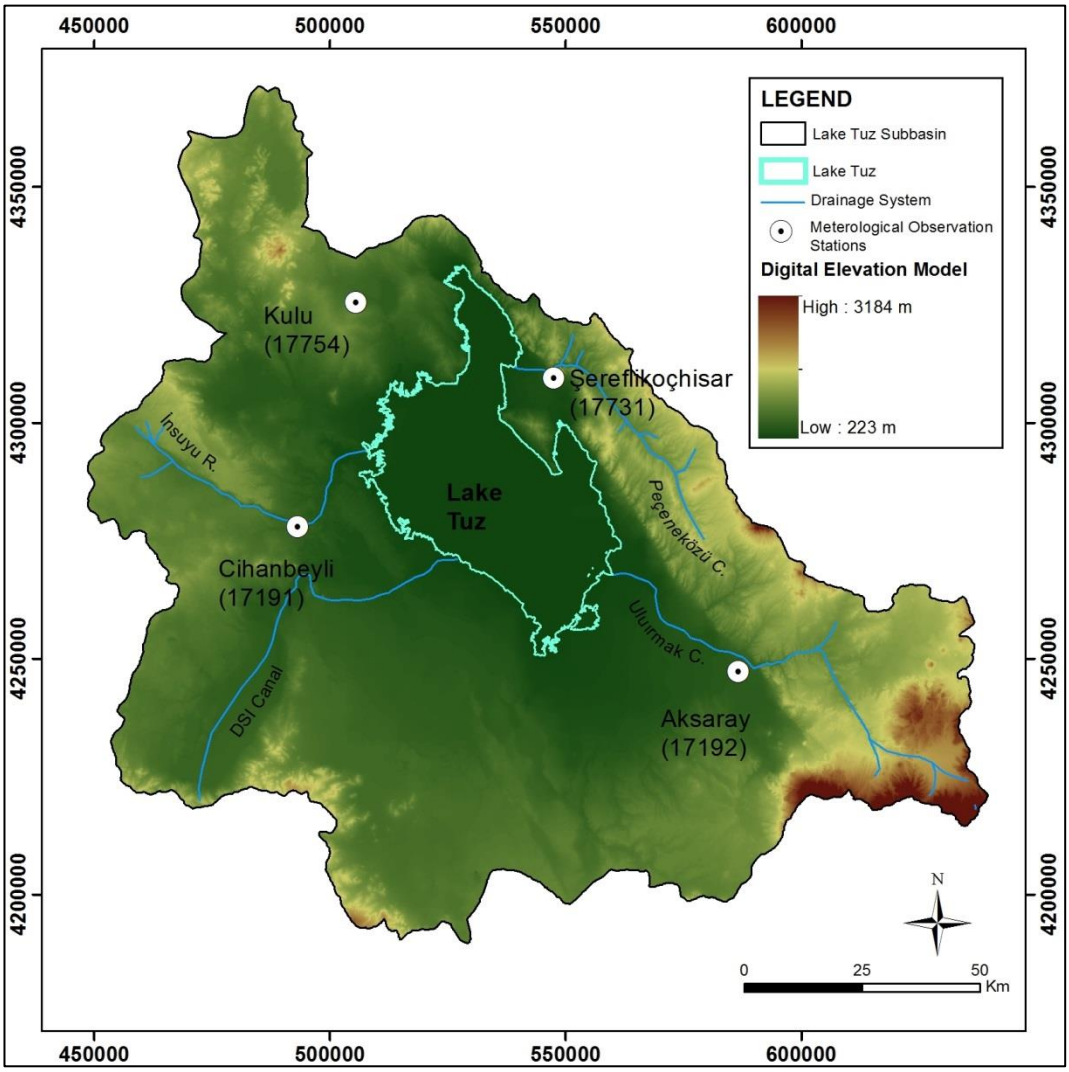

Figure 6: Digital elevation model of Lake Tuz Subbasin and meteorological stations

Table 2: Detailed information about the meteorological stations

Station Name	Coordinates (UTM)		Elevation (m)	Operation Period	Operating Institution
	Easting	Northing			
Aksaray	586668	4247174	960	1938-2015	MGM
Cihanbeyli	493253	4277952	969	1950-2015	MGM
Kulu	505669	4325496	1010	1955-2015	MGM
Şereflikoçhisar	547668	4309520	969	1929-1930, 1951-1995, 2003-2015	MGM

As shown in Figure 6, Şereflikoçhisar Station is the closest station to Lake Tuz. However, due to significant data gaps (Table 2) Şereflikoçhisar Station was excluded from the analysis.

Monthly average precipitation values of Aksaray, Cihanbeyli and Kulu stations during 1970-2015 are shown in Figure 7.

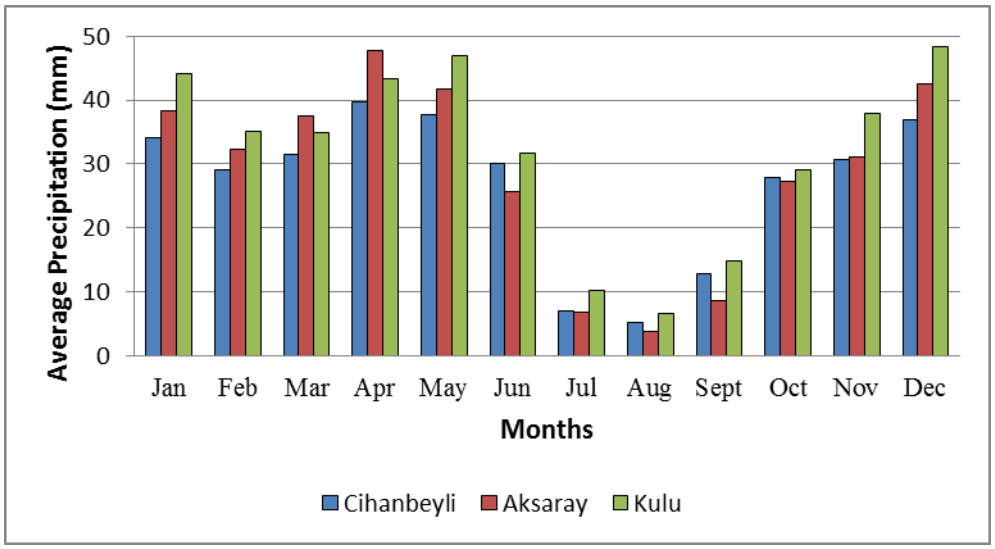

Figure 7 : Montly Average Precipitation (1970-2015)

In general, Kulu station received more precipitation than other stations. In July, August and September, the study area is subjected to significantly less precipitation when compared to other months. The minimum monthly average precipitation was observed in Aksaray station as 3.7mm in August and the maximum was in Kulu

Station as 48.4mm in December. For Aksaray, Cihanbeyli and Kulu stations, precipitation histograms and cumulative deviation from mean annual rainfall graphs were constructed for 1971-2015 water year period (Figure 8).

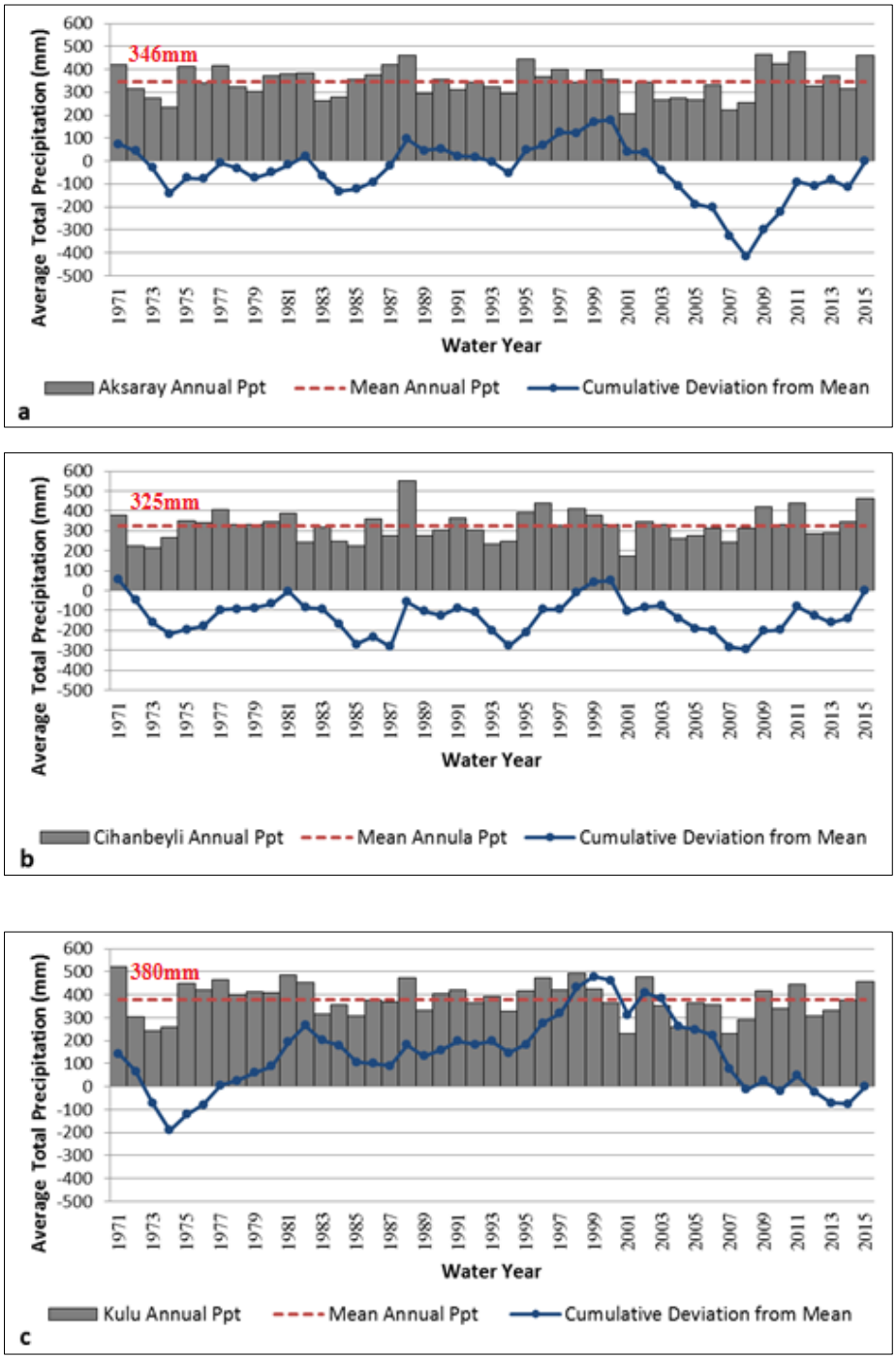

Figure 8: Precipitation histograms and cumulative deviation from mean annual rainfall for a) Aksaray b) Cihanbeyli c) Kulu stations

In Aksaray Meteorological station, the average annual precipitation is 346mm. The minimum annual precipitation was recorded in 2001 as 207mm and the maximum was recorded in 2011 as 447mm. In Cihanbeyli Meteorological Station, the average annual precipitation is 325mm. The minimum annual precipitation was recorded in 2001 as 171mm and the maximum was recorded in 1988 as 550mm. In Kulu Meteorological Station, the average annual precipitation is 380mm. The minimum annual precipitation was recorded in 2001 as 230mm and the maximum was recorded in 1971 as 523mm. In all stations the driest year in record is 2001.

According to all the data obtained from three meteorological stations wet and dry periods were determined. In all stations dry/wet periods are similar where 1971-1974 is dry, 1974-1981 is wet, 1981-1985 is dry, 1985-1988 is wet, 1988-1994 is dry (stable/slightly wet for Kulu Station), 1994-2000 is wet, 2000-2008 is dry, 2008-2011 is wet and 2011-2014 is dry (stable for Aksaray Station) periods. In 2015 high precipitation rates were observed in all stations.

Average monthly temperature values are provided in Figure 9. Aksaray Meteorological Station recorded the highest temperature for all months and Kulu Meteorological Station recorded the lowest temperature values. It can be seen that lowest temperatures are observed in January and highest temperatures are observed in July.

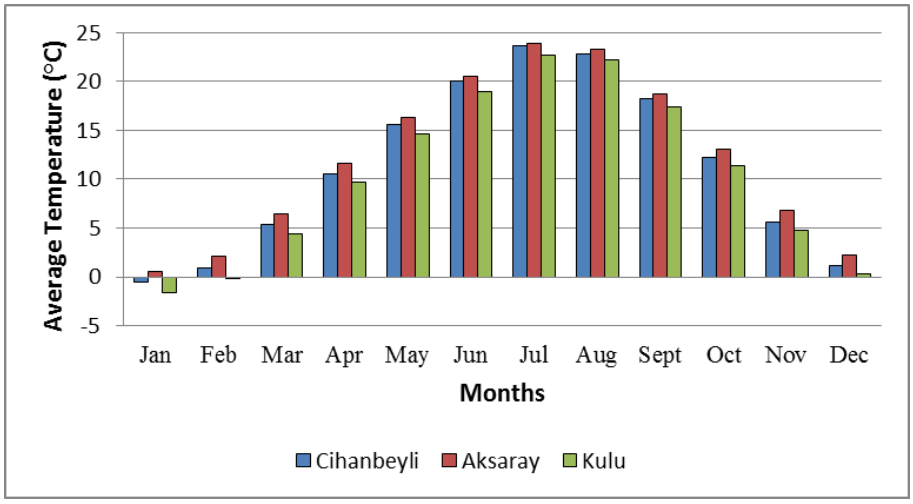

Figure 9: Monthly Average Temperature (1970-2015)

The pan evaporation data obtained from the meteorological stations is continuously available only for the period May-October. The average monthly pan evaporation data for the 1970-2015 periods is provided in Figure 10. As expected, the evaporation data shows a similar trend with the temperature data over months in both Cihanbeyli and Aksaray Stations.

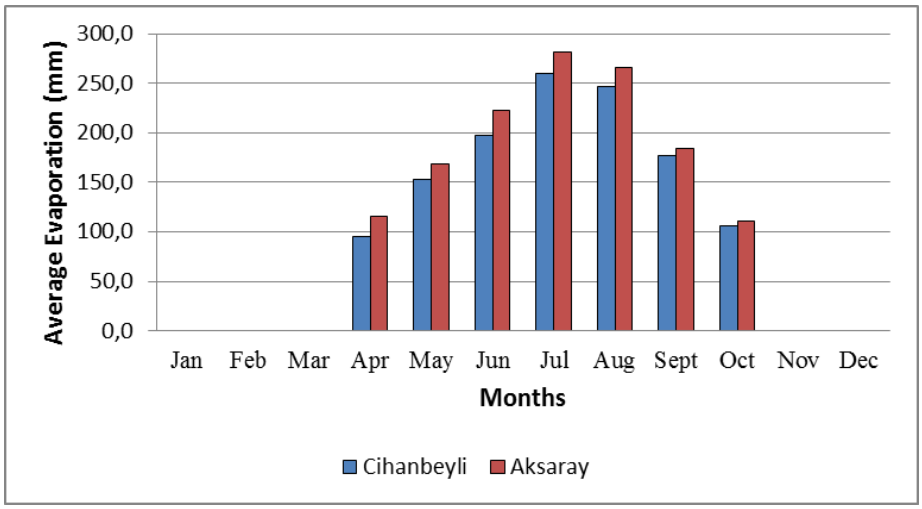

Figure 10: Monthly Average Evaporation (1970-2015)

DSI has two lake level measurement stations. One of the stations was located near the walls of Kaldırım Salina on the northern part of lake and the other station was located near the walls of Yavşan Salina located on the western part of the lake. The walls act like a barrier and the measurements may not reflect the actual lake water levels. However, the relative changes give clues about the overall balance between precipitation and evaporation. Figure 11 and Figure 12 shows the average monthly water levels observed in Kaldırım and Yavşan Salinas, respectively. According to the lake level measurement stations, the driest month of Lake Tuz is September.

In both stations, lake level increases from October to March and decreases from April to September. The maximum and minimum lake levels were measured as 121cm-91cm and 50cm-23cm for Kaldırım and Yavşan Stations, respectively. According to the measurements the maximum lake levels were measured in April while the minimum lake levels were measured in September.

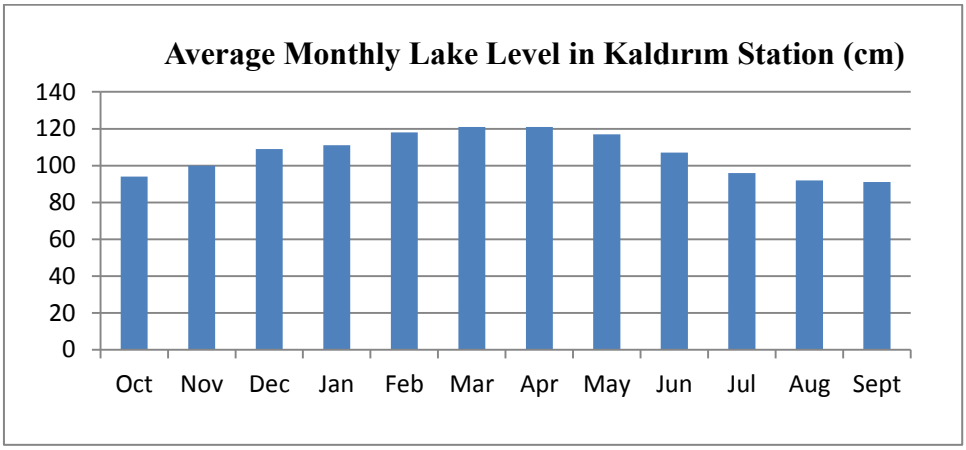

Figure 11: Average monthly lake level measurements of Kaldırım Station (1960-2014)

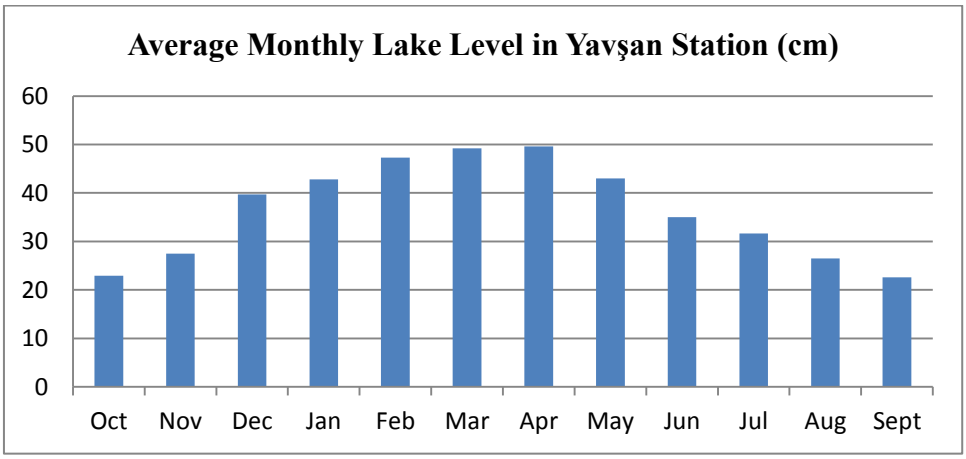

Figure 12: Average monthly lake level measurements of Yavşan Station (2002-2014)

2.2.3. Geology

The Lake Tuz Subbasin is a part of Konya Closed Basin. It is located in a structural depression. The basin is bounded by the Central Anatolian Crystalline Complex from the North and the East, Kütahya-Bolkırdağı Metamorphics from the West and the Southwest, Ulukışla Volcanics from the South and the Southeast. The geological

map of Lake Tuz Subbasin was obtained from General Directorate of Mineral Research and Exploration (MTA) in 1/25000 scale and provided in Figure 13.

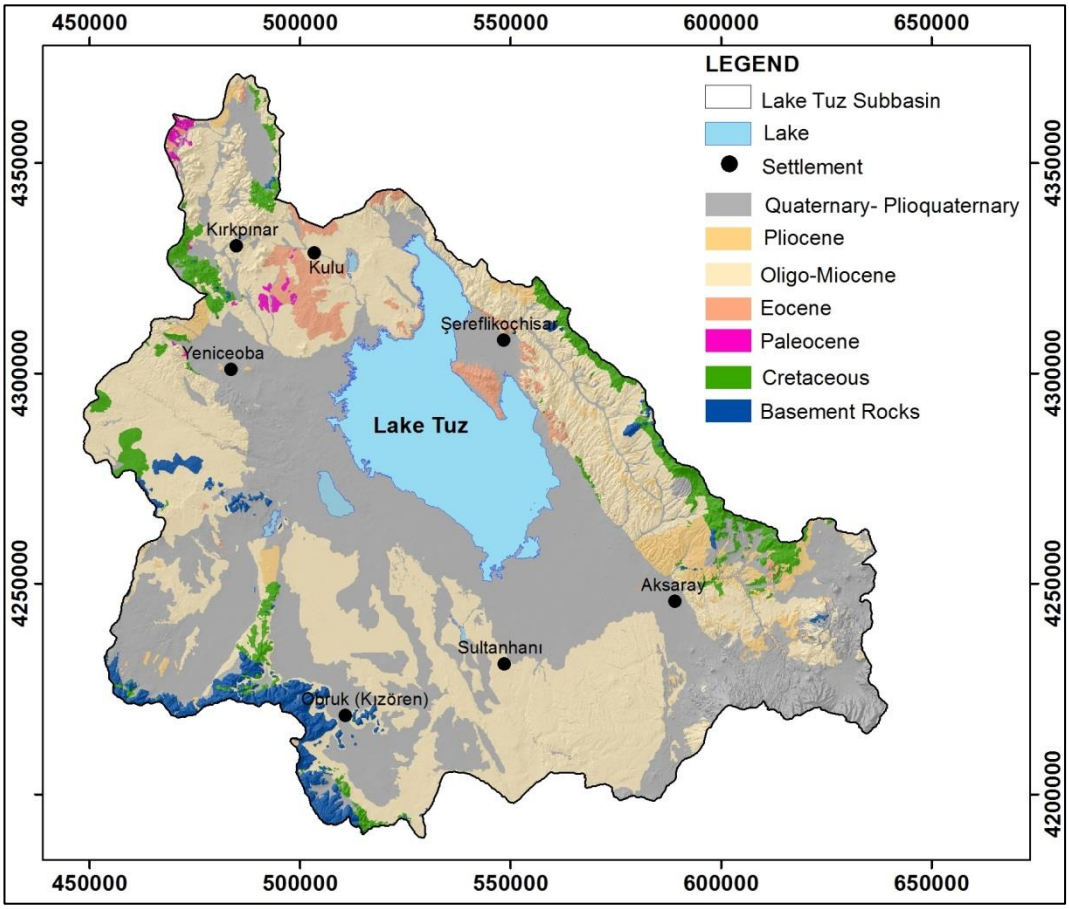

Figure 13: Geological map of Lake Tuz Subbasin (modified from MTA, 2002)

The area of the basin is approximately 15000 km^2 and it has been a sedimentary deposition area since Upper Cretaceous (Turgut, 1978). Two different basement rocks are present on the western and the eastern part of the basin. On the western part the Central Anatolian Crystalline Complex and on the eastern part the Kütahya-Bolkardağı Belt are exposed. These basement rocks can be correlated with each other in the stratigraphic columnar section because their lithology and age are similar (Göncüoğlu et al., 1992). The sedimentary succession in the basin is approximately 5000 m. On the contrary to basement rocks, the eastern and western margins of the basin are characterized by different stratigraphic successions. The

generalized columnar sections representing western and eastern parts of Lake Tuz is shown in Figure 14.

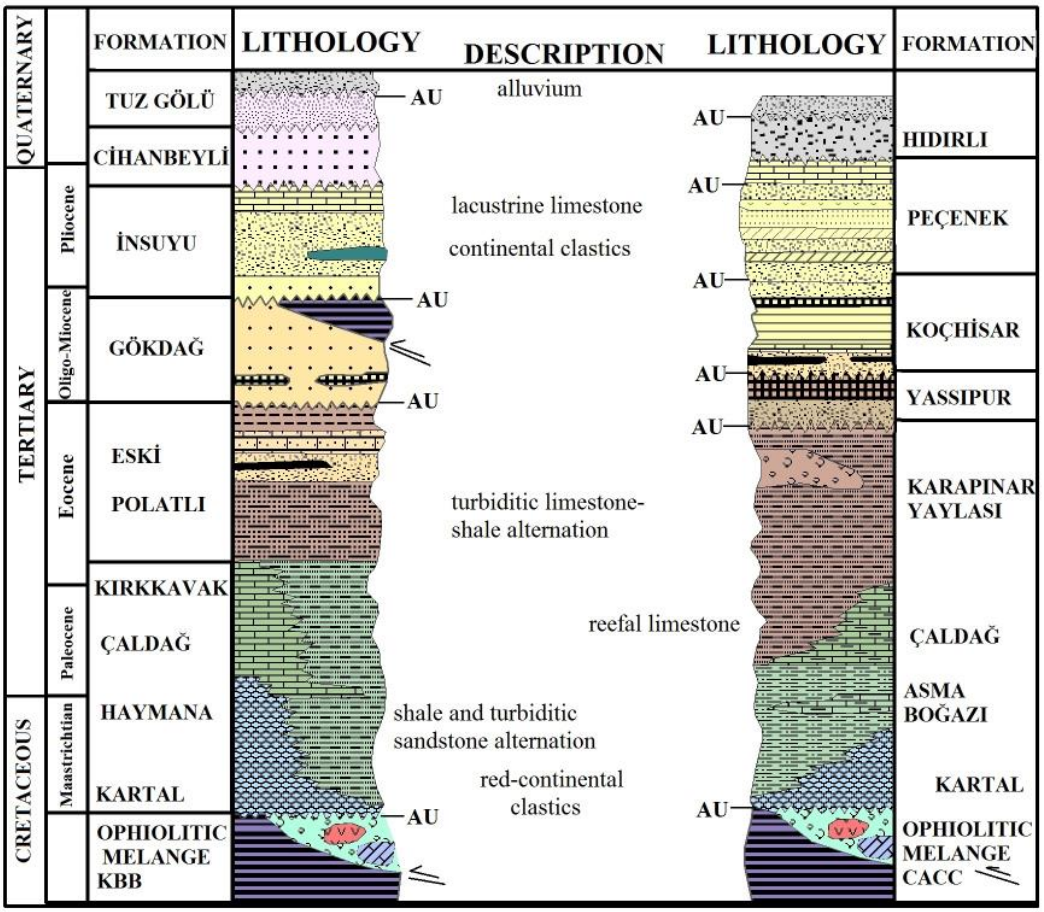

Figure 14: Generalized stratigraphic columnar section of the West (left) and the East (right) of Lake Tuz (Dirik and Erol, 2003)

The Central Anatolian Crystalline Complex was metamorphosed to a lower level than Kütahya-Bolkardağı Belt but they have similar lithologies (Türeli et al.1993). The ophiolitic mélange overlies the basement units tectonically. It mainly composed of serpentinites. Radiolaria and gabbro blocks are also present in the serpentinites. Kartal Formation overlies the basement rocks with angular unconformity. It is composed of red continental clastics such as loose conglomerate, sandstone and mudstone. Haymana Formation consists of turbiditic conglomerate, sandstone and

shale alternation. The bottom parts of Asmaboğazı Formation pass to Kartal Formation vertically and laterally. Asmaboğazı Formation contains sandy limestone, rudist bearing limestone and orbitoides bearing sandstone. Red sandstone and siltstone alternation is present in the formation. Çaldağ Formation mainly contains medium to thick bedded limestone and it is conformable with Asmaboğazı Formation. The main rock type of Kırkkavak Formation is greyish sandtone with laminated shale. Karapınar Yaylası Formation is composed of medium to thick bedded conglomerate and sandstone. Eski Polatlı Formation lies under the unconformity between Eosen and Oligo-Miosen. The lower parts of the formation are composed of turbidic sanstone. The upper parts include volcano-clastics and fossiliferous limestone. The bottom of Gökdağ Formation is not observed. It mainly composed of continental clastics, tuff and evaporates. This formation has a tectonic contact with the Ophiolitic Mélange. Yassıpur Formation is observed between two angular unconformities. The lower part is composed of continental clastics and it passes to massive evaporates in the upper parts. Koçhisar Formation is characterized by continental clastics, mainly sandstone. The sandstone beds may contain clayey limestone or coal lenses and it passes to gypsum and shale alternation through the upper parts. İnsuyu Formation (west) and Peçenek Formation (east) are generally composed continental clastics and tuffite in Pliocene age and the upper parts passes to lacustrine limestone. Cihanbeyli Formation overlies İnsuyu Formation unconformably. This formation is composed of evaporates, clay, pebbly carbonate/limestone which has limited extent. It passes to Lake Tuz Formation vertically and laterally. The unconsolidated pebble, sand, silt, clay and marl deposits in Plio-Quarternary age was named as Tuzgölü Formation. In earlier studies this formation was also included in Cihanbeyli Formation or alluvial deposits (Göncüoğlu et al., 1992; Dirik and Erol, 2003). Hıdırlı Formation is mainly characterized by alluvial fan deposits.

2.2.4. Hydrogeology

In Konya Closed Basin Revised Hydrological Investigation Report published by DSI (2009), the basin was studied in plain bases. Sultanhanı-Obruk, Altınekin and

Cihanbeyli-Yeniceoba-Kulu Plains are located in the borders of Lake Tuz Subbasin. The hydrogeological map prepared by DSI in 1/500000 scale is provided in Figure 15.

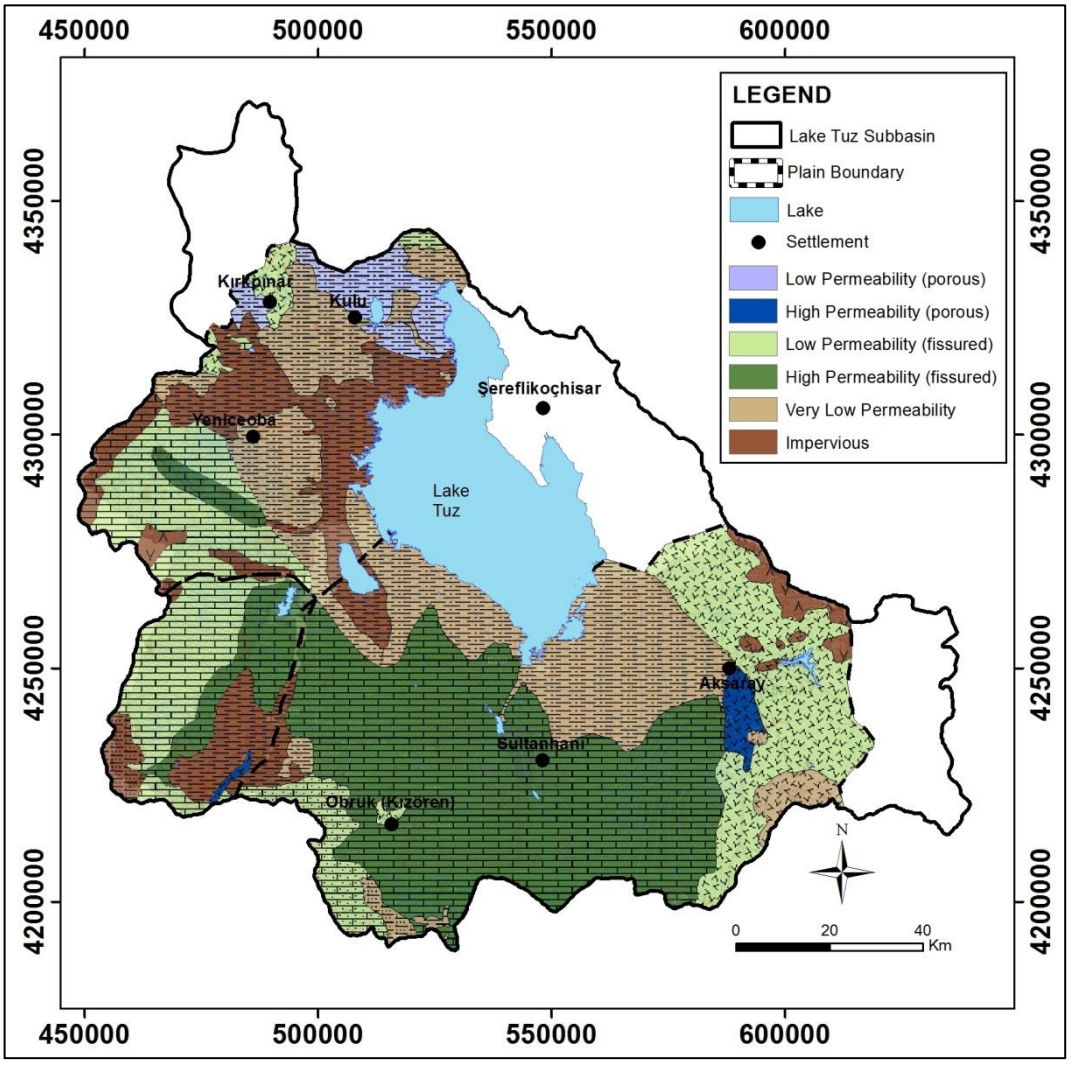

Figure 15: Hydrogeological map of Lake Tuz Subbasin (modified from DSI, 2009)

In Cihanbeyli Plain, the formation containing groundwater is the limestone units in Late Miocene age. Around Yeniceoba Plain, Pliocene aged conglomera and sand units show aquifer properties but they include silt alternations. In Kulu Plain, the units with aquifer properties are conglomerate and sand units and they cover 15km^2 around Değirmenözü Village. Altınekin Plain is located in the southwest of Lake

Tuz. The units containing marl and limestone with marl alterations have the most probability to contain groundwater. Sultanhanı and Obruks Plains are located southern part of Lake Tuz. The limestone units in Cenozoic age contain groundwater and many registered and unregistered wells are located in this unit. There exists pumping wells in the volcanic units and the alluvium. Determination of the extent and the depth of aquifers need further investigations (DSI, 2009).

The conceptual hydrogeological model of Lake Tuz Subbasin was interpreted by Bayarı et al. in 2009 as a part of Konya Closed Basin (KCB). It is an endorheic basin located in the Central Anatolia. KCB has two sub-basins. Konya Sub-Basin is located at the southern part and Lake Tuz Sub-Basin is located at the northern part of KCB. Bayarı et al. (2009) constructed a simplified geological map (Figure 16) and created a cross section demonstrating conceptual hydrogeological flow system in Konya Closed Basin (Figure 17).

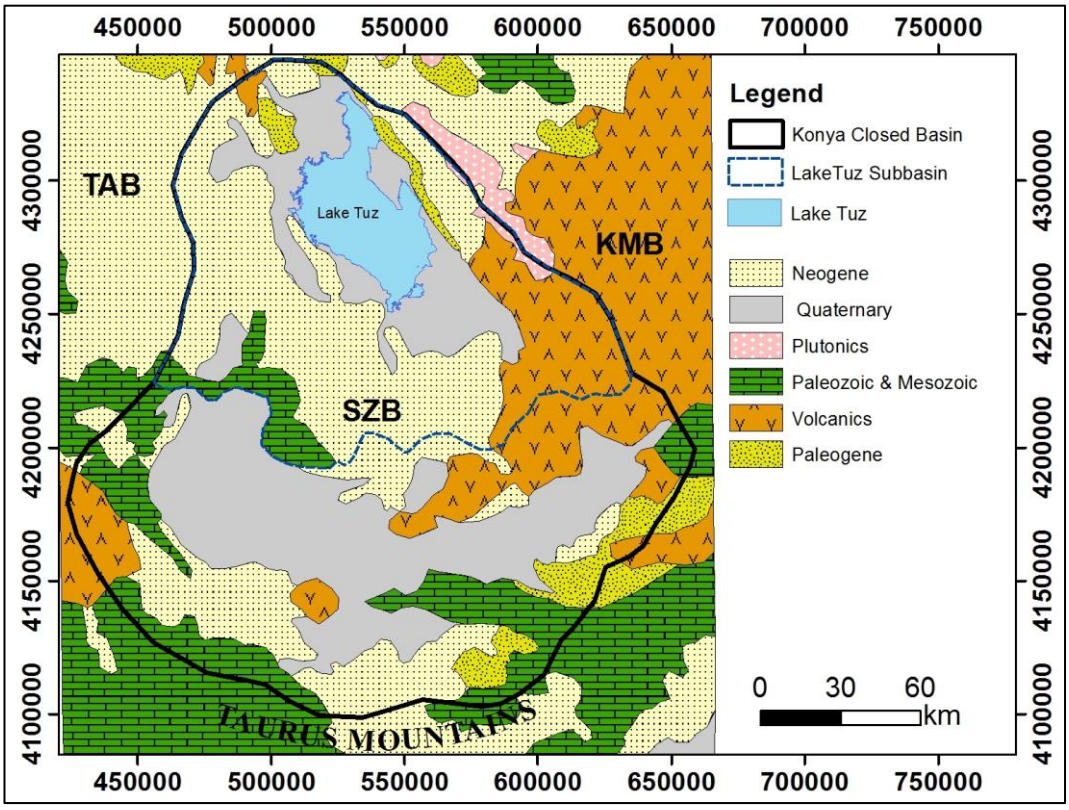

Figure 16: Simplified geological map of Konya Closed Basin (Bayarı et al., 2009)

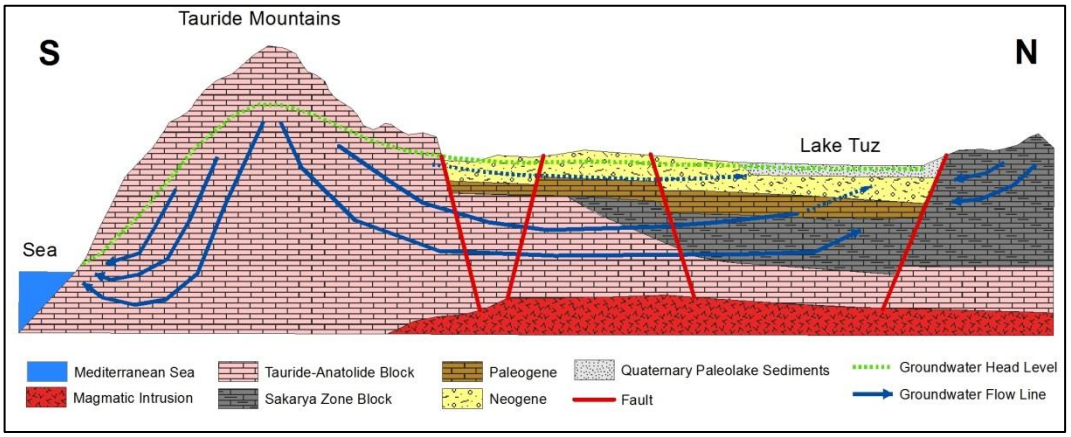

Figure 17: Conceptual hydrogeological flow system of KCB (modified from Bayarı et al., 2009)

The conceptual model is composed of three lithospheric plates; Tauride-Anatolide Block (TAB), Kırşehir Massif Block (KMB) and Sakarya Zone Block (SZB). In hydrogeological point of view; Neogene, Tauride-Anatolide Block and Sakarya Zone Block are the main aquifers in Konya Closed Basins. On the contrary, Paleogene and Quaternary paleolake sediments (QPS) represent aquitard systems. Obruks and karst systems are present in Neogene and TAB. These hydrogeological units constitute two major aquifer systems in KCB. The upper aquifer is located in the Neogene units and it is a shallow, fresh-water bearing, and productive aquifer. In the southern and the northern parts of Lake Tuz Sub-Basin, the Neogene aquifer is confined but in other parts of the KCB it is mainly unconfined. The second aquifer system is separated from the first aquifer system with a weakly permeable Paleogene rocks. This aquifer system contains saline groundwater and it is a confined, poor, deep and thermal aquifer. The deep aquifer system is mainly located in TAB. The Tauride Mountains are the highest point of Konya Closed Basin. Both aquifers in the basin are fed by the recharge from Tauride Mountains. The head in Taurides was 1100 m and it decreases down to 905 m towards Lake Tuz in the Neogene aquifer in 1970s (Bayarı et al., 2009). The study area, Lake Tuz, is a terminal lake in Konya Closed Basin.

2.2.5. Tectonic Setting

Lake Tuz Subbasin is located in a highly faulted area. There are several fault zones located in the basin. These fault zones are Yeniceoba Fault Zone (YFZ), Cihanbeyli Fault Zone (CFZ), Altınekin Fault Zone (AEFZ), Sultanhanı Fault Zone (SFZ) and Lake Tuz Fault Zone (TFZ). These major fault zones were effective during the Plio-Quaternary evolution of the basin (Özsayın et al., 2013). The locations of these major fault zones are shown in Figure 18.

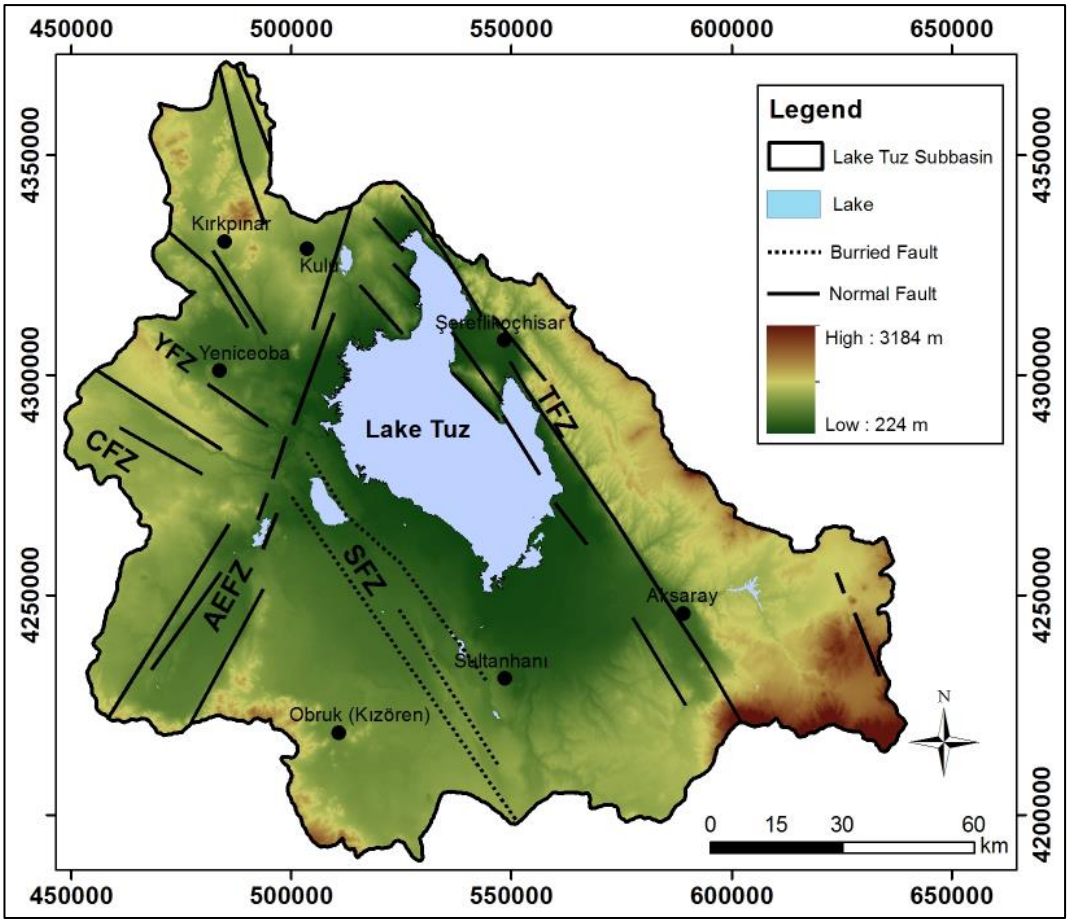

Figure 18: Digital elevation model and tectonic map of the study area (AEFZ: Altınekin Fault Zone, CFZ: Cihanbeyli Fault Zone, YZF: Yeniceoba Fault Zone, TZF: Lake Tuz Fault Zone, SFZ: Sultanhanı Fault Zone) (modified from Özsayın et al., 2013)

Yeniceoba Fault Zone is the middle part of İnönü- Eskişehir Fault Zone and exposed between Yeniceoba and Günyüzü. The length of the fault zone is 130 km. General strike of the fault zone is N50W and N60W. At some locations, YFZ juxtaposes Pliocene limestone units with bedrock units. Akıl (2008) stated that Yeniceoba Fault Zone had three stages and in the last stage YFZ has characteristics of a fault zone. Cihanbeyli Fault Zone is composed of active normal faults and is located on the southern branch of İnönü-Eskişehir Fault Zone. It is a 80km long fault zone located around Sülüklü and Cihanbeyli towns. Sultanhanı Fault Zone forms the Southeast branch of İnönü – Eskişehir Fault Zone. SFZ is composed of normal to strike-slip faults. Lake Tuz Fault Zone is one the major fault zones located in the basin. The fault planes of this zone are dipping Northeast and Southwest and have strike of 40W and N30. The eastern part of Lake Tuz is bounded by TFZ. The major fault of the zone is the Lake Tuz Fault. The fault was interpreted as a strike-slip fault with a thrust component (Şaroğlu et al., 1987), normal fault with a dextral strike-slip component (Çemen et al., 1999) and a dextral strike-slip fault with a normal component (Derman and Engin, 2007). This fault zone juxtaposes bedrock units with Pliocene limestone like Yeniceoba Fault Zone. Altınekin Fault Zone strikes in North-Northeast direction. The fault zone has a length of 100km.

2.3. Early Studies Performed in the Study Area

Lake Tuz Subbasin and Konya Closed Basin have been the target of many studies. Some of the studies are summarized below.

General Directorate of Mineral Research and Exploration (MTA) prepared the geological map of Konya Closed Basin in different scales (MTA, 2002) The hydrogeological map of Konya Closed Basin was conducted by State Hydraulic Works of Turkey (DSI) in 1/500000 scale (DSI, 2009). The hydrogeological map was conducted for each plain and except for the Konya Kapalı plain (16/8) the map has a full coverage of Konya Closed Basin.

Konya Closed Basin Revised Hydrogeological Investigation Report was published by DSI (2009). In the report, the hydrogeological maps prepared by DSI were also

provided. Because of the highly tectonic characteristics of the basin, the extents, depths and aquifer properties of the units are not specified in detail. Main aquifer system of the basin was designated as the limestone units with Cenozoic age.

Lake Tuz is a specially protected environment area since 2000 and a Water Resources Management Project was prepared by Çınar Mühendislik for the Ministry of Environment and Forestry (Çınar Mühendislik, 2010). In this report, the geology, hydrology, hydrogeology and climate characteristics were investigated in a detailed manner.

Ministry of Environment and Urbanization published Lake Tuz Specially Protected Environment Management Plan 2014-2018. The report gives detailed information about the land use, fauna and flora around Lake Tuz. The report also specifies the objectives and activity plans related to them.

Çemen et al. (1998) studied the structural evolution of Lake Tuz Subbasin. In the study a generalized geological map showing the major rock units together with the structural features were provided. In the study, the western and eastern parts of Lake Tuz Subbasin were characterized with different stratigraphic successions. The stratigraphic, sedimentological and structural evidences pointed that the evolution of Lake Tuz Subbasin was first formed during late Maastrichtian tectonism.

Bayarı et al. (2009) focused on the geological and hydrogeological characteristics of Konya Closed Basin (KCB) in association with obruk development. In this study the conceptual hydrogeological model of KCB was proposed. According to this study, mainly two aquifer systems are present in KCB. The upper aquifer system constitutes the Neogene units and contains cool fresh water. The lower aquifer system contains thermal saline water. Obruks are mainly present in Neogene carbonates of the basin. The isotope studies concluded that the obruk formation is related to the dissolution caused by the mixing between the groundwater from two aquifer systems.

Örmeci and Ekerci (2005) analyzed the water quality change using remote sensing techniques. In the study Landsat 2 MSS, Landsat 5 TM and Terra Aster 2004 scenes

were used. Iterative Self Organizing Data Analysis unsupervised classification algorithm was applied on the data and the results show that the water quality of Lake Tuz decreased significantly between 1975 and 2004.

Durduran (2009) studied the extent change of the water bodies in the Konya Closed Basin. In the study Landsat TM and ETM+ scenes were used. The images were geometrically corrected. The lake extent was interpreted by visual interpretation of geometrically corrected images. This study focuses on the changes of the water bodies in the Konya Closed Basin rather than finding the suitable method to differentiate water bodies. Same procedure was employed for all water bodies in the basin. The high albedo cover of the basin of Lake Tuz was not taken into consideration. The extent changes of each water body were shown by comparison of two images. The study concluded that the water resources of Konya Closed Basin tend to disappear.

Başçiftçi et al. (2013) used geographic information systems tools to map groundwater levels in Konya Closed Basin. Data obtained from 18 observation stations were used in the study. In most of the wells employed in the study, a significant drawdown was observed.

CHAPTER 3

DETERMINATION OF THE SUITABLE INDEX

3.1. Description of the Data

In this study, 77 Landsat images were used. The data was obtained from the website of the U.S. Geological Survey (USGS). Ten Landsat 5 TM, five Landsat 7 ETM+ SCL-on and five Landsat 7 ETM+ SLC-off scenes (total number of 20) were used in the selection of the best method (training). 18 images were employed in annual extent change analysis and 61 images were employed in seasonal extent change analysis. The full names, data acquisition dates and the purpose of the selected images are provided in Table 3 below.

In the selection process of a suitable index for extracting water extent of Lake Tuz, Landsat 5 TM and Landsat 7 ETM+ scenes were used. The major criterion employed in the selection of the scenes used in selection of the best method was that in the first visual interpretation wet, moist and dry areas are differentiable. In all training images, there exist wet, moist and dry pixels that can even be differentiated in most of the bands or in natural color images before any processing is applied.

Table 3: File names, data acquisition dates, sensor type and purpose of all scenes used in the study

Image Name	Date	Sensor Type	Purpose		
			Training	Annual	Seasonal
LT51770331984255XXX04	11.9.1984	TM		x	
LT51770331987247XXX02	4.9.1987	TM		x	
LT51770331998213XXX00	1.8.1998	TM	x		
LT51770331998229AAA02	17.8.1998	TM	x		
LT51770331998245XXX02	2.9.1998	TM	x	x	

Table 3 (Continues)

LE71770331999224EDC00	12.8.1999	ETM+ (SLC-on)	x		
LE71760331999265EDC00	22.9.1999	ETM++		x	
LE71760332000140EDC00	19.5.2000	ETM+			x
LE71770332000195EDC00	13.6.2000	ETM+ (SLC-on)	x		
LE71770332000195EDC00	13.7.2000	ETM+			x
LT51760332000228XXX04	15.8.2000	TM			x
LT51760332000260AAA02	16.9.2000	TM		x	x
LE71760332001142SGS00	11.4.2001	ETM+ (SLC-on)	x		
LE71760332001206SGS00	25.7.2001	ETM+			x
LE71770332001213EDC00	1.8.2001	ETM+			x
LE71770332001261EDC00	18.9.2001	ETM+		x	x
LT51770332002160MTI00	9.6.2002	TM			x
LT51770332002176MTI00	25.6.2002	TM	x		
LE71770332002168EDC00	17.7.2002	ETM+ (SLC-on)	x		
LE71760332002225SGS00	13.8.2002	ETM+ (SLC-on)	x		x
LT51770332003179MTI02	28.6.2003	TM	x		x
LT51770332003195MTI01	14.7.2003	TM			x
LT51770332003227MTI01	15.8.2003	TM			x
LE71770332003267ASN01	24.9.2003	ETM+		x	x
LE71760332004167ASN01	15.6.2004	ETM+			x
LE71770332004190ASN01	8.7.2004	ETM+			x
LE71770332004222ASN01	9.8.2004	ETM+			x
LE71770332004270ASN01	26.9.2004	ETM+		x	x
LE71770332005160ASN00	9.6.2005	ETM+			x
LE71770332005192ASN00	11.7.2005	ETM+			x
LE71770332005224ASN00	12.8.2005	ETM+			x
LE71770332005256ASN00	13.9.2005	ETM+		x	x
LE71760332006172ASN00	21.6.2006	ETM+			x
LE71770332006211ASN00	30.7.2006	ETM+			x
LE71770332006227ASN00	15.8.2006	ETM+			x
LE71770332006259ASN00	16.9.2006	ETM+		x	x
LT51770332007174MOR00	23.6.2007	TM			x
LT51770332007190MOR00	9.7.2007	TM			x
LT51770332007222MOR00	10.8.2007	TM			x
LT51770332007254MOR00	11.9.2007	TM		x	x
LE71760332008178ASN00	26.6.2008	ETM+			x
LE71770332008201ASN00	19.7.2008	ETM+			x

Table 3 (Continues)

LE71770332008233ASN00	20.8.2008	ETM+			x
LE71770332008249ASN00	5.9.2008	ETM+		x	x
LT51770332009163MOR00	12.6.2009	TM			x
LE71770332006211ASN00	30.6.2009	TM			x
LT51770332009211MOR00	30.7.2009	TM	x		
LT51770332009227MOR00	15.8.2009	TM	x		
LT51770332009243MOR00	31.8.2009	TM	x		x
LE71770332009267ASN00	24.9.2009	ETM+			x
LT51770332010166MOR00	15.6.2010	TM			x
LT51770332010198MOR00	17.7.2010	TM			x
LT51770332010230MOR00	18.8.2010	TM			x
LT51770332010262MOR00	19.9.2010	TM		x	x
LE71770332011161ASN01	10.6.2011	ETM+			x
LT51770332011201MOR00	20.7.2011	TM	x		x
LT51770332011233MOR00	21.8.2011	TM			x
LT51770332011249MOR00	6.9.2011	TM	x	x	x
LE71760332012157ASN00	5.6.2012	ETM+			x
LE71760332012205ASN00	23.7.2012	ETM+			x
LE71770332012228ASN00	15.8.2012	ETM+			x
LE71770332012260ASN00	16.9.2012	ETM+		x	x
LE71760332013175ASN00	24.6.2013	ETM+			x
LE71760332013191ASN00	10.7.2013	ETM+			x
LE71760332013223ASN00	11.8.2013	ETM+			x
LE71770332013246ASN00	3.9.2013	ETM+		x	x
LE71770332014169SG100	18.6.2014	ETM+			x
LE71760332014194SG100	13.7.2014	ETM+			x
LE71770332014169SG100	18.7.2014	ETM+ (SLC-off)	x		
LE71760332014226SG100	14.8.2014	ETM+			x
LE71760332014258SG100	15.9.2014	ETM+		x	x
LE71760332014322SG100	18.11.2014	ETM+ (SLC-off)	x		
LE71770332015172NSG00	21.6.2015	ETM+			x
LE71770332015188NSG00	7.7.2015	ETM+			x
LE71770332015220NSG00	8.8.2015	ETM+ (SLC-off)	x		x
LE71770332015252NSG00	9.9.2015	ETM+ (SLC-off)	x	x	x
LE71770332015252NSG00	25.9.2015	ETM+ (SLC-off)	x		

USGS offers different product types based on their processing levels. All scenes used in this study were obtained as Level 1 product type. As a general description, Level 1 products are provided as geocoded products by using parameters like resampling algorithms, projection and orientation. There are three types of level 1 product. L1G is the basic product where the area is lack of ground control points and all geocoding is applied purely from sensor data. L1Gt is geocoded and also terrain corrected by basic ortho-correction. L1T products are the most accurately corrected products of Landsat output products offered by USGS. This product is referred as terrain corrected products because it is corrected by using GCPs all over the scene and a digital elevation model. All scenes used in this study are L1T product type.

On 31 May, 2003 the scanline corrector of Landsat 7 has failed. Without scan line corrector (SCL) the line of sight of Landsat 7 follows a zig-zag pattern. The uncorrected pattern results in duplicated and gap areas. However, even in SLC-off mode Landsat 7 is still capable of capturing useful images especially in the center parts of the scenes. Landsat SLC-off images are at the same spectral quality of SLC-on mode images but the edges of scenes should be used carefully.

3.2. Pre-Processing

Pre-processing of the remotely sensed data was performed by ENVI Software version 5.1. Firstly, the data gaps in each band of Landsat 7 (SLC-off) scenes were filled by ENVI software. In the procedure, the software recalculates the missing values by using the neighboring available values around the area by Delaunay triangulation method.

Figure 19 shows the 8^{th} (panchromatic) band of Landsat 7 (SLC-off) scene captured on August 8, 2015 before and after correction.

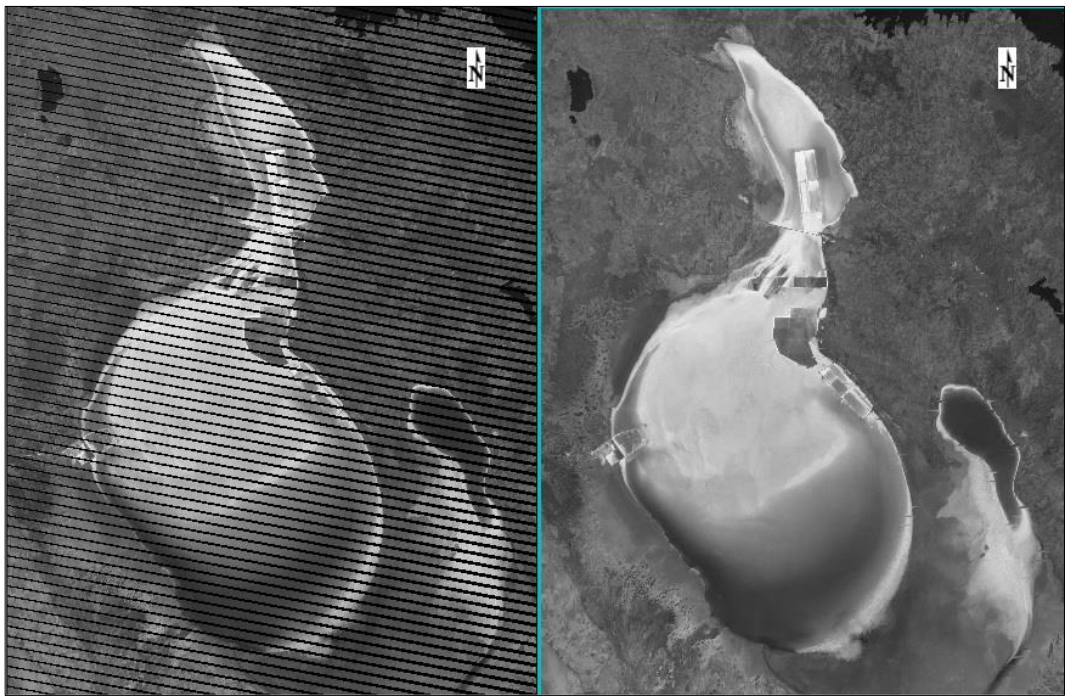

Figure 19: Landsat ETM+ (SLC-off) scene captured on August 8, 2015 before (left) and after (right) replacing the bad values

Second pre-processing applied to the Landsat data was gain and bias correction. The L1T images are composed of digital numbers (DN), not radiance or reflectance. The images have to be corrected to obtain the radiance or reflectance values. There are two methods to convert DNs to radiance. These methods are gain and bias correction and spectral radiance scaling. In the study, gain and bias correction method was employed. The equation of the correction is given in Equation 9, where L_λ is the cell value as radiance. Gain and bias values of each band were supplied by the metadata file of the scenes.

$$L_\lambda = \text{gain} \times \text{DN} + \text{bias} \quad (9)$$

3.3. Method

Each band of satellite images are provided as individual layers in L1T products and every band was pre-processed on an individual basis. After pre-processing, multi-band indices were calculated by using cell values of related bands (Figure 20).

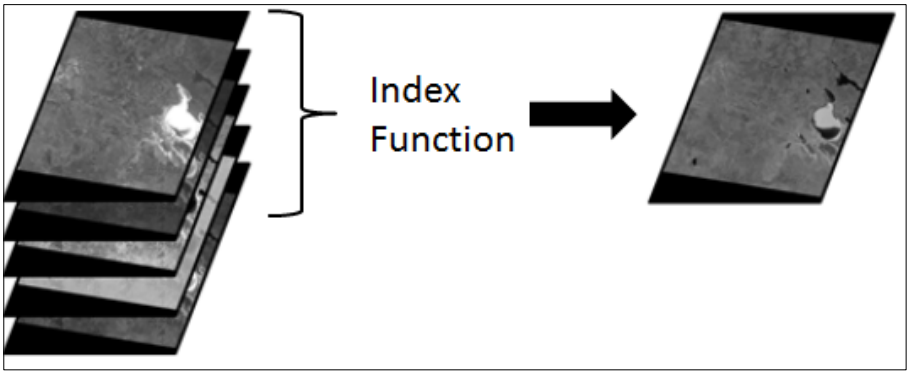

Figure 20: Illustration of multi-band index calculation

In this study five multi-band indices have been used. The indices and their equations adapted to spectral width of TM and ETM+ bands (denoted as ρ) are given in Table 4. In addition to the multi-band indices, individual bands of the imagery were also investigated.

Table 4: The selected multi-band indices and their equations

$MNDWI = (\rho2 - \rho4) / (\rho2 + \rho4)$	Xu (2006)
$NDWI = (\rho2 - \rho5) / (\rho2 + \rho5)$	McFeeters (1996)
$AWEI_{nsh} = 4 \times (\rho2 - \rho5) - (0.25 \times \rho4 + 2.75 \times \rho7)$ $AWEI_{sh} = \rho1 + 2.5 \times \rho2 - 1.5 \times (\rho4 + \rho5) - 0.25 \times \rho7$	Feyisa et al. (2014)
$TCW = 0.1446\ \rho1 + 0.1761\ \rho2 + 0.3322\ \rho3 + 0.3396\ \rho4 - 0.6210\ \rho5 - 0.4186\ \rho7$	Christ and Cicone (1984)

As expected, pre-processed single bands and the calculated indices resulted in different water extents. For the selected dates (Table 3), five dry, moist and wet control points were selected. The points were selected so that in possibly maximum number of layers the points represent the same feature such as dry, moist or wet. As an example, for 25th June, 2002 all bands, the calculated indices and selected points were given in Figure 21.

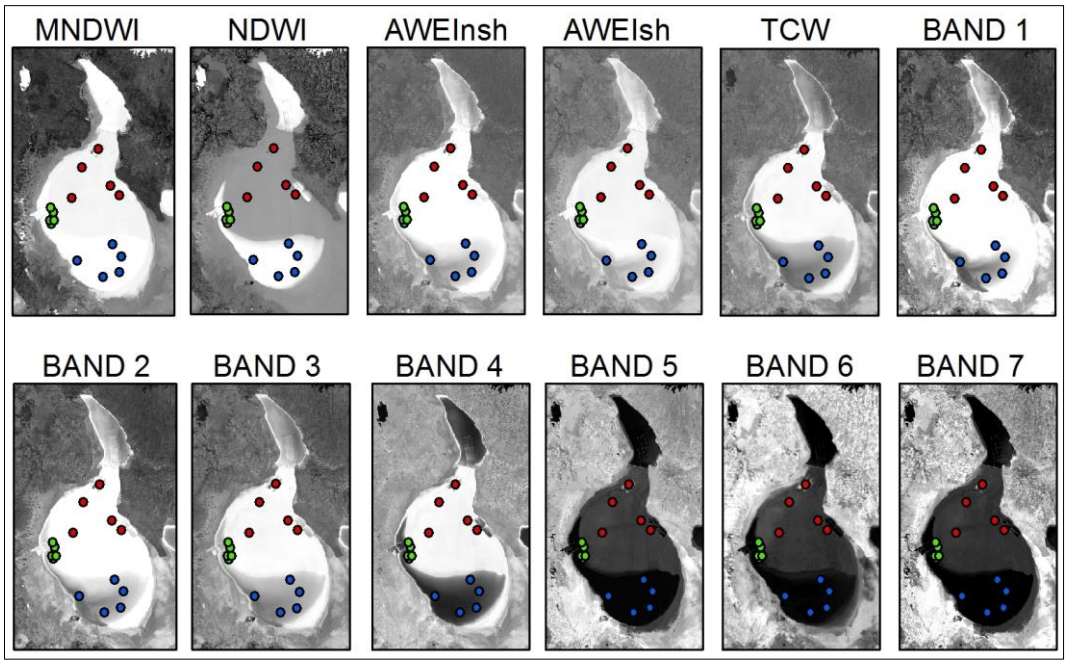

Figure 21: Selected control points on individual bands and calculated indices for 25th June, 2002 (red: dry, green: moist, blue: wet)

On the example date given in Figure 21, the wet points were located on the southern part whereas the dry points were on the northern part of the lake. The moist area was observed around the Yavşan Salina so moist control points were concentrated on the west of Lake Tuz. Other points were scattered on the lake surface. Five dry, five moist and five wet control points were selected for all Landsat TM and Landsat ETM+ scenes. The coordinates and radiance values corresponding to the selected points were recorded. The minimum, maximum, mean, range and standard deviation values were listed in Table 5 and Table 6 for Landsat TM and ETM+, respectively.

Band 6 corresponds to the thermal band of both TM and ETM+ sensors. Thermal band images provide information about the Earth surface temperature regardless of the cover type. This information cannot be used for water extent mapping hence they were excluded from the summary tables.

These summary tables (Table 5 and Table 6) show the results of the training images listed in Table 3. In these tables the minimum, maximum, mean, range and deviation values of each index and single band are provided for Landsat 5 (TM) and Landsat 7 (ETM+) separately. The suitable index/band should not have overlaps between minimum and maximum values of wet, moist and dry classes. Moreover, the mean values of classes should be as separated as possible. These values will be shown and discussed in detail in Selection of the Best Index and the Threshold section (Section3.4)

Table 5: Min, max and mean values of control points (Landsat 5 TM)

WET											
	NDWI	MNDWI	AWEInsh	AWEIsh	TCW	Band1	Band2	Band3	Band4	Band5	Band7
min	0.58	0.99	493.46	395.04	78.38	104.19	124.58	109.49	13.38	0.11	-0.02
max	0.84	1.00	921.64	695.20	156.47	193.04	234.63	201.37	60.69	0.83	0.18
mean	0.73	1.00	738.18	586.24	118.41	166.05	186.91	155.20	30.11	0.40	0.11
range	0.26	0.01	428.18	300.17	78.09	88.86	110.05	91.87	47.30	0.72	0.20
deviation	0.06	0.00	106.15	82.03	18.41	27.13	27.14	21.10	11.14	0.15	0.06
MOIST											
	NDWI	MNDWI	AWEInsh	AWEIsh	TCW	Band1	Band2	Band3	Band4	Band5	Band7
min	0.30	0.98	906.66	601.96	178.53	193.04	234.63	213.89	107.99	0.35	0.11
max	0.39	1.00	1089.12	708.54	206.99	193.04	280.97	252.52	144.78	2.75	0.77
mean	0.34	0.99	983.00	641.69	191.99	193.04	254.73	234.06	124.63	1.10	0.31
range	0.09	0.02	182.45	106.58	28.46	0.00	46.34	38.63	36.79	2.40	0.66
deviation	0.02	0.00	51.56	28.40	7.32	0.00	13.00	9.96	8.23	0.57	0.17
DRY											
	NDWI	MNDWI	AWEInsh	AWEIsh	TCW	Band1	Band2	Band3	Band4	Band5	Band7
min	0.21	0.92	714.45	477.68	163.64	192.28	194.09	190.93	126.39	4.07	0.97
max	0.27	0.97	1017.56	628.20	210.84	193.04	270.83	251.48	164.93	8.63	1.96
mean	0.25	0.95	909.41	572.23	191.83	193.03	243.52	227.30	146.81	6.02	1.42
range	0.07	0.05	303.11	150.52	47.20	0.77	76.74	60.55	38.54	4.56	0.99
deviation	0.02	0.01	78.36	37.66	12.11	0.11	19.80	16.69	9.09	0.88	0.18

Table 6: Min, max and mean values of control points (Landsat 7 ETM+)

WET												
	NDWI	MNDWI	AWEInsh	AWEIsh	TCW	Band1	Band2	Band3	Band4	Band5	Band7	Band8
min	0.61	0.98	235.12	205.74	38.94	71.75	60.15	44.98	10.26	0.26	-0.02	29.46
max	0.80	1.00	880.56	720.53	146.65	227.64	223.50	180.77	47.23	2.06	0.57	119.25
mean	0.69	0.99	555.86	447.66	93.83	133.61	141.46	124.80	25.60	0.76	0.19	76.55
range	0.19	0.02	645.45	514.79	107.71	155.89	163.35	135.79	36.97	1.79	0.59	89.79
deviation	0.04	0.01	183.41	149.79	29.34	46.65	46.44	37.06	9.10	0.41	0.12	23.99
MOIST												
	NDWI	MNDWI	AWEInsh	AWEIsh	TCW	Band1	Band2	Band3	Band4	Band5	Band7	Band8
min	0.25	0.98	320.56	237.37	66.28	90.64	83.14	75.16	39.70	0.01	0.05	57.76
max	0.38	1.00	1036.07	751.58	209.83	279.60	268.27	234.52	133.47	2.25	0.57	192.45
mean	0.32	0.99	764.28	539.78	153.93	198.34	198.43	169.16	102.23	0.83	0.21	154.68
range	0.12	0.02	715.51	514.21	143.55	188.96	185.13	159.37	93.77	2.24	0.53	134.69
deviation	0.03	0.00	187.52	134.93	38.87	49.19	48.60	47.63	24.56	0.43	0.11	37.08
DRY												
	NDWI	MNDWI	AWEInsh	AWEIsh	TCW	Band1	Band2	Band3	Band4	Band5	Band7	Band8
min	0.06	0.89	317.30	219.16	74.14	93.00	86.77	82.70	58.26	2.03	0.44	69.48
max	0.24	0.98	956.58	661.10	209.66	265.43	257.38	233.58	174.16	8.07	1.70	227.59
mean	0.17	0.94	696.80	451.50	155.58	188.85	189.11	160.89	134.16	5.74	1.15	170.10
range	0.18	0.09	639.29	441.94	135.52	172.43	170.61	150.88	115.90	6.04	1.26	158.11
deviation	0.05	0.02	149.17	99.98	32.12	37.74	39.58	36.77	30.24	1.35	0.30	41.75

3.4. Selection of the Best Index and the Threshold

The values corresponding to selected control points on individual bands and multi-band indices were analyzed to determine the best method to extract water extent. Since the bands of Landsat 5 TM and Landsat 7 ETM+ are located at almost the same spectral range (Table 1), the values corresponding to control points from these satellites were analyzed collectively in determining the best index and setting the threshold value. The results were summarized using box plots given in Figure 22-32. The horizontal axis shows the condition of the pixel. In a box-plot, the box contains horizontal lines at the 25th, 50th and 75th percentiles of the distribution and the box range represents the interquartile range (IQR). The vertical lines (whiskers) extend from each end of the box show the maximum and the minimum values of the data within the 1.5 times of the interquartile range. The mild outliers (>1.5*IQR) were represented with a circle (o) and extreme outliers (>3*IQR) were represented with an asterisk (*).

The box plot results of Modified Normalized Difference Index (MNDWI) for Landsat 5 TM (on the left) and Landsat 7 ETM+ (on the right) are shown in Figure 22. This index can differentiate dry pixels but moist and wet pixels are located at the same range. The moist and dry clusters have mild and extreme outliers. MNDWI values have a small range (0.89 -1.00) rather than being scattered between -1 and 1. Therefore, the separation between wet, moist and dry classes is imprecise.

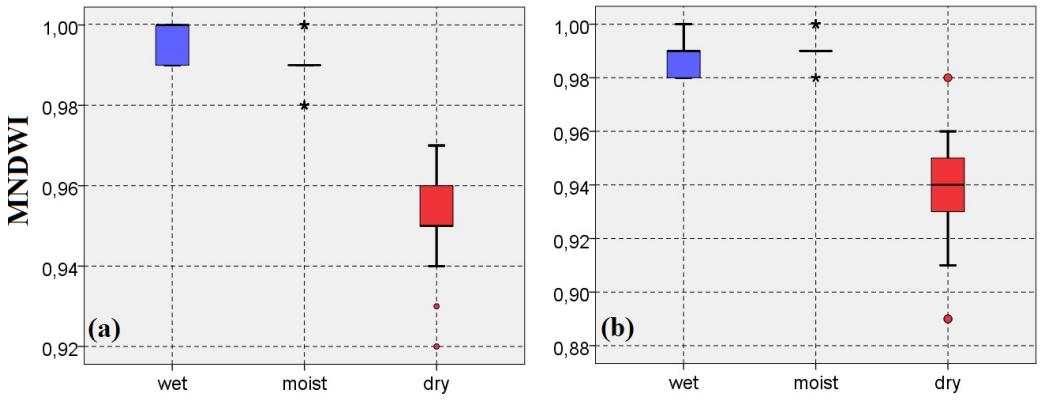

Figure 22: The box plots showing MNDWI results of the control points in (a) Landsat 5 TM and (b) Landsat 7 ETM+

The results of Normalized Difference Water Index (NDWI) are shown in Figure 23. The results of NDWI are scattered between 0.0 and 0.9 approximately. This range allows enough separation between classes. It is seen from Figure 23 that the wet class have significantly different (greater) NDWI values compared to moist and dry classes with a distinct separation. Although there is an outlier of wet class in ETM+ dataset, the differentiation of classes are not affected because the dry and moist classes have significantly lower NDWI values and the outlier has even a higher value than the wet class. Moreover, NDWI is capable of differentiating moist and dry classes. The moist class is located between 0.30 and 0.39 in Landsat 5 (TM) and between 0.25 and 0.38 in Landsat 7 (ETM+).The dry class between 0.21 and 0.27 in Landsat 5 (TM) and 0.06 and 0.24 in Landsat 7 (ETM+).

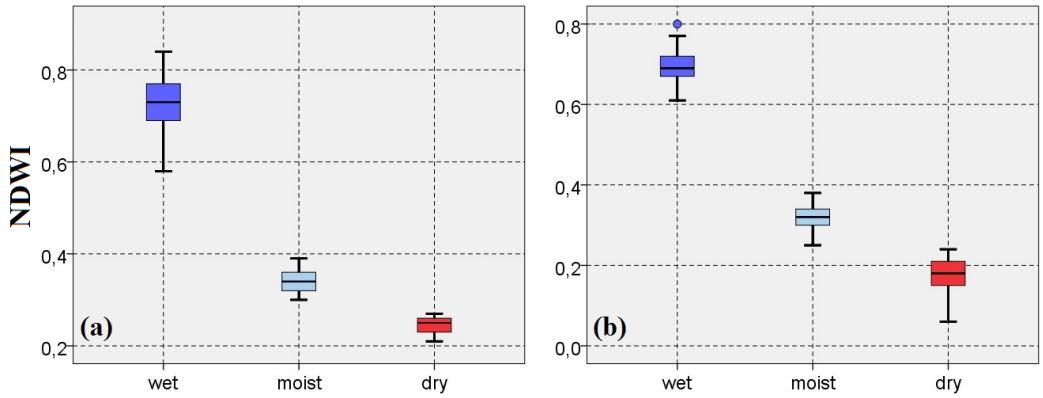

Figure 23: The box plots showing NDWI results of the control points in (a) Landsat 5 TM and (b) Landsat 7 ETM+

The results of AWEInsh are shown in Figure 24. The wet, moist and dry classes show significant overlaps. In the ETM+ dataset, the classes are located in the same range and dry class contains significant number of outliers overlapping with other classes.

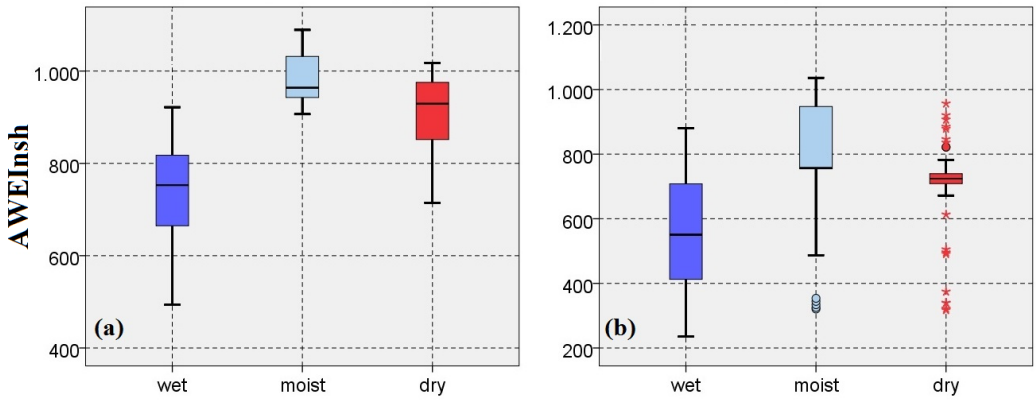

Figure 24: The box plots showing AWEInsh results of the control points in (a) Landsat 5 TM and (b) Landsat 7 ETM+

The boxplots for AWEIsh are shown in Figure 25. The wet class spans a wide range of AWEIsh values. This extent also overlaps with moist and dry classes; hence the differentiation of wet, moist and dry pixels is not possible. In the ETM+ dataset, the moist and dry classes have outliers within the range of wet class.

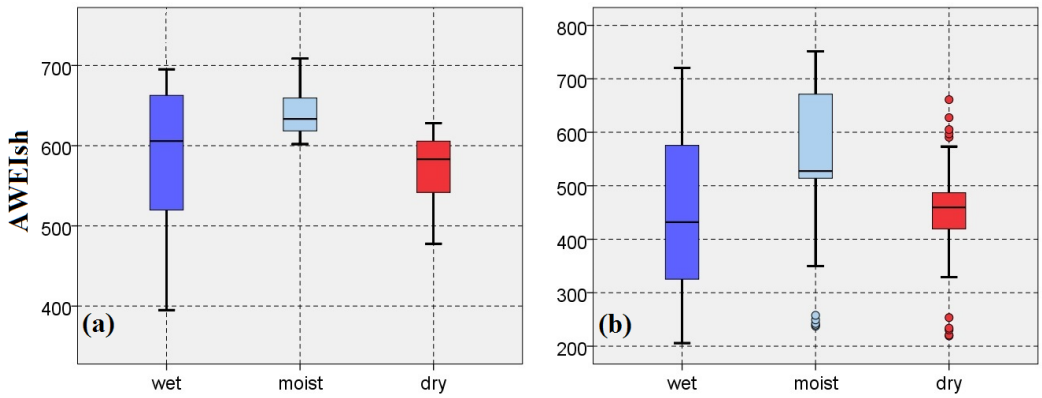

Figure 25: The box plots showing AWEIsh results of the control points in (a) Landsat 5 TM and (b) Landsat 7 ETM+

TCW results corresponding to wet, moist, dry classes are shown in Figure 26. In TM dataset, the wet class is differentiated from moist and dry class but moist and dry classes have similar ranges. In ETM+ dataset all classes have overlaps and dry class includes several outliers. The wet, moist and dry classes cannot be differentiated.

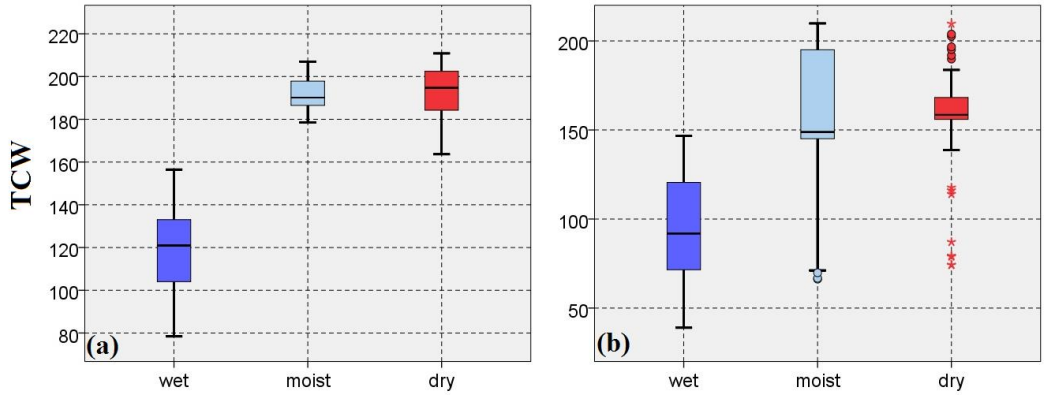

Figure 26: The box plots showing TCW results of the control points in (a) Landsat 5 TM and (b) Landsat 7 ETM+

Band-1 radiance values corresponding to wet, moist, dry classes are shown in Figure 27. In the TM dataset, wet class has a wide range while moist and dry classes are fixed to the same value. In ETM+ dataset, the classes cover a similar range. The dry class is composed of several extreme outliers and the moist class has mild outliers.

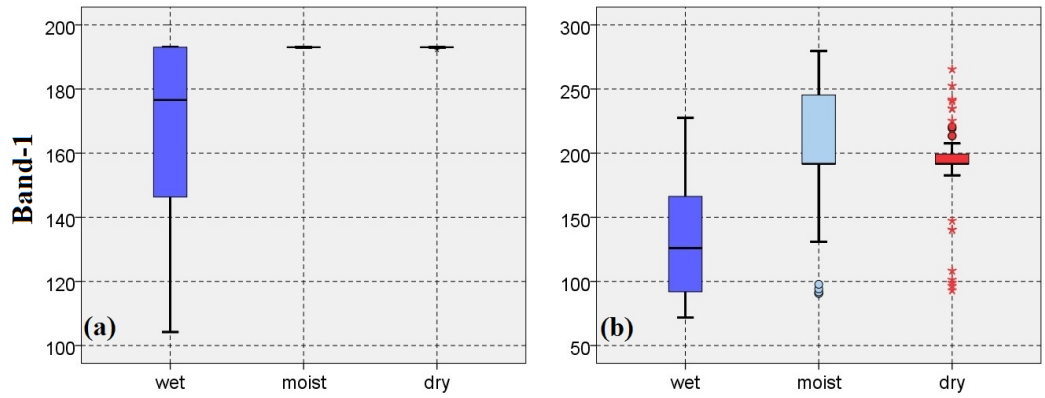

Figure 27: The box plots showing Band-1 results of the control points in (a) Landsat 5 TM and (b) Landsat 7 ETM+

The box plots of Band-2 results are shown in Figure 28. The ETM+ dataset shows a very similar pattern to ETM+ dataset of Band-1. The classes are located in almost similar range; moreover the moist and dry datasets include outliers. The TM dataset does not have outliers but there exist overlaps in all classes.

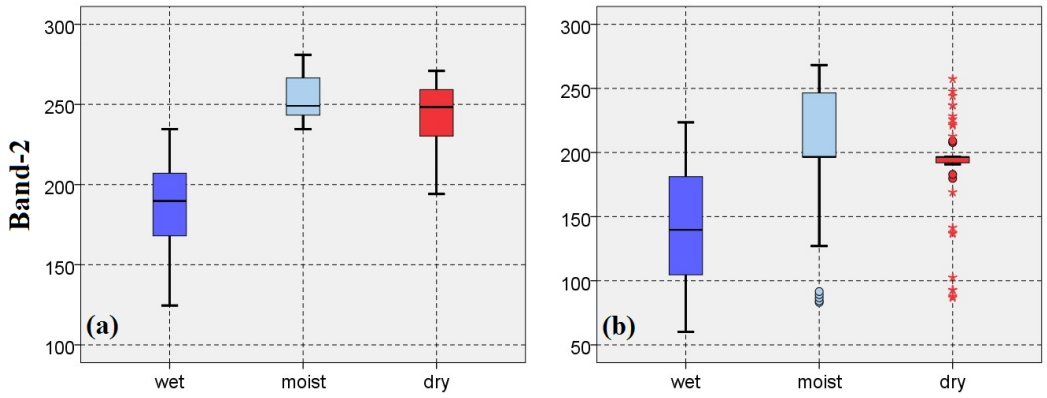

Figure 28: The box plots showing Band-2 results of the control points in (a) Landsat 5 TM and (b) Landsat 7 ETM+

The results of Band-3 are shown Figure 29. In TM dataset, wet class is differentiated from the moist but shows overlaps with the dry class. This position of classes shows an irrational alignment. Moreover, all three classes are located in a similar range in the ETM+ dataset.

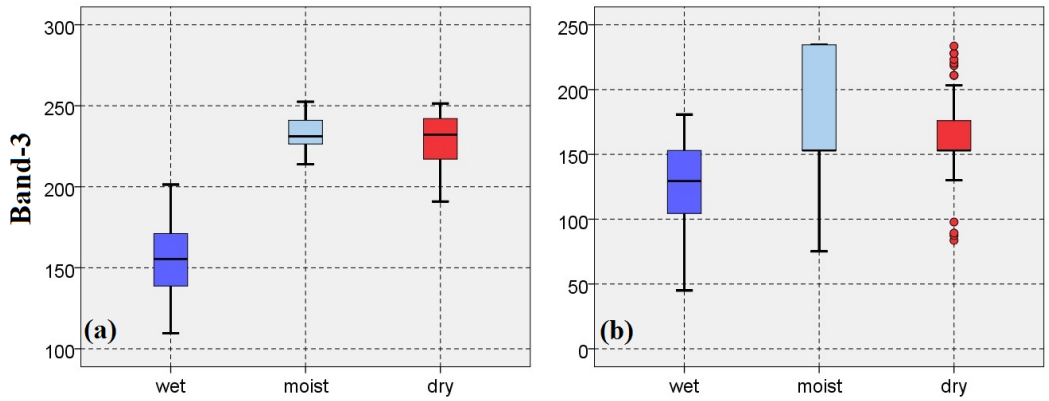

Figure 29: The box plots showing Band-3 results of the control points in (a) Landsat 5 TM and (b) Landsat 7 ETM+

The results of Band-4 are provided in Figure 30. The wet class of TM dataset is significantly differentiated from the moist and the wet class. On the contrary, the moist and dry classes share a major portion of their ranges. The wet class of ETM+ dataset is still differentiable from the dry dataset although it has some overlaps with the outliers of moist class. In both datasets, the moist and dry classes are not

differentiated from each other. When two datasets were investigated collectively, all classes contain several outlier points.

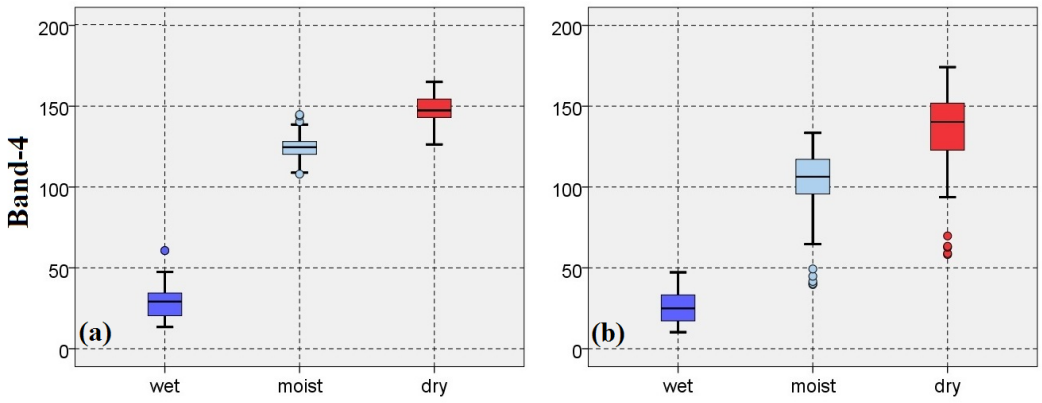

Figure 30: The box plots showing Band-4 results of the control points in (a) Landsat 5 TM and (b) Landsat 7 ETM+

Figure 31 shows the classification based on Band-5. As seen from the vertical axes of both plots, the wet and moist classes are located in a narrow and overlapping data range and that makes differentiation of classes more problematic. The dry class seems more differentiable but in ETM+ dataset it shows some overlaps with the outliers of other classes.

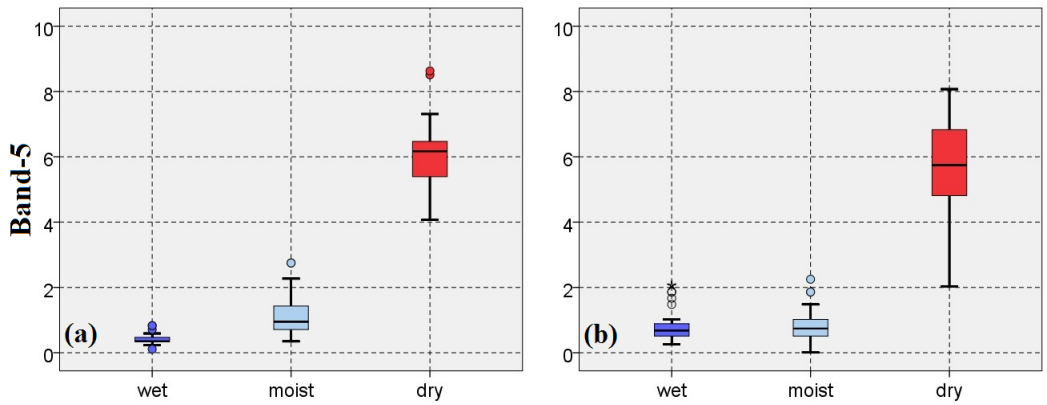

Figure 31: The box plots showing Band-5 results of the control points in (a) Landsat 5 TM and (b) Landsat 7 ETM+

The results of Band-7 are shown in Figure 32. The wet and moist classes are almost completely overlapping. In TM dataset, the dry class seems to be differentiable from other classes but its range is not quite consistent with the dry class of ETM+ dataset.

There are overlaps between the dry class and the other classes in ETM+ dataset. Moreover, all classes are located in a significantly limited range.

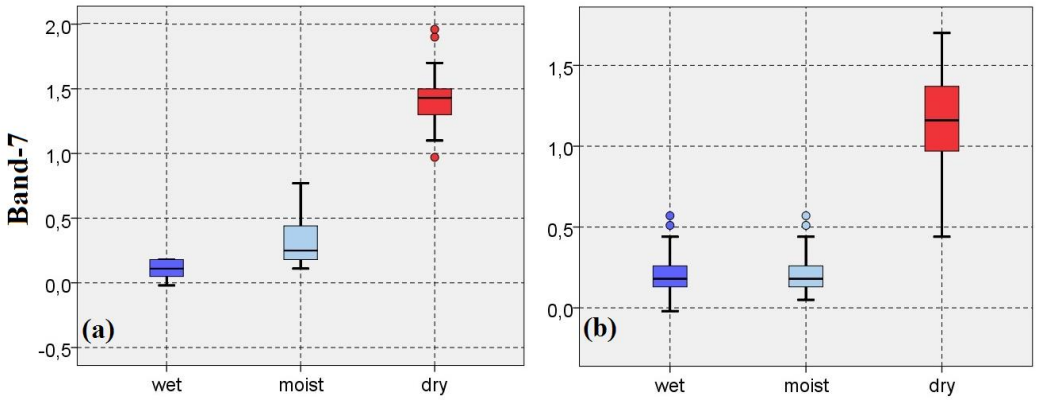

Figure 32: The box plots showing Band-7 results of the control points in (a) Landsat 5 TM and (b) Landsat 7 ETM+

The results of the last band, Band-8, are provided in Figure 33. Band 8 is the panchromatic band of ETM+ and has a spatial resolution of 15m. The wet, moist and dry classes show overlaps with each other. Moreover, the moist and wet classes have outliers corresponding to the range of wet class.

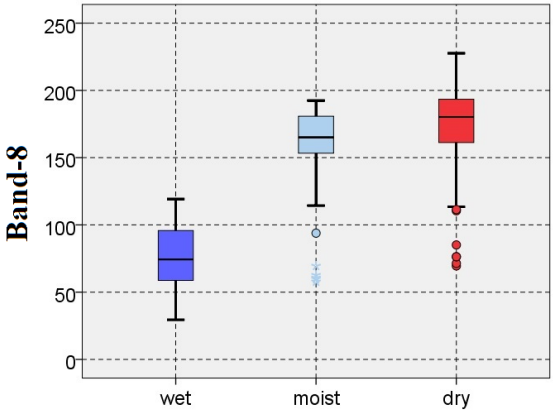

Figure 33: The box plots showing Band-8 results of the control points (Landsat 7 ETM+)

When results of all indices and single bands are compared it is clearly seen that NDWI is the best method to differentiate wet, moist and dry classes in the study area. It is clearly seen from Figure 23 that NDWI shows distinct separation between all classes without overlap. Among the investigated indices and single bands, NDWI is the only method successfully differentiating wet, moist and dry classes and hence it is selected as the water extent extraction method for Lake Tuz.

The water height in moist class designated above is negligible. Hence, in selecting the threshold values, the moist class was interpreted as dry. The minimum, maximum and mean NDWI values of wet/moist/dry classes for TM and ETM+ datasets are summarized in Table 7. The NDWI threshold between wet and dry pixels was set to 0.4 which approximately corresponds to the upper limit of the moist class. Above this threshold was interpreted as wet and below as dry.

Table 7: The summary of NDWI results

NDWI		wet	moist	dry
min	TM	0.58	0.30	0.21
	ETM+	0.61	0.25	0.06
max	TM	0.84	0.39	0.27
	ETM+	0.80	0.38	0.24
mean	TM	0.73	0.34	0.25
	ETM+	0.69	0.32	0.17

CHAPTER 4

CHANGES IN THE LAKE EXTENT

4.1. Multi-Temporal Changes

4.1.1. Seasonal Changes

Seasonal lake extent change of Lake Tuz was investigated from the wettest through the driest month. In July, August and September Lake Tuz receive the least amount of precipitation. In other months, Lake Tuz receives significantly more precipitation as discussed in Climate section (Section2.2.2) in detail. June corresponds to the end of nine consecutive wet months and September corresponds to the end of three consecutive dry months. Therefore, the seasonal lake extent change of Lake Tuz was investigated from June to September between 2000 and 2015. In the selection of the scenes two criteria were employed; the scene should not have cloud cover around Lake Tuz and the data acquisition day should be as close to 15^{th} of the month as possible based on the data availability. The list of the data used in this analysis is provided in Table 3.

An example showing the NDWI image before and after the threshold is given in Figure 34. In the example 17 July 2010 NDWI is calculated. A threshold of 0.4 was applied to differentiate wet and dry classes and the results are shown in the figure below.

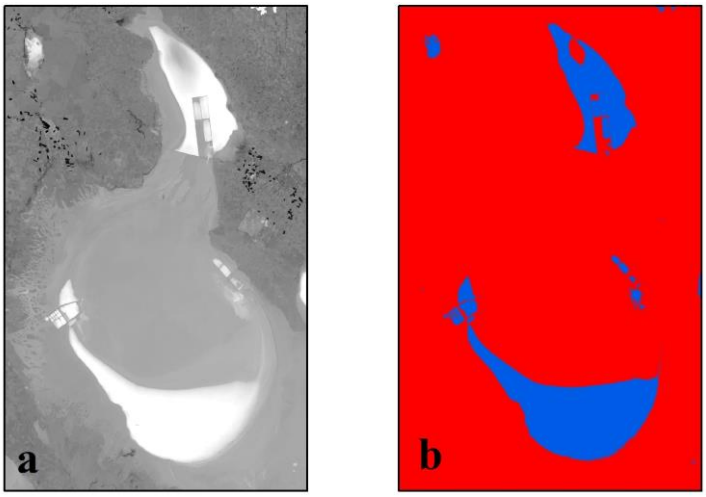

Figure 34: Water extent analysis for 17 July 2010 a) NDWI before the threshold is applied b) after 0.4 thresholds is applied (blue: wet, red: dry)

The results of the seasonal water extent change are summarized in Table 8. The maximum lake extent was obtained in 10 June, 2011. As discussed earlier in the Climate section, the water year 2011 is wettest year between 1971-2015 period. The water extent at this date is accepted as the maximum outline of the lake in this study. Hence the maximum area of the Lake Tuz water extent is 883.89 km^2 within the study time period.

Table 8: The summary of the seasonal lake extent change results (2000-2015), (Note that % Area values are based on the lake extent on 10 June 2011)

Date	Area(km^2)	Area(%)	Date	Area(km^2)	Area(%)
19 May 2000	804,1	91	26 Jun 2008	104,11	11,8
13 Jul 2000	442,5	50,1	19 Jul 2008	13,02	1,5
15 Aug 2000	170,52	19,3	13 Aug 2008	0	0
16 Sept 2000	86,85	9,8	05 Sept 2008	0	0
25 Jul 2001	13,28	1,5	12 Jun 2009	811,47	91,8
01 Aug 2001	4,78	0,5	30 Jul 2009	293,5	33,2
18 Sept 2001	4,71	0,5	31 Aug 2009	126,8	14,3
09 Jun 2002	798,53	90,3	24 Sept 2009	71,86	8,1
13 Aug 2002	118,17	13,4	15 Jun 2010	695,81	78,7

Table 8 (Continues)

15 Jun 2004	144,32	16,3	20 Jul 2011	679,43	76,9
08 Jul 2004	79,34	9	21 Aug 2011	228,42	25,8
09 Aug 2004	52,99	6	06 Sept 2011	185,79	21
26 Sept 2004	0	0	05 Jun 2012	745,29	84,3
09 Jun 2005	247,57	28	23 Jul 2012	168,56	19,1
11 Jul 2005	69,34	7,8	15 Aug 2012	103,01	11,7
12 Aug 2005	11,9	1,3	16 Sept 2012	36,14	4,1
13 Sept 2005	0,06	<0.1	24 Jun 2013	267,96	30,3
21 Jun 2006	255,38	28,9	10 Jul 2013	125,35	14,2
30 Jul 2006	60,34	6,8	11 Aug 2013	24,79	2,8
15 Aug 2006	30,84	3,5	03 Sept 2013	3,16	0,4
16 Sept 2006	0,8	0,1	18 Jun 2014	334,52	37,8
23 Jun 2007	82,07	9,3	13 Jul 2014	136,64	15,5
09 Jul 2007	24,49	2,8	14 Aug 2014	27,92	3,2
10 Aug 2007	0,3	0	15 Sept 2014	10,15	1,1
11 Sept 2007	0	0	21 Jun 2015	805,85	93,5
			07 Jul 2015	696,16	80,2
			08 Aug 2015	401,73	45,5
			09 Sept 2015	214,64	24,3

Note that due to unavailability of imagery in June, 2000, the imagery of May, 2000 was used instead. The lake extent decreases every month from June to September. The only exception is 2003. In 2003, the lake extent observed in September is larger than August. This exception can be linked to the excessive precipitation recorded in September, 2003. The average precipitation values observed in Aksaray, Cihanbeyli and Kulu stations are 8.6mm, 12.9mm, 14.8mm while in 2003 the precipitation values are 11.4mm, 44.4mm and 69.5mm, respectively. In 2001, 2004, 2005, 2006, 2007, 2008, 2010, 2013 and 2014 the lake almost (water extent is less than 2%) or completely dries out. The seasonal changes in water extent are depicted in detail in Figure 35-38.

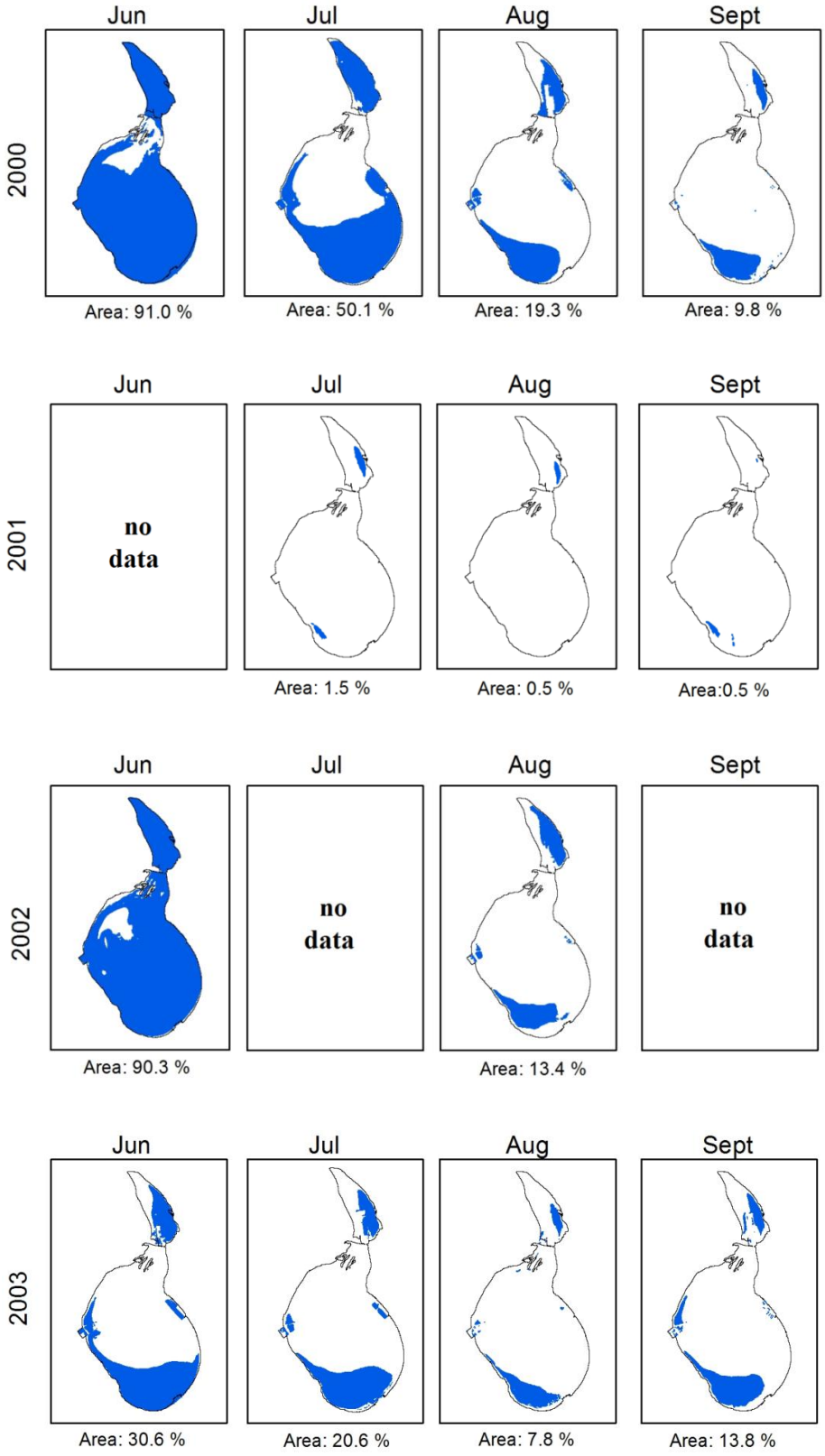

Figure 35: Seasonal change of lake extent (2000, 2001, 2002, 2003)

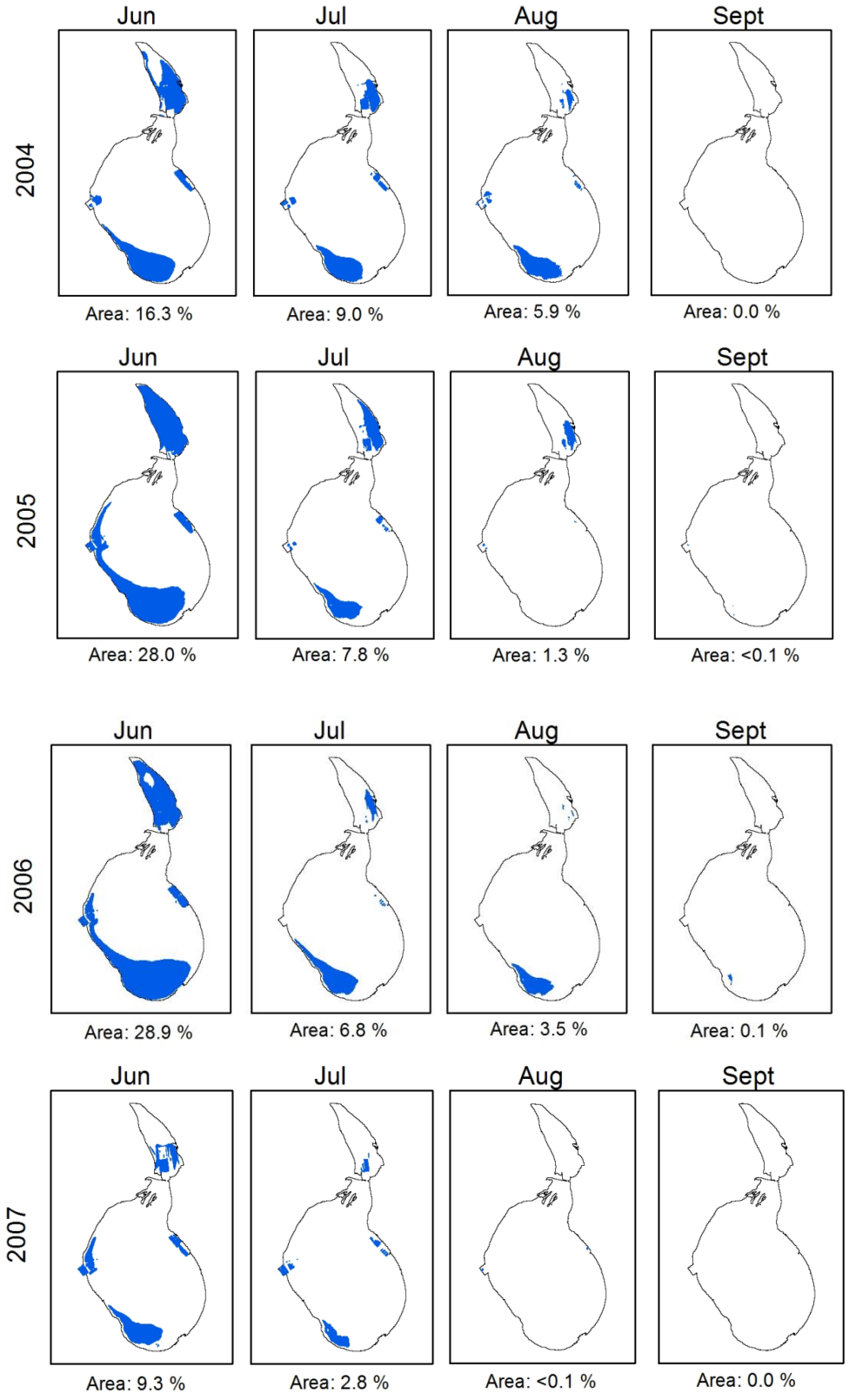

Figure 36: Seasonal change of lake extent (2004, 2005, 2006, 2007)

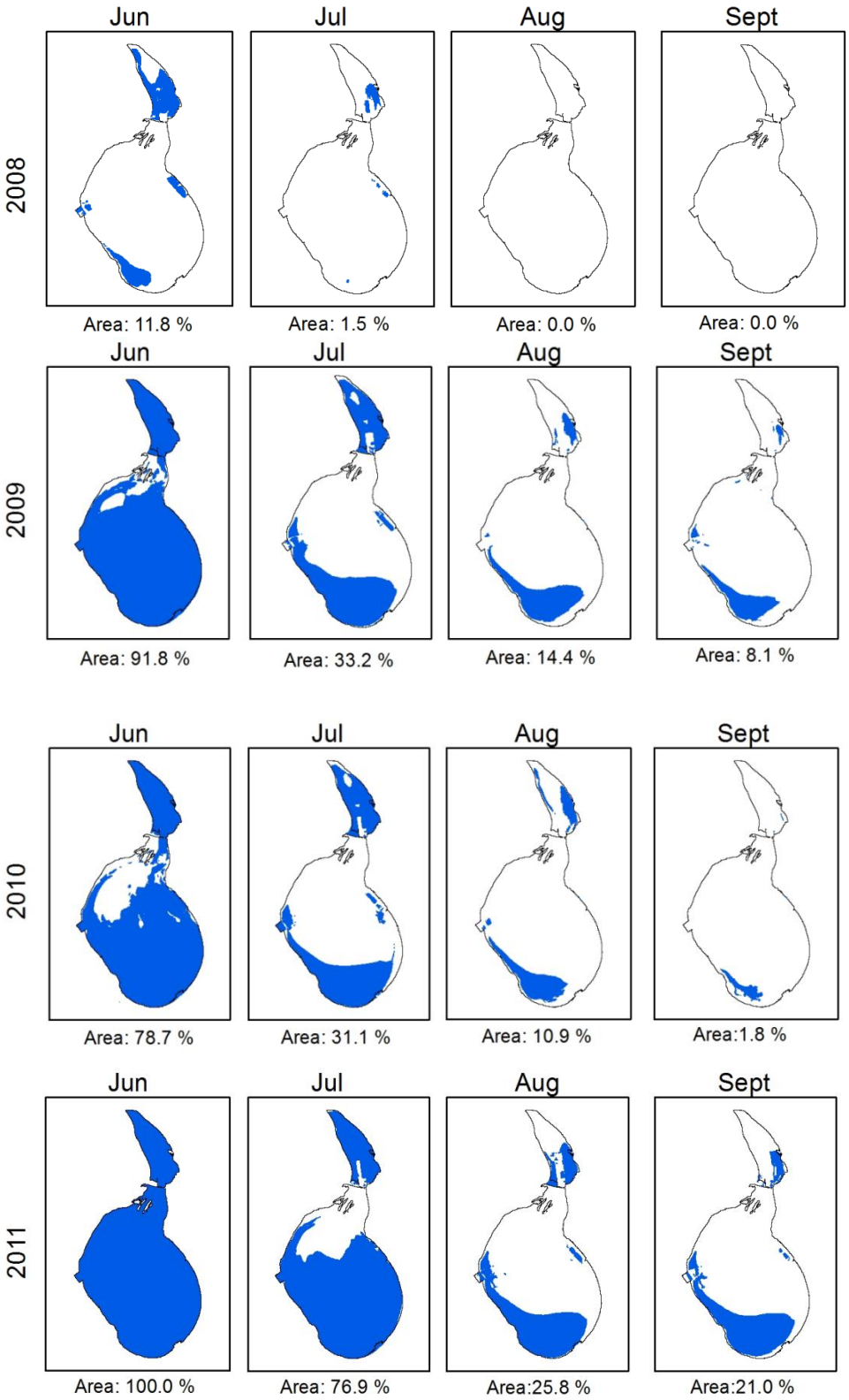

Figure 37: Seasonal change of lake extent (2008, 2009, 2010, 2011)

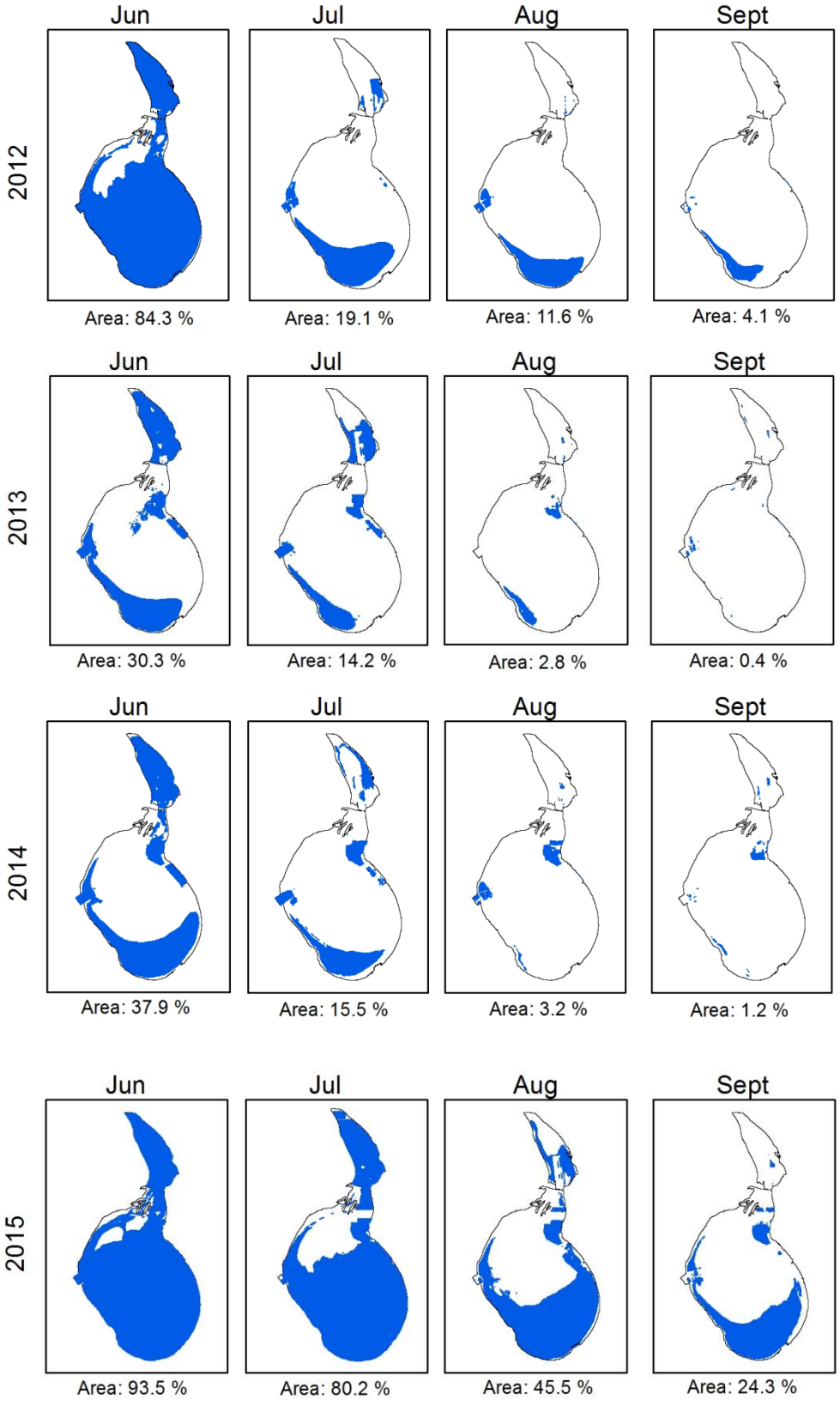

Figure 38: Seasonal change of lake extent (2012, 2013, 2014, 2015)

It can be seen from these figures that the drying always starts from north and proceeds towards the south. In other words, at the end of the drying phase the last water extent always remains in the south or the lake completely dries out. The seasonal drying patterns observed between 2000 and 2015 are shown in Figure 39 on yearly basis.

Determination of the drying pattern has significant implications in lake water budget computation efforts. For example, in designing in-situ lake level measurement networks this drying pattern should be considered for proper estimation of lake water volume. It can also be seen from these figures that in the driest month, only salinas or DSI canal outlet can retain some water. The drying pattern of Lake Tuz potentially provides valuable information on lake bathymetry, prevailing wind directions and lake recharge zones.

The reasons behind the decreasing pattern of the lake extent from June to September and reaching the maximum extent in June is investigated in detail in Chapter 5.

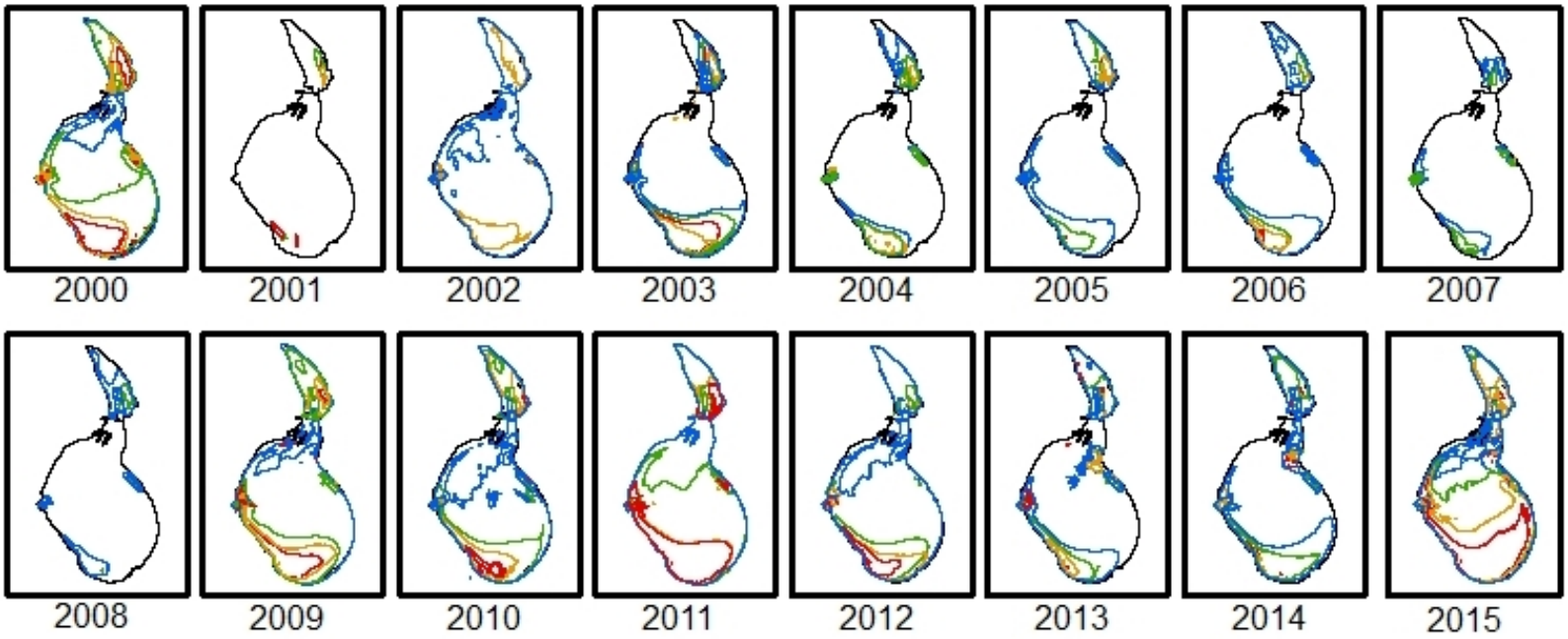

Figure 39: The seasonal drying pattern of Lake Tuz between 2000 and 2015 (black: outline of the lake, blue: June, green: July, orange: August, red: September)

4.1.2. Annual Changes

When multi-temporal scenes of Lake Tuz were investigated, it was seen that the driest month for Lake Tuz is September. The annual lake extent change was investigated by the driest month. In this study, one Landsat 5 TM or Landsat 7 ETM+ scene of Lake Tuz in September was employed for each year based on the data availability. The list of the scenes used in annual change extent analysis is provided in Table 3.

As discussed earlier, the maximum lake area was obtained in 10 June, 2011 and accepted as 100%. The annual lake extent percentages were calculated based on that day. The results of the analysis are summarized in Table 9.

Table 9: The summary of the end-of-dry season annual lake extent change results

Sensor	Date	Area (km^2)	Area (%)
TM	11 Sept 1984	343,74	38,9
TM	04 Sept 1987	364,39	41,2
TM	02 Sept 1998	276,38	31,3
ETM+	22 Sept 1999	123,23	13,9
TM	16 Sept 2000	86,85	9,8
ETM+	18 Sept 2001	4,71	0,5
ETM+	24 Sept 2003	122,04	13,8
ETM+	26 Sept 2004	0	0
ETM+	13 Sept 2005	0,06	<0,1
ETM+	16 Sept 2006	0,8	0,1
TM	11 Sept 2007	0	0
ETM+	05 Sept 2008	0	0
ETM+	24 Sept 2009	71,86	8,1
TM	19 Sept 2010	16,08	1,8
TM	06 Sept 2011	185,79	21
ETM+	16 Sept 2012	36,14	4,1
ETM+	03 Sept 2013	3,16	0,4
ETM+	15 Sept 2014	10,15	1,1
ETM+	09 Sept 2015	214,64	24,3

The maximum water extent at the end of the dry season was reached in 1987 as 41.2 %. Note that no imagery is available between 1988 and 1997. Starting from 2000 the lake extent decreases significantly. There is a dry period between 2004 and 2008. During this period the lake dries out completely every September.

The lake water had its maximum extent during 1980s. After that period, the lake extent showed variations. The driving mechanisms behind these variations were investigated in Chapter 5. The annual change of the lake extent was shown Figure 40.

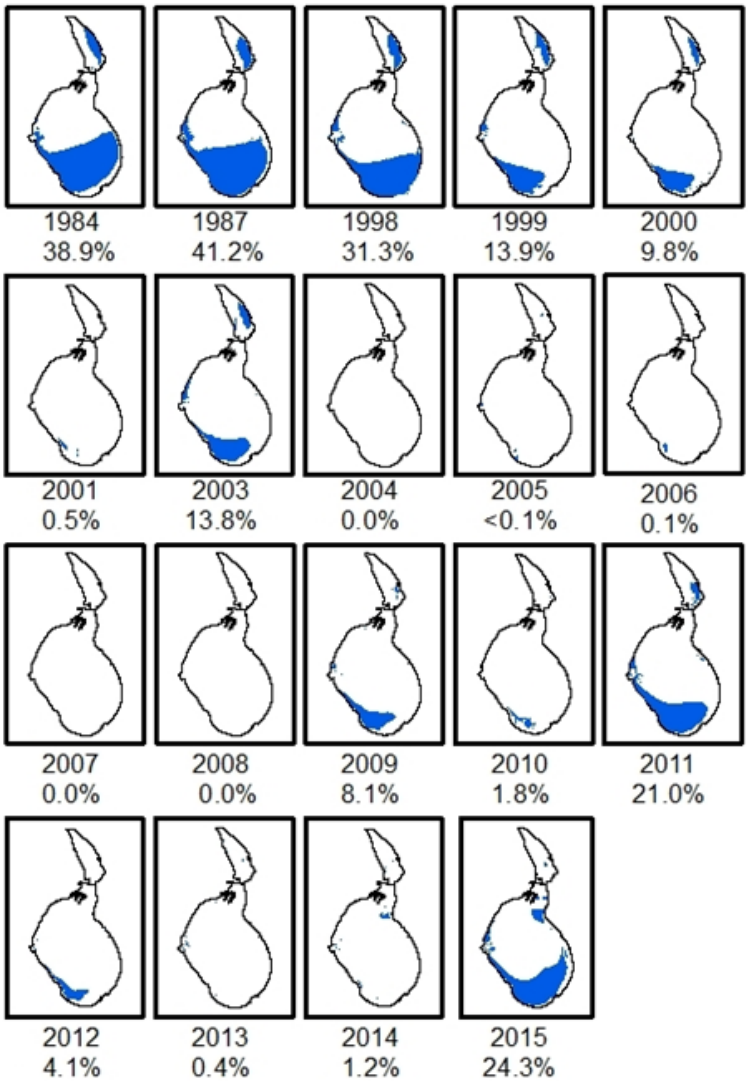

Figure 40: The annual change of lake extent at the end of the dry season (September)

4.2. Spatial Changes

Spatial changes of lake extent were investigated for a better understanding of the drying pattern of Lake Tuz. For this task, the centroid of the main water body (excluding north of the barrier wall if not connected to the main water body) of the lake is determined. Moreover, four control points were selected and for each scene coordinates of these control points were listed. The first point is the road junction of the barrier road of Lake Tuz and Bozan Village Road. The second point is selected as the junction of the barrier road and a wall of Kaldırım Salina. The third point is the south corner of Kayacık Salina and the fourth point is the east corner of Yavşan Salina. The locations of the selected points and the centroid of the main water body on May 19, 2000 are shown in Figure 41.

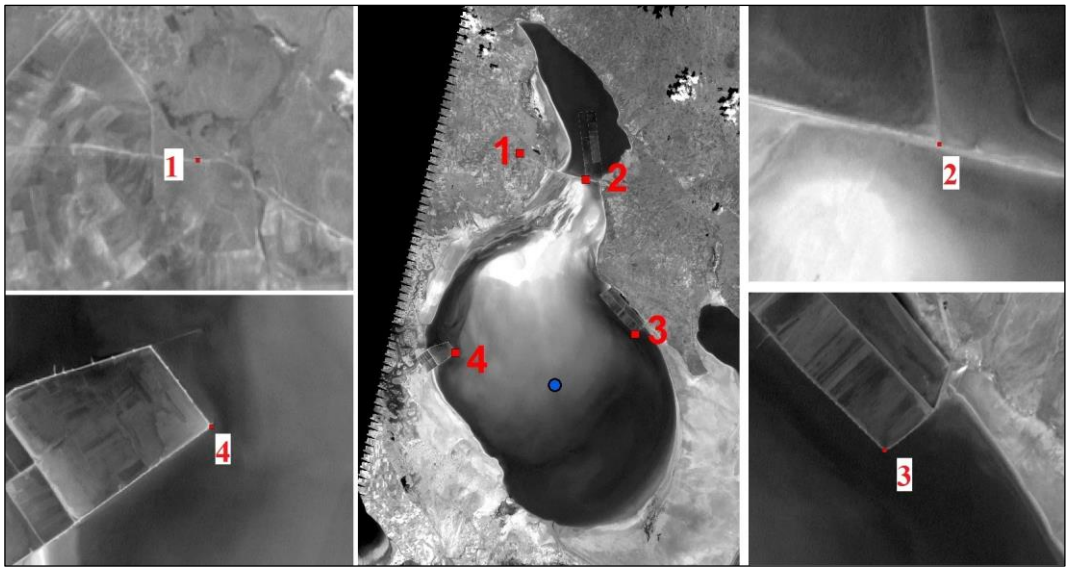

Figure 41: Location of control points (red) and the centroid of the main water body (blue) on May 19, 2000

The distances between the centroid of the main water body and each control points were calculated for every scene used in annual and seasonal change investigation. This makes a total of 68 scenes. The relationships between lake extent and distance to control points are shown in Figures 43-46. The p-values for all relationships shown in these figures are smaller than 0.0005.

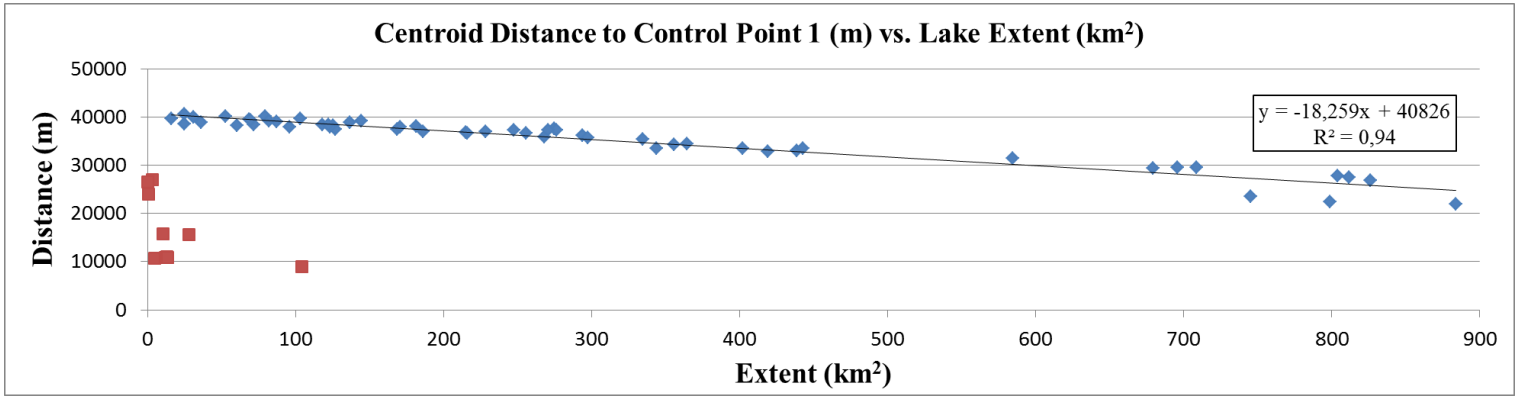

Figure 42:Relationship between the lake extent and the distance between the centroid of the main water body and Control point 1 (red point: outlier, $\alpha=0.05$, $p<0.0005$)

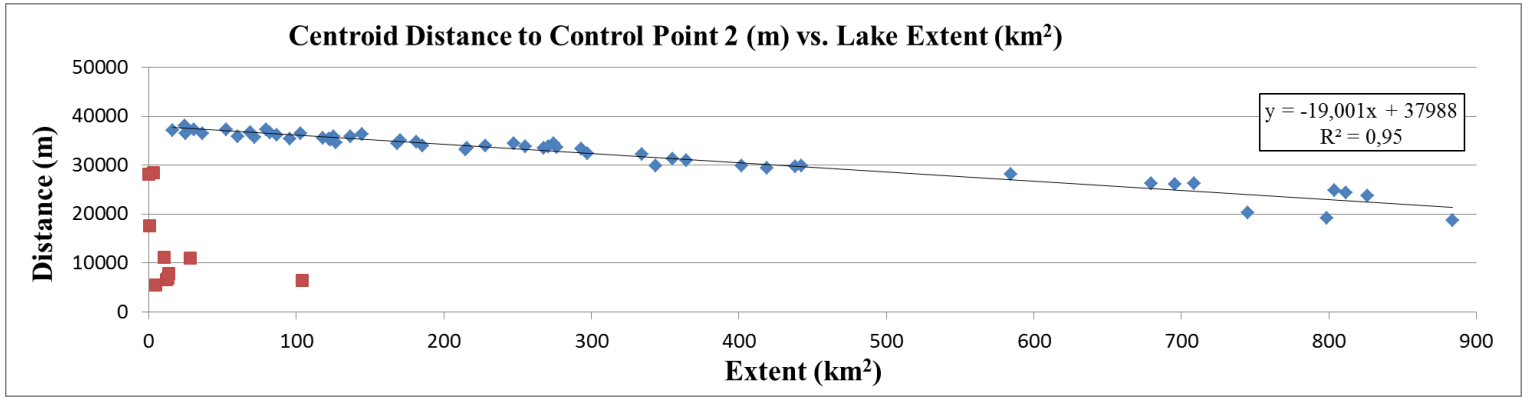

Figure 43:Relationship between the lake extent and the distance between the centroid of the main water body and Control point 2 (red point: outlier, $\alpha=0.05$, $p<0.0005$)

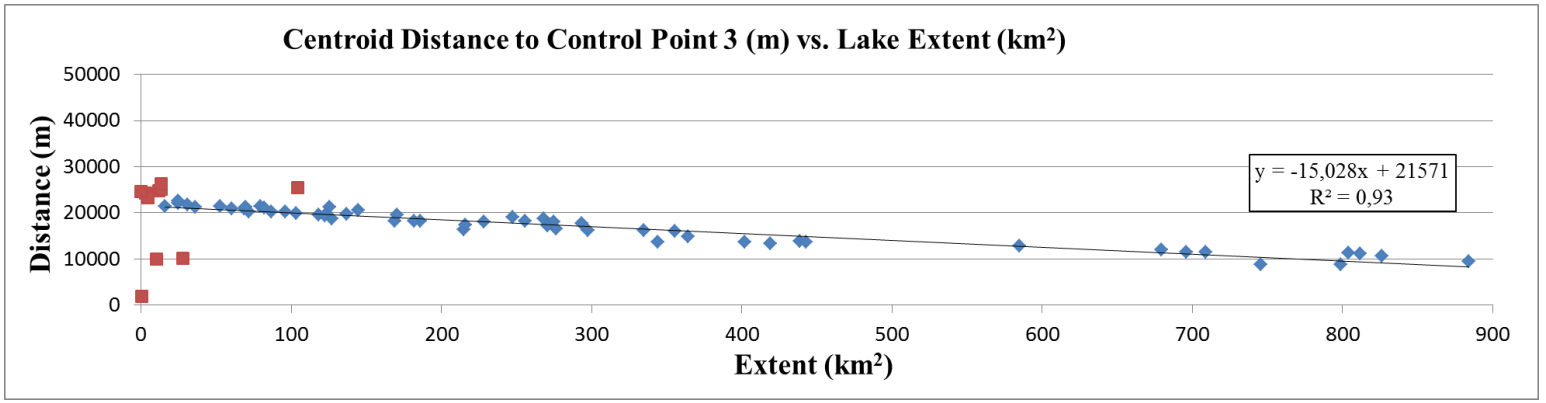

Figure 44:Relationship between the lake extent and the distance between the centroid of the main water body and Control point3 (red point: outlier, α=0.05, p<0.0005)

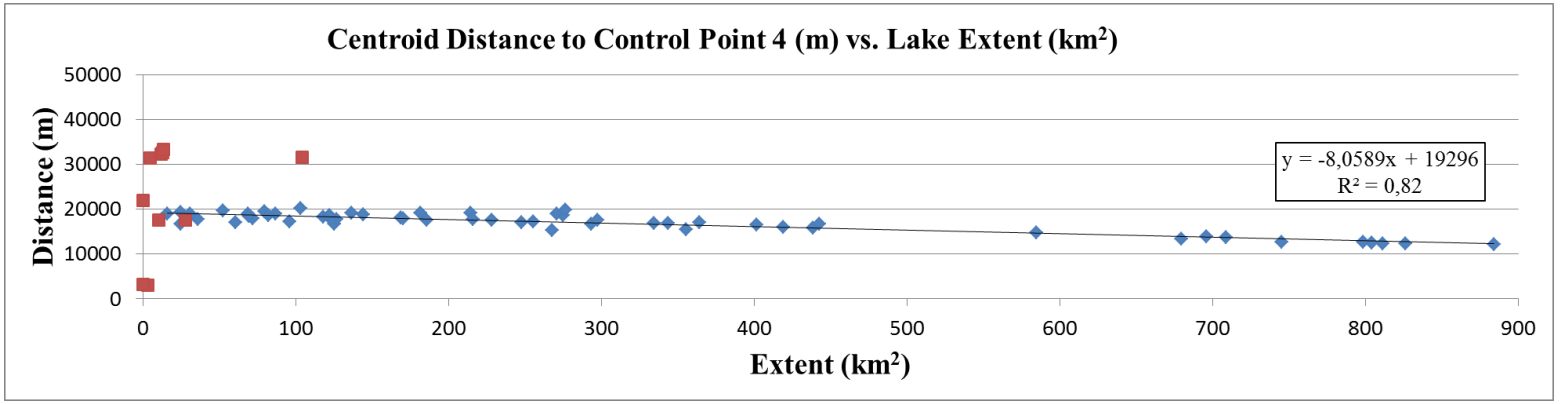

Figure 45:Relationship between the lake extent and the distance between the centroid of the main water body and Control point4 (red point: outlier, α=0.05, p<0.0005)

As the water extent decrease, the centroid of the main water body moves towards South and becomes more distant to all control points. The red points on the plots belongs the outliers of the datasets. The outlier data represent the artificial water extent. On these dates, the lake only retains some water in salinas or behind the barrier. Since these values do not reflect the natural drying pattern of the lake, they are not included in the analysis.

Spatial changes of the water extent were investigated by directly comparing the extent and coordinates of the centroid of the water body using all images selected for annual and seasonal change analysis. The relationship between the water extent and the longitude of the centroid is shown in Figure 46. As shown in the figure the relation between the water extent and the longitude cannot be explained by linear relationship. The relationship between the water extent and the latitude of the centroid is shown in Figure 47. The water extent and the latitude of the centroid are linearly correlated with an R^2 value of 0.95. This relation shows that as the lake extent increases the centroid moves towards the North.

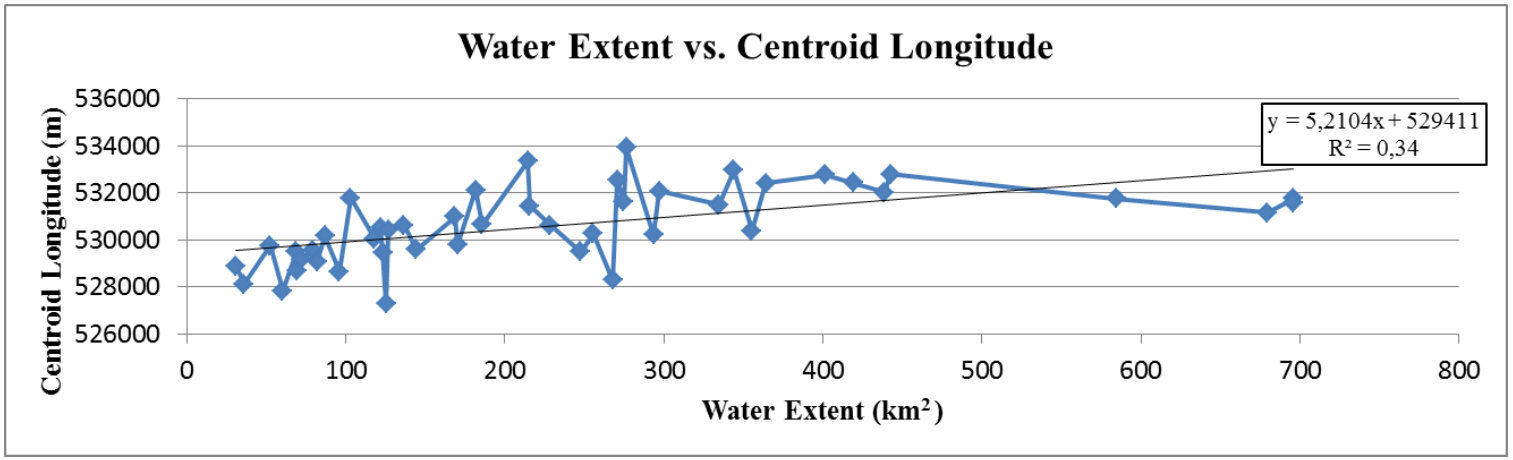

Figure 46: Water extent vs. centroid longitude (α=0.05, p:0.03)

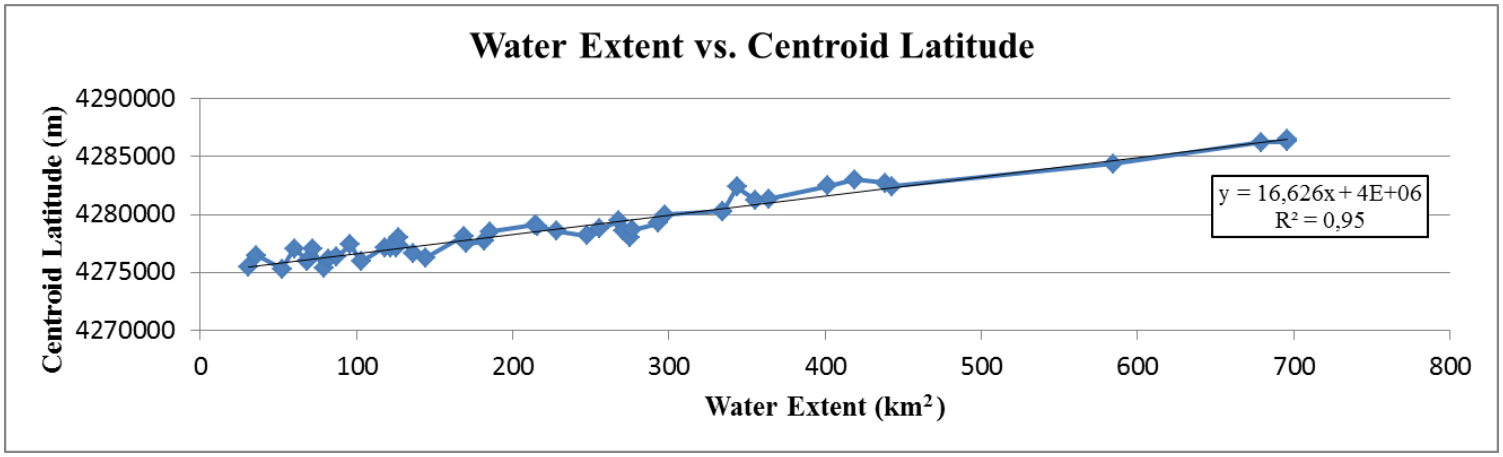

Figure 47: Water extent vs. centroid latitude **(**α=0.05, p:0.02)

CHAPTER 5

RELATIONSHIP BETWEEN METEOROLOGICAL VARIABLES AND THE LAKE EXTENT

5.1. Precipitation

There are four meteorological stations in the study area. The data obtained from these stations were used in the investigation of the relationship between precipitation and the lake extent. The mean monthly precipitation histograms and the lake extents observed in June, July, August and September are compared and provided in Figure 48 through Figure 51 for Aksaray, Cihanbeyli, Kulu and Şereflikoçhisar stations, respectively.

Starting from April, the precipitation starts to decrease significantly. The study area receives the least precipitation in June, July and August as discussed in Climate chapter in detail. The precipitation fluctuations are similar in all stations. The seasonal change of lake extent shows quite similar pattern with change of mean monthly precipitation and decreases significantly with decreasing precipitation observed in all stations.

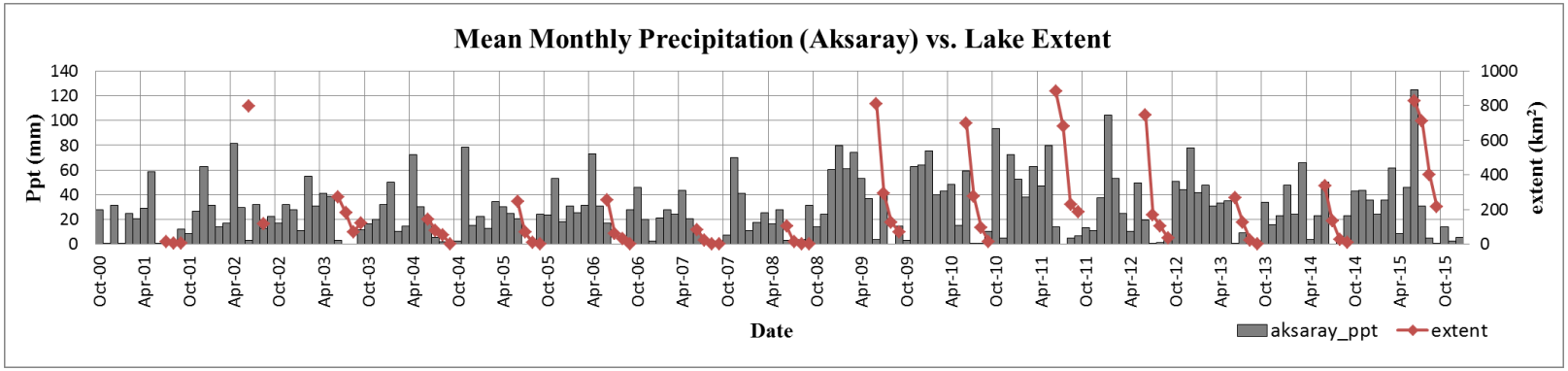

Figure 48: Mean monthly precipitation vs. lake extent (Aksaray) time series

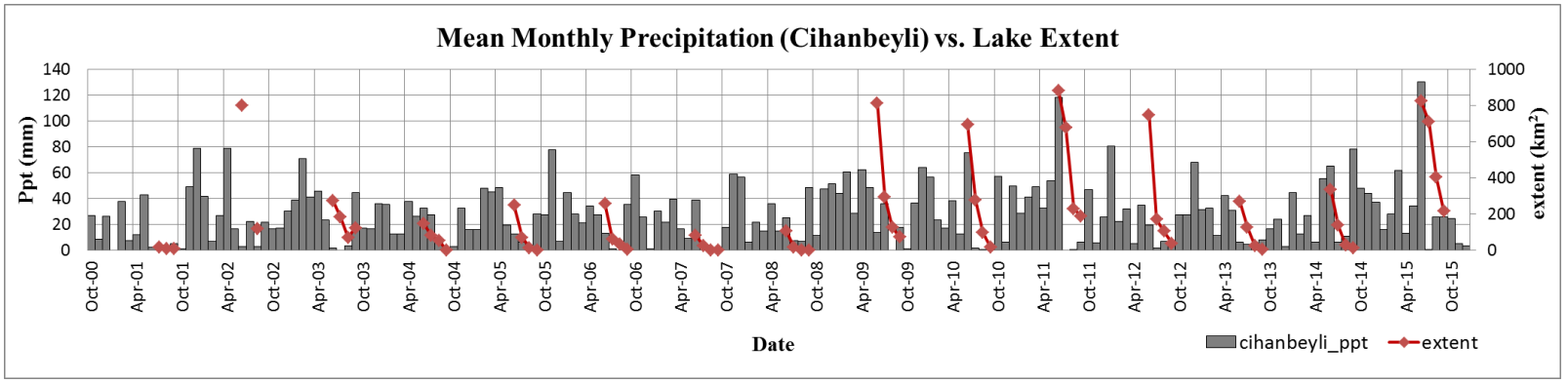

Figure 49: Mean monthly precipitation vs. lake extent (Cihanbeyli) time series

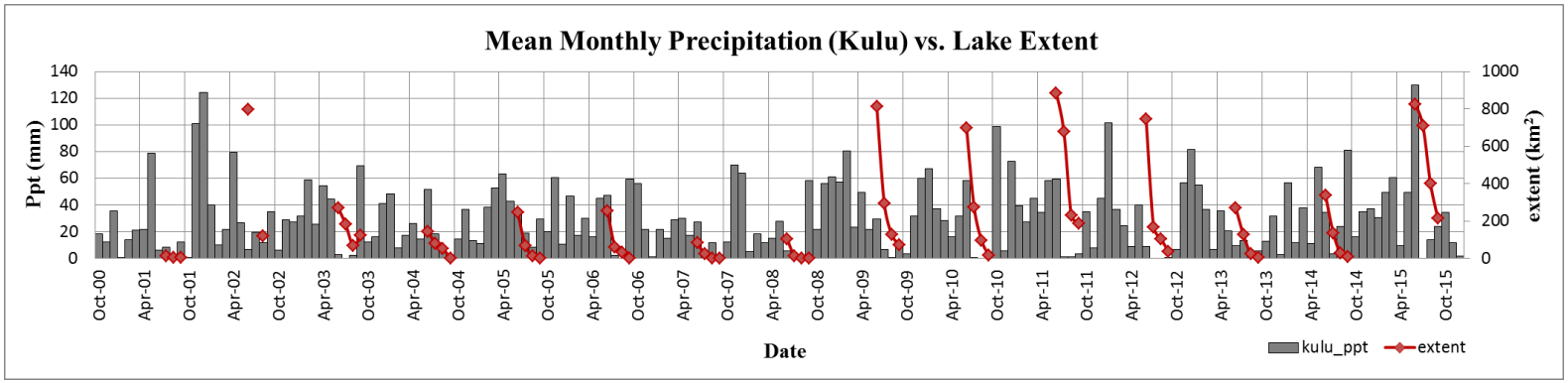

Figure 50: Mean monthly precipitation vs. lake extent (Kulu) time series

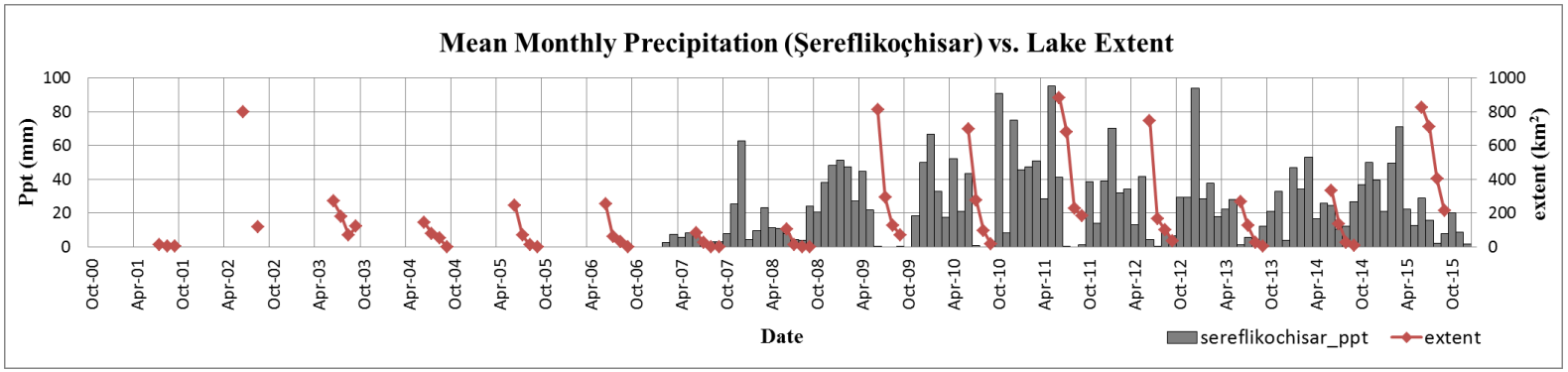

Figure 51: Mean monthly precipitation vs. lake extent (Şereflikoçhisar) time series

The relationship between precipitation and lake extent was also investigated in terms of annual changes. The maximum precipitation is observed between October and June while the minimum is between July and September. Therefore, the relationship between cumulative precipitation observed between October and June and the lake extent in June was investigated for years 2001 and 2015. The time series of total precipitation between October-June period vs. the lake extent in June is provided in Figure 52.

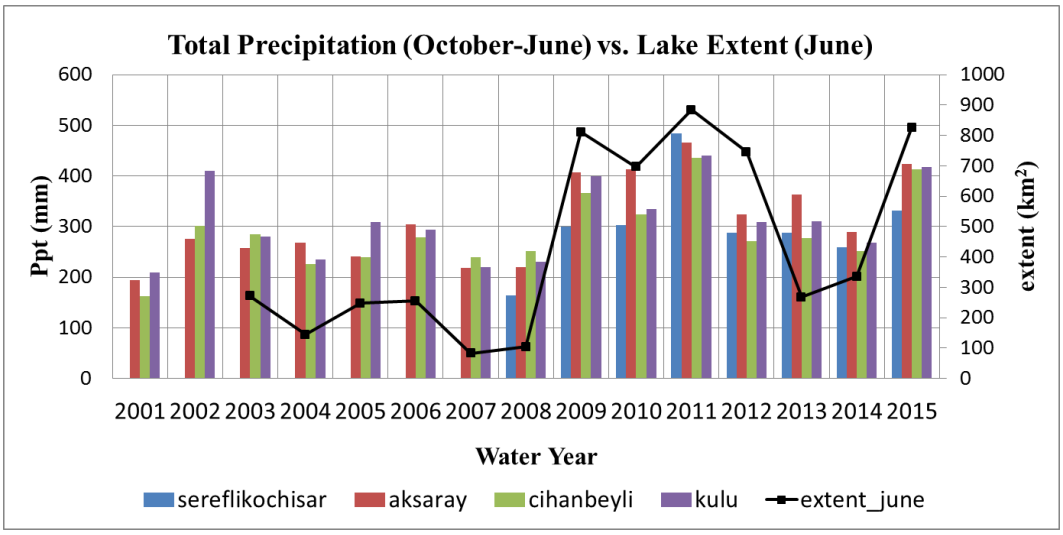

Figure 52: Total precipitation (October-June) vs. lake extent of June time series

The annual lake extent change is quite responsive to total precipitation observed in the study area between October and June, as expected. The lake reaches to its minimum extent in September. The precipitation observed between October and June fills the lake and the extent reaches to its maximum in June. As shown in Figure 52 the lake extent increases with increasing precipitation and decreases with decreasing precipitation. The direct relationship was not observed only in 2013 and 2014. Although the total precipitation remained constant or slightly increased in 2013 when compared to 2012, the lake extent of June 2013 is less than June 2012. In 2014 the lake extent slightly increases even though there is a little decrease in the total precipitation.

The relationship between the lake extent and precipitation is further investigated by directly comparing total precipitation between October and June and the lake extent observed in June. In this analysis precipitation data obtained from Aksaray, Cihanbeyli and Kulu stations are used. Şereflikoçhisar Station was excluded from the study because of the long data gaps and limited data points. The results of the analysis are provided in Figure 53 for Aksaray, Figure 54 for Cihanbeyli and Figure 55 for Kulu Station. For all relations, the significance level (α) is set to 0.05.

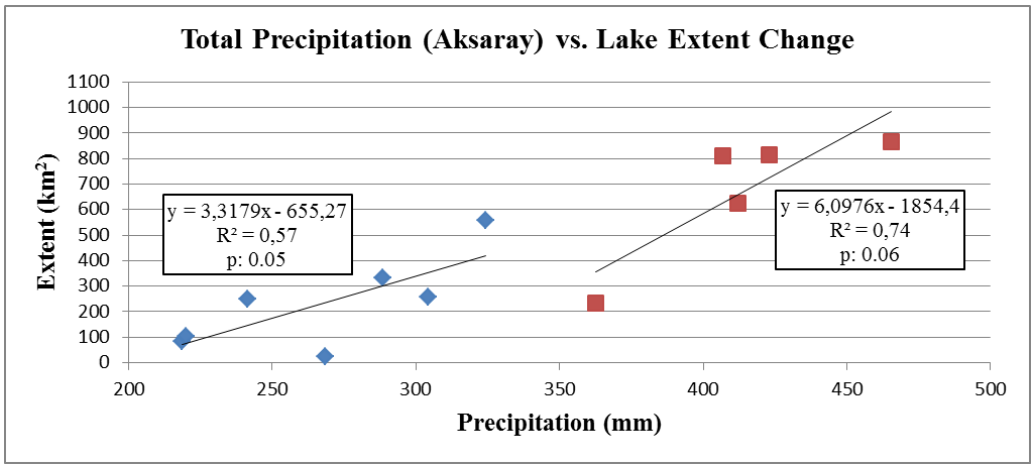

Figure 53: Total precipitation Oct-Jun (Aksaray) vs. lake extent (Jun) (blue: low precipitation, red: high precipitation, α: 0.05)

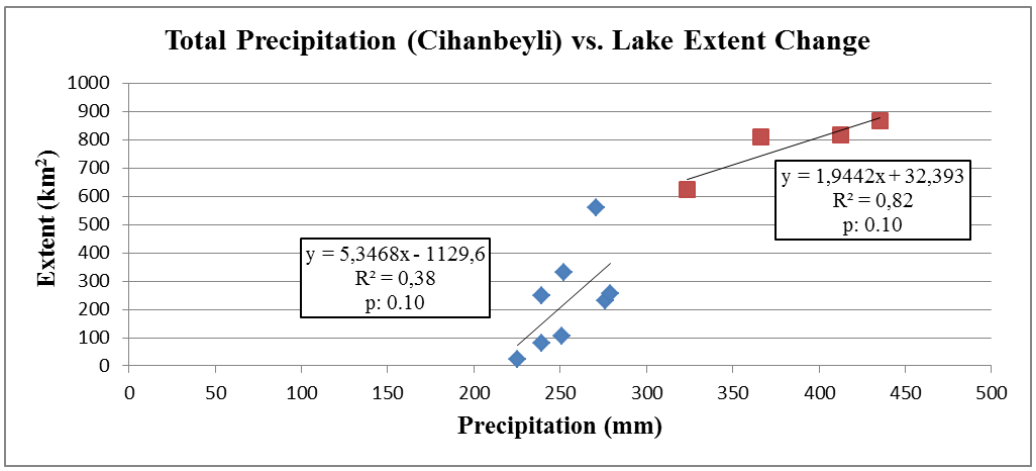

Figure 54: Total precipitation Oct-Jun (Cihanbeyli) vs. lake extent (Jun) (blue: low precipitation, red: high precipitation, α: 0.05)

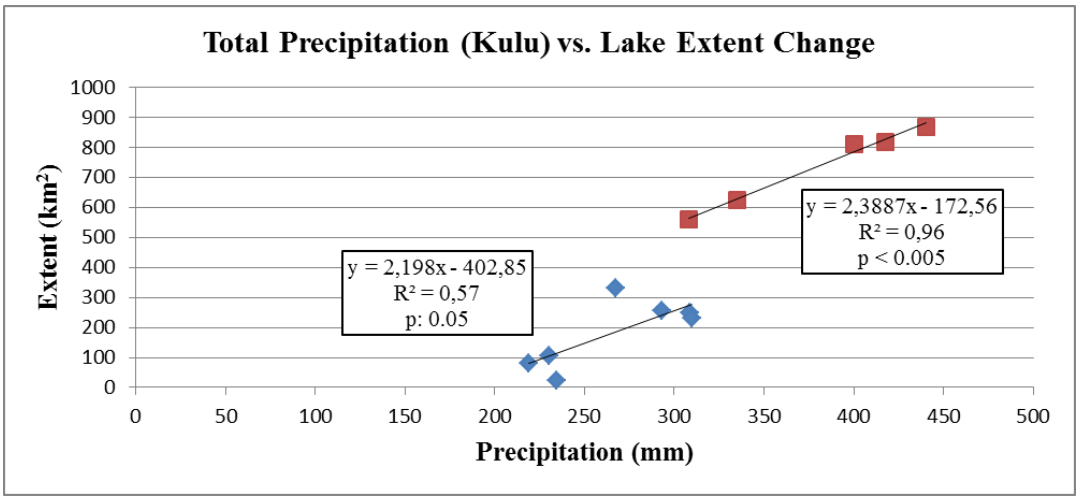

Figure 55: Total precipitation Oct-Jun (Kulu) vs. lake extent (Jun) (blue: low precipitation, red: high precipitation, α: 0.05)

The relationship was investigated in two clusters. The extent of 2012 was not correlated either of the cluster, thus accepted as outlier and excluded from the analysis. The first cluster is composed of low precipitation (approximately <375mm) and the second of high precipitation (approximately >375mm). The data points of high precipitation cluster are less than low precipitation. Both high and low precipitation clusters shows strong correlation between total precipitation (October-June) and the lake extent of June.

5.2. Evaporation and Temperature

Evaporation measurements were obtained from Aksaray and Cihanbeyli meteorological stations. Both data sets include gaps starting from November until April in their records. The evaporation histograms and the lake extents are provided in Figure 56 for Aksaray and in Figure 57 for Cihanbeyli Stations.

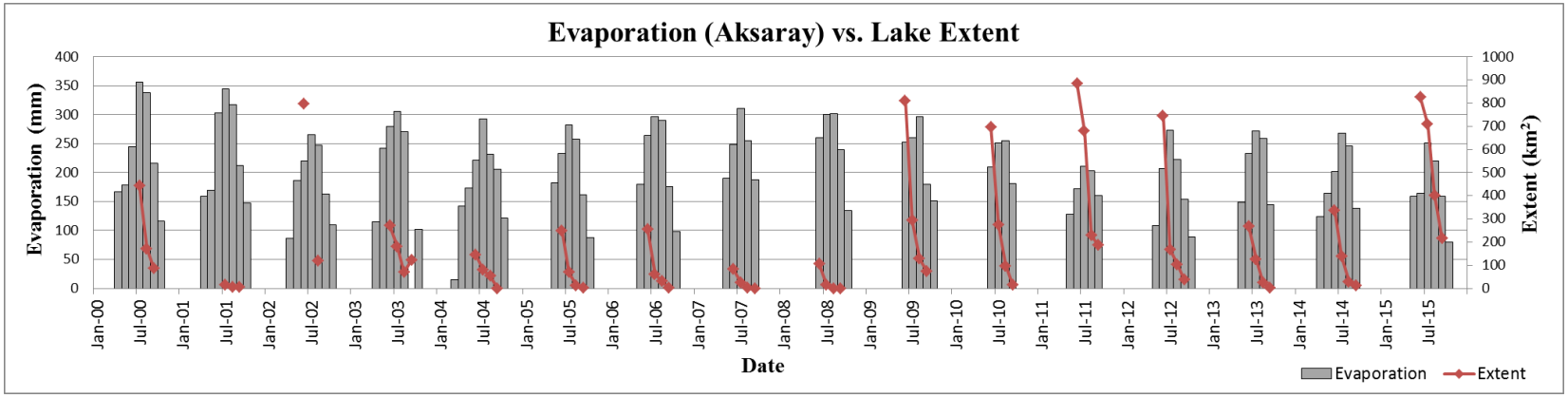

Figure 56: Evaporation (Aksaray) vs. lake extent

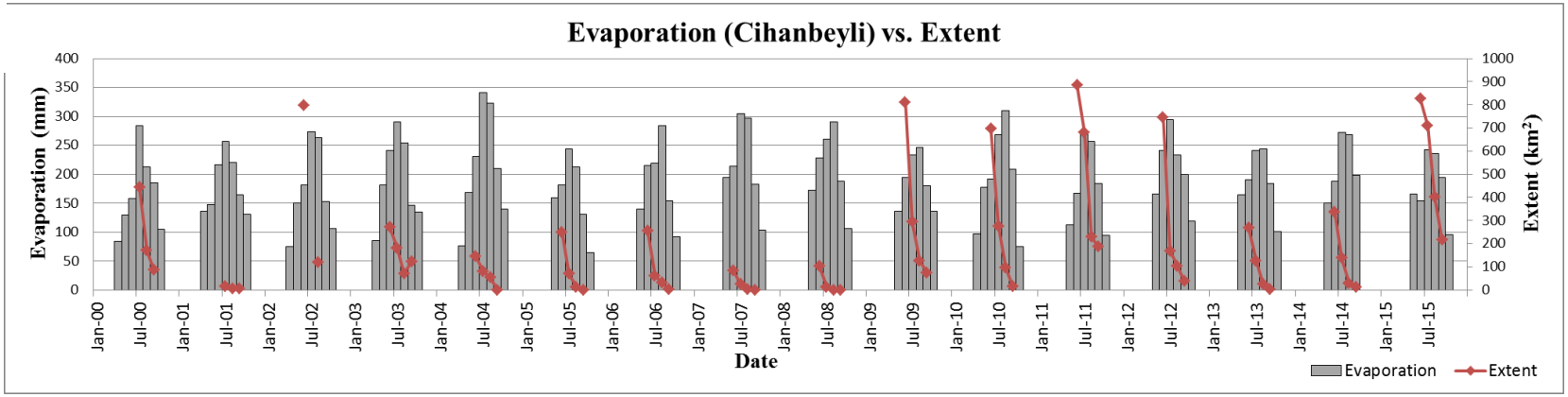

Figure 57: Evaporation (Cihanbeyli) vs. lake extent

Evaporation patterns of Aksaray and Cihanbeyli Stations show similarities. Until July the evaporation increases. Starting from July until October (or the end of record) the evaporation decreases.

Temperature data is available for all four meteorological stations. The measured temperature values of these stations are very similar to each other. Monthly average temperatures versus lake extent time series are shown in Figure 58 for Aksaray and Cihanbeyli Stations and Figure 59 for Şereflikoçhisar and Kulu Stations. As expected, the evaporation and temperature trends show similarities. Temperature has an increasing trend between January and July. Lake extent decreases from June to September. The major decrease in the lake extent is also observed between June and July.

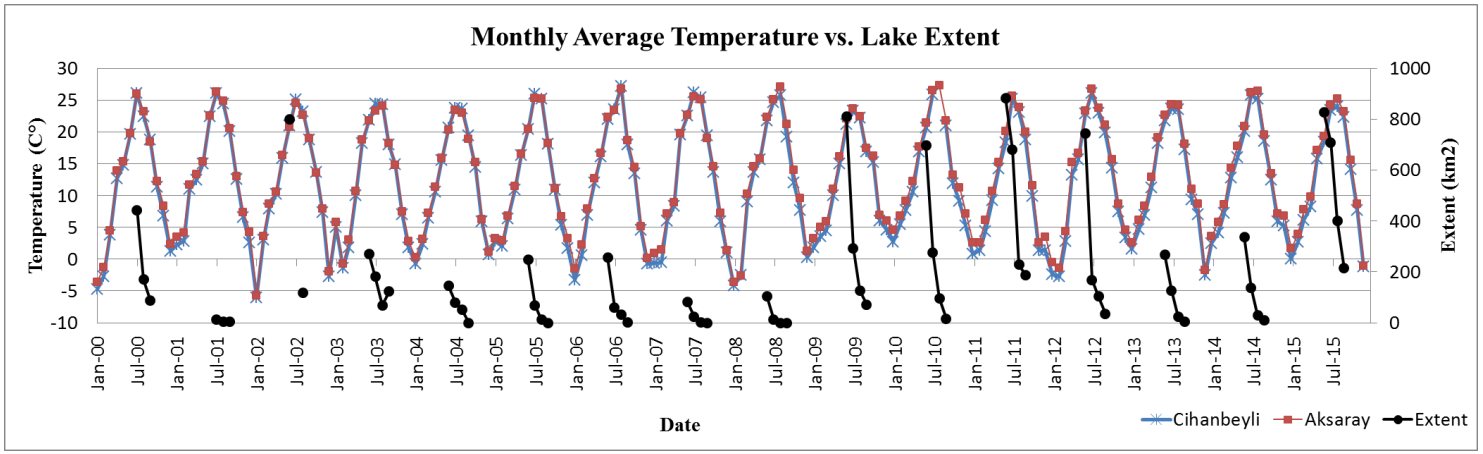

Figure 58: Monthly average temperature vs. lake extent (Aksaray & Cihanbeyli)

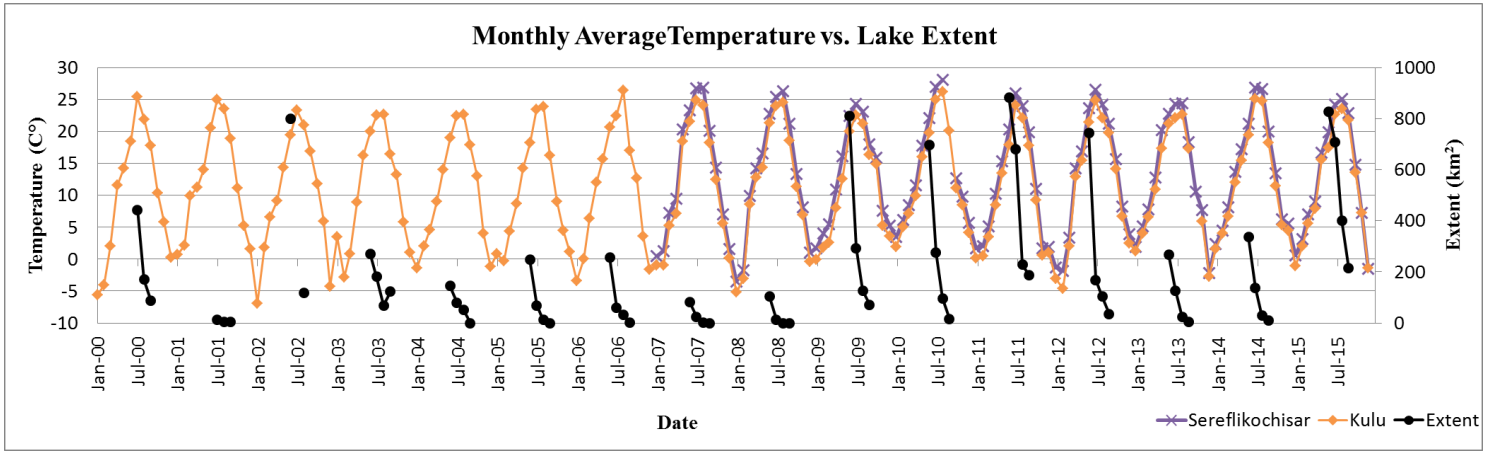

Figure 59: Monthly average temperature vs. lake extent (Şereflikoçhisar & Kulu)

5.3. Wind

The wind data is obtained from Şereflikoçhisar Station between 2007 and 2014. The wind rose showing the wind speed and wind direction is provided in Figure 60 .

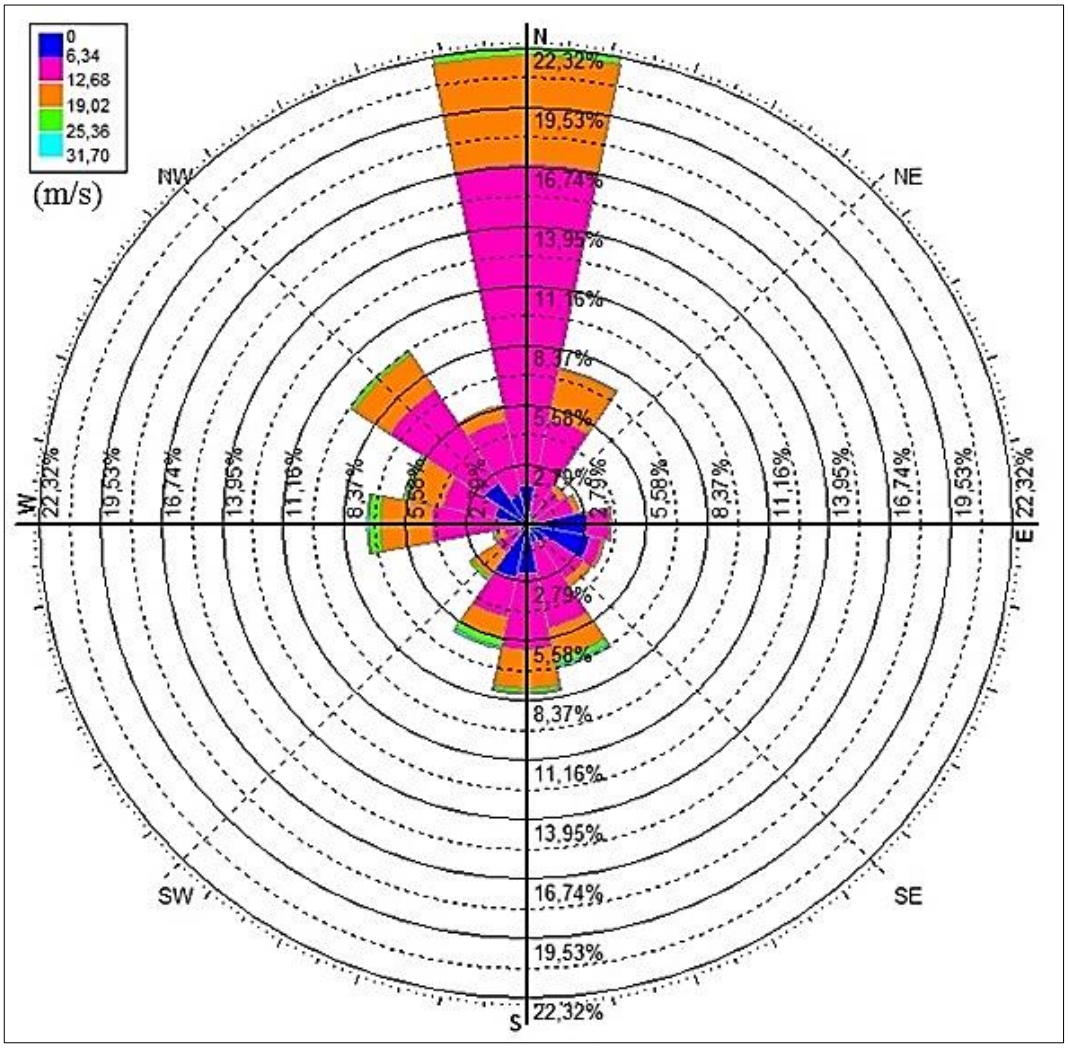

Figure 60: Wind rose showing the wind speed and wind direction

The rose diagram shows that northerly winds are dominant in the study area. The speed of the majority of the northerly winds is between 6 and 13 meter per second (m/s). The general information about the wind pattern is summarized in Table 10 .

Table 10: General information about the winds affecting the study area

Direction	Total Wind Count	Wind Count of the Max Data Month	Most Windy Month	Mean Speed in the Most Windy Month (m/s)	Max Mean Month/Speed (m/s)
N	636	100	Aug	11.08	Jul/12.39
NNE	213	49	Jul	12.19	Jun/12.60
NE	64	11	Jul	10.46	Jul/10.46
ENE	71	20	Aug	10.19	Jun/12.85
E	112	32	Nov	4.62	Jun/12.70
ESE	105	20	Nov	4.93	Jun/17.50
SE	102	22	Feb	8.61	May/12.60
SSE	197	35	Jan	11.59	Jun/14.70
S	227	33	Jan	9.12	Jun/12.29
SSW	171	21	Mar/Apr	10.66/13.75	Apr/13.75
SW	91	18	May	12.96	Jun/16.48
WSW	46	7	May	14.66	May/14.66
W	209	35	Apr	13.72	May/14.17
WNW	165	20	Apr	12.84	Jun/15.56
NW	278	34	Mar	10.94	Aug/12.31
NNW	162	19	Oct/Jan	7.39/7.91	Apr/11.39

Northerly winds are more frequent in the study area and they generally occur in August. The mean speed of these winds is 11.08 m/s. The maximum mean speed of northerly winds is 12.19 m/s and it is achieved in July. The majority of the maximum speeds were recorded in June and May. The minimum mean wind speed is observed at E and ESE directions in November. The relationship between wind speed and lake extent is shown in Figure 61.

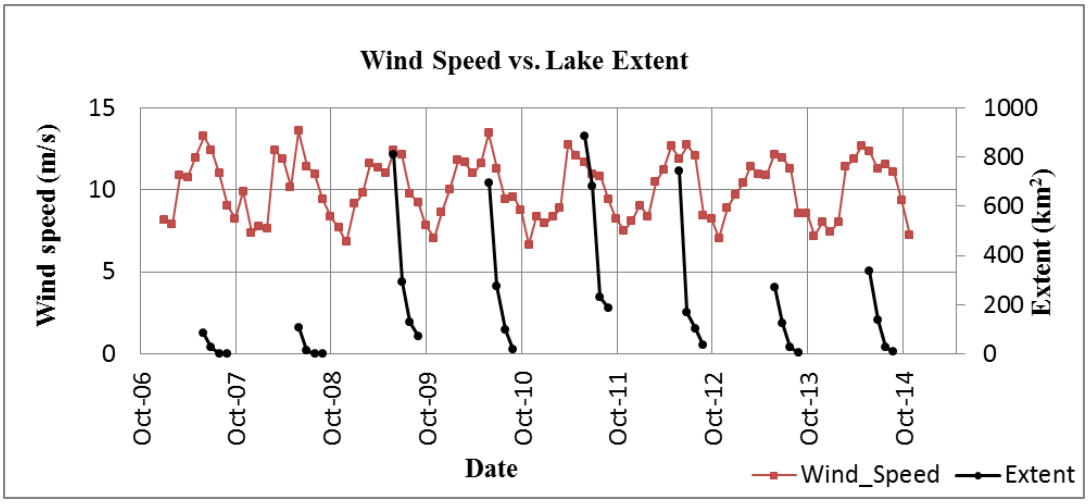

Figure 61: Wind speed vs. lake extent (2007-2014)

Wind speed starts to decrease in May and continues to decrease until November. The lake extent is also shows a decreasing pattern between June and September. When the drying pattern of the lake and the prevailing wind direction is considered, the lake extent is expected to decrease with increasing wind speed.

CHAPTER 6

SUMMARY, CONCLUSIONS & RECOMMENDATIONS

The objective of this study is to determine the best method to extract water extent of Lake Tuz by using remotely sensed image and investigate its relationship with meteorological variables. The salt crust covering the bottom of Lake Tuz creates problems in extracting water extent by using remotely sensed images. The seasonal changes of the lake extent were investigated between 2000-2015 and the annual changes were investigated between 1984-2015 (including data gaps). Landsat 5 TM and Landsat 7 ETM+ scenes obtained from the website of USGS and meteorological data provided by General Directorate of Meteorology were used in the analysis.

Ten Landsat 5 TM and ten Landsat 7 ETM+ scenes in which wet, moist and dry parts of the lake are visually identifiable were selected as training scenes. Landsat 7 ETM+ SLC-off scenes were filled by linear interpolation. All scenes were pre-processed by means of gain and offset. Five indices were selected among multi-band indices used in water body mapping. MNDWI, NDWI, AWEInsh, AWEIsh and TCW indices were calculated for selected control dates. Five absolute wet, moist and dry points were selected for each training scene. The values of single bands and multi-band indices corresponding to the control points were investigated. NDWI was the only method to successfully differentiate wet, moist and dry points. The results of NDWI showed zero overlap and maintained maximum separation between the classes. Single bands and other multi-band indices were incapable of differentiating the classes. Hence NDWI was selected as the best method in differentiating dry/moist/wet classes over salt crust.

The moist class was interpreted as dry since the water in moist class is very limited and can switch into dry conditions easily. The upper limit of moist class was set as the threshold for differentiating water pixels from its surroundings.

Multi-temporal and spatial changes of Lake Tuz were investigated by using NDWI and the selected threshold. In this analysis Landsat 5 TM and Landsat 7 ETM+ scenes were used. The annual changes of Lake Tuz were investigated by its driest month for 1984,1987,1998,1999 and between 2000-2015. The meteorological data and the satellite images showed that the driest month of Lake Tuz is September. The investigation of the annual changes of the lake extent showed that starting from 2000s the extent of Lake Tuz decreased significantly. In majority of the years after 2000s, the lake dries out completely in September rarely retaining some water in built up areas like salinas. The shrinking of the lake extent is not observed continuously in yearly basis. In some years the lake extent may be larger than the year before based on the wetness of the year. Yet the long term investigation of the lake extent proves that the shrinkage is more prevalent in recent years. For example, in September 1984, the lake is 38.9 % full and it corresponds to the end of two successive dry years while in September 2014, the lake is 1.2 % full and it corresponds to the end of three successive wet years. Even though the precipitation is most effective factor on the lake extent other factors such as groundwater levels can be affecting the lake extent in the long term.

Analysis of the seasonal drying pattern of Lake Tuz between 2000 and 2015 indicated that the lake extent significantly decreases from June to September. In this period precipitation decreases and with increasing temperature and wind effect evaporation becomes dominant. The major decrease in the extent is observed between June and July. From July to September the decrease continues and in 2004, 2007 and 2008 Lake Tuz completely dries out. In both annual and seasonal changes of lake extent shows that the lake consistently dries from north to south. The analysis on the spatial change of the lake extent also shows that as the extent of the lake decreases, the centroid of the main water body moves towards south.

The final scope of the study is the investigation of the relationship between the changes in the lake extent and the meteorological variables. The strongest relationship was observed between the lake extent and precipitation. The lake area is very responsive to precipitation since it is a shallow lake. The friction between lake water surface and wind creates a drag force. The drag force moves the surface of the water in the direction of the wind. The movement becomes more significant in shallow water and can have an effect on the drying pattern and it was also emphasized in Bowen et al. (1968). The study area is subjected to prevailing northerly winds throughout the year, mostly in August. Lake Tuz is a shallow lake located in a flat topography. Thus, the wind pattern can be an assertive factor on the North to South drying pattern of Lake Tuz.

Based on the results of this study, following recommendations can be made. The lake bathymetry data is not available hence the link between lake bottom elevation and drying pattern could not be established. There exists an artificial canal in the south of the lake that discharges city of Konya's treated waste water. The discharge rate of this canal is less affected by natural climatic conditions. This waste-water disposal from the South can also be a factor in determining the drying pattern of the lake. Future works should include determination of the bathymetry of the lake and amount of waste-water disposal from the city of Konya. Moreover, quantification of possible groundwater recharge into Lake Tuz and surface water inflows will provide valuable insight into the lake water balance estimation. Together with the suggested work, lake water balance estimations will shed further light into the recharge-discharge mechanism of Lake Tuz. The results of this study can be used as a baseline for future lake water balance estimation studies.

REFERENCES

Akıl, B., 2008. İnönü-Eskişehir Fay Sistemi'nin Günyüzü (Eskişehir) - Yeniceoba (Konya - Türkiye) arasındaki bölümünün yapısal evrimi, Hacettepe Üniversitesi Doktora Tezi, 126 s, Ankara (unpublished).

Baraj Arama. (2014). URL: http://www.dsi.gov.tr/baraj-arama.

Başçiftçi F., Durduran S.S., İnal C., 2013. Mapping Ground Water Level with Geographic Information System (GIS) In Konya Closed Basin. Electronic Journal of Map Technologies, 5 (2) 1-15.

Bayarı S., Özyurt N., Kilani S., 2009. Radiocarbon age distribution of groundwater in the Konya Closed Basin, Central Anatolia, Turkey. Hydrogeology J. 17:347–365.

Bowen, A. J., Inman D. L., Simmons V. P., 1968. Wave set-down and set-up. Journal of Geophysics, 73(8), 2569–2577.

Campbell, J. B., Wynne R. H., 2011. Introduction to Remote Sensing. 5th ed., Guilford Press, New York, pp. 205–206.

Crist, E. P., Cicone R. C., 1984. Application of the Tasseled Cap concept to simulated Thematic Mapper data. Photogrammetric Engineering and Remote Sensing 50(3):343-352.

Çamur, M. Z., Mutlu, H., 1996. Major ion geochemistry and mineralogy of the Salt Lake (Tuz Gölü) Basin, Turkey. Chemical Geology, 127, p.313-329.

Çemen, İ., Göncüoğlu, M.C., Dirik, K., 1999. Structural evolution of the Tuzgölü basin in Central Anatolia. Turkey, Journal of Geology, 107 (6), 693-706.

Çınar Mühendislik, 2010. Lake Tuz Specially Protected Area Water Resources Management Project.

Derman, A. S., Engin, M. A., 2007. Tuzgölü (Koçhisar-Aksaray) Fay Zonunun Yeraltı ve Yerüstü Verileri Yardımıyla Karakterinin Belirlenmesi ve Basen Evrimine Katkısı 60th Geological Congress of Turkey, Ankara.

Dirik, K., Erol, O., 2003. Tectonomorphologic Evolution of Tuzgölü and Surrounding Area, Central Anatolia-Turkey. TPJD Special Issue 5, 27-46.

Durduran, S. S., 2010. Coastline change assessment on water reservoirs located in the Konya Basin Area, Turkey, using multitemporal landsat imagery. Environ Monit Assess, 164:453–461.

DSİ, 2009. Konya Closed Basin Revised Hydrological Investigation Report, General Directorate of State Hydraulics Works, Ankara.

Feyisa, G.L., Meilby, H., Fensholt, R., Proud, S.R., 2014. Automated Water Extraction Index: A new technique for surface water mapping using Landsat imagery. Remote Sensing Environment 140, 23–35.

Gao, B.C., 1996. NDWI—A normalized difference water index for remote sensing of vegetation liquid water from space. Remote Sensing Environment, 58, 257–266.

Göncüoğlu, M. C., Erler, A., Toprak, V., Yalınız, K., Olgun, E., Rojay, B., 1992. The Geology of the Western Margins of the Central Anataolian Massif , TPAO Report No: 3535.

Gürol, S., Behnert, I., Özen, H., Deadman, A., Fox, N., Leloğlu, U.M., 2010. Tuz Gölü: New CEOS Reference standard test site for infrared visible optical sensors. Can. J. Remote Sensing, 36, 553–565.

Kauth R.J., Thomas G.S., 1976. The tasseled Cap -- A Graphic Description of the Spectral-Temporal Development of Agricultural Crops as Seen by LANDSAT. Proceedings of the Symposium on Machine Processing of Remotely Sensed Data, Purdue University of West Lafayette, Indiana, pp. 4B-41 to 4B-51.

Kriegler, F.J., Malila, W.A., Nalepka, R.F., Richardson, W., 1969. Preprocessing transformations and their effects on multispectral recognition. Proceedings of the Sixth International Symposium on Remote Sensing of Environment, p. 97-131.

Landsat Missions. (2016, January 15).

URL: http://landsat.usgs.gov/band_designations_landsat_satellites.php

McFeeters, S. K., 1996. The use of Normalized Difference Water Index (NDWI) in the delineation of open water features, International Journal of Remote Sensing, 17(7):1425–1432.

Ministry of Environment and Urbanization, General Directorate of Natural Heritage, (2014). Lake Tuz Specially Protected Area Management Plan 2014-2018.

MTA, 2002. 1/500 000 Scale Geological Map of Turkey, Ankara.

Örmeci, C., Ekercin, S., (2005). Water quality monitoring using satellite image data: a case study at the Salt Lake, Turkey, Proceedings, 11th SPIE International Symposium on Remote Sensing, 19–20 September, Bruges, Belgium; 59770K1–59770K11.

Özsayın, E., Çiner, A., Dirik, K., Rojay, B., Fernandez-Blanco, D., Melnick, D., Garcin, Y.,Bertotti, G., Strecker, M., Schildgen, T., Sudo, M., 2013. Plio-Quaternary extensionaltectonics of the Central Anatolian Plateau: a case study from the Tuz Gölü Basin,Turkey. In: Çiner, Attila, Strecker, Manfred, Bertotti, Giovanni (Eds.), T. Journal of Earth Sciences, 22, pp. 691–714.

Parker, D.C., M.F. Wolff, 1965. Remote sensing, International Science and Technology, 43:20-31.

Richards, J.A., Jia, X. (1999). Remote Sensing Digital Image Analysis, third edition, 363 pp.

Rogers, A. S., Kearney, M. S., 2004. Reducing signature variability in unmixing coastal marsh ThematicMapper scenes using spectral indices. International Journal of Remote Sensing, 25, 2317–2335.

Rokni, K., Ahmad, A., Selamat, A., and Hazini, S., 2014. Water feature extraction and change detection using multitemporal landsat imagery. Remote Sensing, v. 6, p. 4173-4189.

Şaroğlu, F., Emre Ö., Boray, A., 1987. Türkiye'nin Diri Faylari ve Depremsellikleri: Maden Tetk. Arama Genel Müdürlüğü Jeoloji Etüd Dairesi Başkanlığı, Ankara.

The Electromagnetic Spectrum. (2013, February 07).
URL: http://landsat.usgs.gov/electromagnetic_spectrum.php

Turgut, S., 1978. The stratigraphical and depositional Evolution of Lake Tuz Basin: IV. Turkey Petroleum Congress Bulletin Turkey, p. 115-126.

Türeli, T. K., Göncüoğlu, M. C., Akiman, O., 1993. Origin and petrology of Ekecikdag Granitoid in Western Central Anatolian Crystalline Complex. MTA Bull. 115:15–28.

Xu, H., 2006. Modification of normalized difference water index (NDWI) to enhance open water features in remotely sensed imagery, International Journal of Remote Sensing, 27(14):3025–3033.